AD-783 851

NONDESTRUCTIVE EVALUATIONS OF COMPOSITE HEATSHIELD MATERIALS BEFORE AND AFTER AN UNDERGROUND NUCLEAR EXPOSURE

James R. Brown, Jr., et al

Southern Research Institute

Prepared for:

Air Force Weapons Laboratory

June 1974

DISTRIBUTED BY:

NTIS

National Technical Information Service
U. S. DEPARTMENT OF COMMERCE
5285 Port Royal Road, Springfield Va. 22151

AFWL-TR-73-247

AIR FORCE WEAPONS LABORATORY
Air Force Systems Command
Kirtland Air Force Base
New Mexico 87117

When US Government drawings, specifications, or other data are used for any purpose other than a definitely related Government procurement operation, the Government thereby incurs no responsibility nor any obligation whatsoever, and the fact that the Government may have formulated, furnished, or in any way supplied the said drawings, specifications, or other data, is not to be regarded by implication or otherwise, as in any manner licensing the holder or any other person or corporation, or conveying any rights or permission to manufacture, use, or sell any patented invention that may in any way be related thereto.

DO NOT RETURN THIS COPY. RETAIN OR DESTROY.

UNCLASSIFIED
Security Classification

DOCUMENT CONTROL DATA - R & D AD 783851

(Security classification of title, body of abstract and indexing annotation must be entered when the overall report is classified)

1. ORIGINATING ACTIVITY (Corporate author) Southern Research Institute Birmingham, Alabama 35205	2a. REPORT SECURITY CLASSIFICATION UNCLASSIFIED 2b. GROUP

3. REPORT TITLE

NONDESTRUCTIVE EVALUATIONS OF COMPOSITE HEATSHIELD MATERIALS BEFORE AND AFTER AN UNDERGROUND NUCLEAR EXPOSURE

4. DESCRIPTIVE NOTES (Type of report and inclusive dates)

Final Report; May 1972-November 1973

5. AUTHOR(S) (First name, middle initial, last name)

James R. Brown, Jr.; H. G. Sanders; C. D. Pears

6. REPORT DATE June 1974	7a. TOTAL NO. OF PAGES 122	7b. NO. OF REFS None
8a. CONTRACT OR GRANT NO. F29601-72-C-0058 b. PROJECT NO. 627A c. Task No. 0 d.	9a. ORIGINATOR'S REPORT NUMBER(S) AFWL-TR-73-247 9b. OTHER REPORT NO(S) (Any other numbers that may be assigned this report)	

10. DISTRIBUTION STATEMENT

Approved for public release; distribution unlimited.

11. SUPPLEMENTARY NOTES	12. SPONSORING MILITARY ACTIVITY AFWL (DYV) Kirtland AFB, NM 87117

13. ABSTRACT

Distribution Limitation Statement A

Nondestructive evaluations were performed on various composite heatshield materials before and after underground nuclear exposure. Quality control nondestructive evaluations were used to select representative rings from a larger sample. Additional nondestructive testing and nondestructive mechanical (NDM) evaluations were used to characterize the selected rings before and after exposure. Improved methods of characterizing rings after exposure were developed and will be implemented in Carbon-Carbon Design Program. The materials evaluated included an angled, tape-wrapped carbon-phenolic (R6300); 3D carbon/quartz-phenolic (3DC/QP); 3D carbon-phenolic (3DCP); 3D carbon-carbon (3DCC); and felt carbon-carbon (felt CC). All materials were evaluated before underground exposure. After exposure the R6300, 3DCC, and felt CC were evaluated. In the follow-on program, the two CC materials will receive further evaluations.

Reproduced by
NATIONAL TECHNICAL
INFORMATION SERVICE
U S Department of Commerce
Springfield VA 22151

DD FORM 1 NOV 65 1473

UNCLASSIFIED
Security Classification

14 KEY WORDS	LINK A ROLE	LINK A WT	LINK B ROLE	LINK B WT	LINK C ROLE	LINK C WT
Composite materials						
Nondestructive testing						
Mechanical properties evaluation						
Thermal properties evaluation						
Carbon-carbon						
Carbon-phenolic						

NONDESTRUCTIVE EVALUATIONS OF COMPOSITE HEATSHIELD MATERIALS BEFORE AND AFTER AN UNDERGROUND NUCLEAR EXPOSURE

James R. Brown, Jr.
H. G. Sanders
C. D. Pears
Southern Research Institute
Birmingham, AL 35205

Final Report for Period May 1972 through November 1973

TECHNICAL REPORT NO. AFWL-TR-73-247

Approved for public release; distribution unlimited.

FOREWORD

This report was prepared by the Southern Research Institute, Birmingham, Alabama, under Contract F29601-72-C-0058. The research was performed under Program Element 63311F, Project 627A, Task 0, and was funded by the Space and Missile Systems Organization (SAMSO).

Inclusive dates of research were May 1972 through November 1973. The report was submitted 22 April 1974 by the Air Force Weapons Laboratory Project Officer, Captain John A. Gordon (DYV)

This technical report has been reviewed and is approved.

JOHN A. GORDON
Captain, USAF
Project Officer

for CARL D. STUBER
Major, USAF
Chief, Materials/Vulnerability
Hardening Branch

DAVID M. ERICSON
Lt Colonel, USAF
Chief, Technology Division

ABSTRACT

(Distribution Limitation Statement A)

Nondestructive evaluations were performed on various composite heatshield materials before and after underground nuclear exposure. Quality control nondestructive evaluations were used to select representative rings from a larger sample. Additional nondestructive testing and nondestructive mechanical (NDM) evaluations were used to characterize the selected rings before and after exposure. Improved methods of characterizing rings after exposure were developed and will be implemented in Carbon-Carbon Design Program. The materials evaluated included an angled, tape-wrapped carbon-phenolic (R6300); 3D carbon/quartz-phenolic 3DC/QP); 3D carbon-phenolic (3DCP); 3D carbon-carbon (3DCC); and felt carbon-carbon (felt CC). All materials were evaluated before underground exposure. After exposure the R6300, 3DCC, and felt CC were evaluated. in the follow-on program the two CC materials will receive further evaluations.

CONTENTS

Page

SECTION 1

INTRODUCTION 1

SECTION II

MATERIALS EVALUATED 3

AVCO 3D Carbon-Carbon (3DCC) 3
Sandia Felt Carbon-Carbon (Felt CC) 3
AVCO R6300 3
AVCO 3D Carbon/Quartz-Phenolic (3DC/QP) 3
AVCO 3D Carbon-Phenolic (3DCP) 4

SECTION III

APPARATUSES AND PROCEDURES 5

Nondestructive Testing and monitor Evaluations 5

Visual 5
Gravimetric Bulk Density 5
Radiography 5
Ultrasonics 6
Liquid Penetrant Inspection 7

Nondestructive Mechanical Evaluations (NDM) 8

Ring Flexure 8
Hydrostatic Compression 8

SECTION IV

DATA AND RESULTS 10

Nondestructive Testing and Monitors 10

AVCO R6300 10
AVCO 3DCP 11
AVCO 3DC/QP 12
AVCO 3DCC 13
Sandia Felt CC 14

Nondestructive Mechanical Evaluations 15

CONTENTS - Continued

Page

SECTION V

IMPROVED METHODOLOGY 17

Eddy Current. 17
Circumferential Segment Velocity. 18
Turntable X-ray 18
Curved Coupon Compression 18
Ring Segment Testing. 19

Ring Segment Compression (RSC) 20
Ring Segment Tension (RST) 20
Ring Segment Results 20
Comparison of Ring Tests 21

SECTION VI

ADDITIONAL EVALUATIONS 22

Matrix for 3DCC and Felt CC Underground Exposure and Kaman Sciences Equivalent Rings 22

LIST OF ILLUSTRATIONS

Figure		Page
1	AVCO Orthogonal 3D Carbon-Carbon - Material 8	24
2	AVCO R6300 - Single Phase, 2D, 20-Degree Angle Tape-Wrapped Carbon-Phenolic	25
3	AVCO Two-Phase 3D, Orthogonal, Carbon/Quartz-Phenolic-Material #15.	26
4	SoRI Indexing and Orientation System for Rings.	27
5	Definition of Structure-Change Terms.	28
6	Ultrasonic Attenuation Setup Using the Pulsed Through-Transmission Technique	29
7	Schematic of Ring Flexure Setup Used for Modulus of Elasticity in Flexure (MOE) Evaluations.	30
8	Schematic of Hydrostatic Ring Evaluation Setup Used for Compressive Modulus Evaluation.	31
9	Photographs Showing Typical AVCO R6300.	32
10	Thickness Variation for Ring 83301-305-1 from AVCO R6300	33
11	Sketch Showing Inspection Results on Ring 83301-400 from AVCO R6300	34
12	Sketch Showing Inspection Results on Ring 83301-305-4 from AVCO R6300	35
13	Sketch Showing Inspection Results on Ring 83301-305-1 from AVCO R6300	36
14	Photograph Showing Outer Surface of Exposed Ring 83301-305-1 from AVCO R6300	37
15	Photograph Showing Typical AVCO 3DCP for Rings 1, 2, 4, 8, 9, and 11	38
16	Photograph Showing Typical AVCO 3DCP for Rings 83301-200, 83301-202A, 83301-305-2, and 83301-305-3 . .	39

LIST OF ILLUSTRATIONS - Continued

Figure		Page
17	Photograph Showing Visual Resin-Starved Areas Around Radials in Ring 2 from AVCO 3DCP	40
18	Photograph Showing Bumped Outer Edge on Ring 2 from AVCO 3DCP	41
19	Photograph Showing Visual Resin-Starved Areas Around Radials in Ring 8 from AVCO 3DCP	42
20	Sketch Showing Inspection Results on Ring 1 from AVCO 3DCP	43
21	Sketch Showing Inspection Results on Ring 2 from AVCO 3DCP	44
22	Sketch Showing Inspection Results on Ring 83301-200 from AVCO 3DCP	45
23	Sketch Showing Inspection Results on Ring 83301-202A from AVCO 3DCP	46
24	Sketch Showing Inspection Results on Ring 83301-305-2 from AVCO 3DCP	47
25	Sketch Showing Inspection Results on Ring 83301-305-3 from AVCO 3DCP	48
26	Photograph Showing Typical AVCO 3DC/QP for Ring 3	49
27	Photograph Showing Typical AVCO 3DC/QP in Rings 83301-202B and 83301-305-5	50
28	Sketch Showing Inspection Results on Ring 83301-202B from AVCO 3DCP/QP	52
29	Sketch Showing Inspection Results on Ring 83301-305-5 from AVCO 3DCP/QP	53
30	Photograph Showing Typical AVCO 3DCC	54

LIST OF ILLUSTRATIONS - Continued

Figure		Page
31	Sketch Showing Inspection Results on Ring 1109-35-2 from AVCO 3DCC	55
32	Sketch Showing Inspection Results on Ring 1109-35-3 from AVCO 3DCC	56
33	Photographs Showing As-Received Ring 1109-35-2 from AVCO 3DCC After Exposure	57
34	Photographs Showing As-Received Ring 1109-35-3 from AVCO 3DCC After Exposure	59
35	Photographs Showing Structural Change After Exposure in Ring 1109-35-2 from AVCO 3DCC	62
36	Photographs Showing Structural Change After Exposure in Ring 1109-35-3 from AVCO 3DCC	65
37	Photographs Showing Typical Sandia Felt CC	71
38	Sketch Showing Inspection Results on Ring 9N-2 from Sandia Felt CC	72
39	Sketch Showing Inspection Results on Ring 9P-2 from Sandia Felt CC	73
40	Photographs Showing As-Received Ring 9N-2 from Sandia Felt CC After Exposure	74
41	Photographs Showing As-Received Ring 9P-2 from Sandia Felt CC After Exposure	76
42	Photographs Showing Structural Change After Exposure in Ring 9N-2 from Sandia Felt CC	78
43	Photographs Showing Structural Change After Exposure in Ring 9P-2 from Sandia Felt CC	80
44	Curved Specimen Compression Test Fixture	83

LIST OF ILLUSTRATIONS - Continued

Figure		Page
45	Comparison of Initial Portions of Stress-Strain Curves of Several Compressive Evaluation Methods on Felt CC Material	84
46	Circumferential Compression 3DCC Curved Specimen 5-0 Supported Laterally	85
47	Circumferential Compression 3DCC Curved Specimen 4-0 - No Lateral Support Showing Cumulative Effects of Repeated Loading	86
48	Compressive Modulus vs Strain History-Curved 3DCC - No Lateral Support	87
49	Stress-Strain Curve for a 3DQP Curved Compression Specimen with Lateral Support	88
50	Schematic of Ring Segment Tension/Compression Fixture	89
51	Felt CC Ring Segment Compression, Ring #1	90
52	Load Unload at 100% P/A Felt CC Ring #1 (Debug)	91
53	Ring Segment Tensile/Compressive Cycle of Felt CC	92
54	Comparison of Clip-On vs Strain Gage Data in Compression for Curved Felt CC Specimen 3-1-Unsupported	93

LIST OF TABLES

Table		Page
1	Evaluations Completed on Rings for the Underground Exposure Program	94
2	NDT and Monitor Inspection Results on AVCO R6300 Rings Before and After Underground Nuclear Exposure	95
3	NDT and Monitor Results on AVCO 3DCP Rings Before Underground Nuclear Exposure	96
4	NDT and Monitor Inspection Results on AVCO 3DC/QP Rings Before Underground Nuclear Exposure	98
5	NDT and Monitor Inspection Results on AVCO 3DCC Rings Before and After Underground Nuclear Exposure	100
6	NDT and Monitor Inspection Results on Sandia Felt CC Rings Before and After Underground Exposure	101
7	Dimensions of Underground Exposure and Kaman Sciences Equivalent Rings	103
8	Bulk Modulus of Elasticity for Underground Exposure and Kaman Sciences Equivalent Rings	104
9	Felt CC Curved Compression Test Results (Fixed End Test)	105
10	3DCC Curved Compression Test Results (Fixed End Test)	106
11	Comparison of Clip-On Versus Strain Gage Data in Compression for Curved Felt CC Specimen 3-1 Unsupported	107
12	Comparison of Modulus of Elasticity at Different Locations for 3DQP Rings	108

SECTION 1

INTRODUCTION

Nondestructive evaluations were performed on various composite heatshield materials before and after nuclear exposure. Quality control (QC) nondestructive evaluations were used to select representative rings from a larger sample which included specimens for both this program (underground exposure) and the Advanced Heatshield Concept Assessment (AHCA) program. Additional nondestructive testing (NDT) and nondestructive mechanical (NDM) evaluations were used to characterize the selected rings before and after their underground nuclear exposure. The materials evaluated included an angled, tape wrapped, carbon-phenolic (R6300); 3D carbon/quartz phenolic (3DC/QP); 3D carbon-phenolic (3DCP); 3D carbon-carbon (3DCC) and felt carbon-carbon (felt CC).

The underground exposure and the related AHCA program were concerned with the effects of hostile encounter as simulated by nuclear exposure or flyer plate impact on the properties of carbon-carbon and phenolic composite heatshield materials. For these two programs QC evaluations consisting of ulk density, visual inspection (with photographic documentation) and radiography were completed on a total of 67 rings. Using the QC results as a guide, ten rings were selected for application in the underground exposure, and six rings were selected for more extensive evaluations in the AHCA program. Results of the QC evaluations on the 67 rings are given in Nondestructive, Thermal and Mechanical Properties Evaluations of Composite Heatshield Materials, Technical Report AFWL-TR-73-189 prepared for the Air Force Weapons Laboratory.

An unexpected failure mode of the 3D carbon/quartz-phenolic (3DC/QP) rings and 3D carbon-phenolic (3DCP) rings during flyer plate testing at Kaman Sciences dictated a change in application of seven of the ten rings selected for this program. These seven rings had received little more than QC NDT when their application was redirected. Eight rings were supplied as replacements for the redirected seven rings. Two additional rings (felt CC) had been designated for this program by Sandia Laboratories.

The test matrix, Table 1, outlines the specific evaluations completed on each ring in this program. Seven rings received only QC NDT evaluations. Thirteen rings received QC NDT plus additional NDT consisting of penetrant inspection, sonic transmission, and sonic velocity. An attempt to polish the rings for photomicrography (40X) using trimethylpentane was unsuccessful. These 13 rings were subjected to NDM evaluations consisting of hydrostatic compression and ring flexure. After underground exposure, 4 carbon-carbon rings were reevaluated using all of the previous nondestructive evaluations. Three R6300s were also reevaluated after underground exposure using all of the previous nondestructive evaluations except hydrostatic compression.

During the course of these evaluations, the need for improved techniques to determine material properties of rings after exposure to hostile environments became apparent. New techniques were developed and included compressive evaluations on a curved coupon specimen, tensile or compressive evaluations on a segment of a complete ring, eddy current evaluations on the carbon-carbon materials, circumferential velocity of a segment of a complete ring, and improved X-ray techniques for rings.

SECTION II

MATERIALS EVALUATED

AVCO 3D CARBON-CARBON (3DCC)

The 3DCC cylinders were orthogonal, three-dimensional, carbon-carbon composites manufactured by AVCO Corporation. The composite was fabricated, densified by phenolic impregnation, pyrolyzed and graphitized. The construction of this material is shown in Figure 1.

The 3DCC rings evaluated were identified as 1109-35 #2 and 1109-35 #3 and received all evaluations before and after the underground exposure.

SANDIA FELT CARBON-CARBON (FELT CC)

The felt CC was a multidirectional carbon-carbon composite from Sandia Laboratories. A rayon felt carcass was reinforced by needling, a process which pulled some of the fibers through the thickness direction The carcass was infiltrated by vapor deposition and graphitized.

The felt CC rings evaluated were identified as 9N-2 and 9P-2 and were evaluated using all NDT and NDM before and after the underground exposure.

AVCO R6300

The R6300 Composite was a single-phase, 2D, 20-degree angle tape-wrapped phenolic-carbon from AVCO Corporation. A sketch of the construction of this material is shown in Figure 2.

The three R6300 rings evaluated were identified as 83301-400, 83301-305-1 (#9) and 83301-305-4. All rings received NDT and NDM evaluations before and after the underground exposure.

AVCO 3D CARBON/QUARTZ-PHENOLIC (3DC/QP)

The 3DC/QP rings were a two-phase material made of 3D, orthogonal, phenolic-graphite over a 3D, orthogonal, phenolic-quartz manufactured by AVCO Corporation. The radials were phenolic-carbon. A sketch showing the construction of this material is shown in Figure 3.

The 3DC/QP ring identified as 3DC/QP ring #3 received only QC NDT. Rings 83301-202B and 83301-305-5 received full NDT and NDM evaluations before the underground exposure only.

AVCO 3D CARBON-PHENOLIC (3DCP)

The 3DCP material was a single-phase, 3D, orthogonal, phenolic-graphite identical in construction to the 3DC/QP material except without the phenolic-quartz substructure.

The six 3DCP rings identified as #1, #2, #4, #8, #9, and #11 received QC NDT only. Rings 83301-200, 83301-202A, 83301-305-2, and 83301-305-3 received the full NDT and NDM evaluations before the underground exposure only.

SECTION III

APPARATUSES AND PROCEDURES

NONDESTRUCTIVE TESTING AND MONITOR EVALUATIONS

VISUAL - For virgin (unexposed) material, visual inspections (1X to 10X) were made on surfaces to determine material macro-level typicality and surface anomalies. This was effective for detecting surface variations such as yarn bundle fraction variations, separations, macrovoids, discolorations, resin-rich and resin-starved areas, yarn bundle wrinkling and spacing variations, ply spacing variations, and void clusters. Results were documented photographically.

For exposed (hit) materials, visual inspections (1X to 10X) were performed on the edges and surfaces of the specimens to assess macro-level structural change. Results were documented photographically. Results from these inspections were compared to those from virgin material for assessment of structural change. The Southern Research indexing and orientation systems used to locate specific features are shown in Figure 4. Angular locations without any additional designation are relative to the exposure centerline. Angular locations such as SoRI 90° are relative to the SoRI chosen 0° reference. Definitions of terms used to describe structural change are shown in Figure 5.

GRAVIMETRIC BULK DENSITY - Bulk density measurements for specimens were calculated from direct measurements of weights and dimensions. An analytical balance having a sensitivity of ±0.1-gram was used for weighing. Micrometers read to the nearest 0.0005-inch were used for measuring lengths.

RADIOGRAPHY - Radiography was performed using state-of-the-art X-ray techniques for low-absorptive materials. The radiographic unit used was a Radifluor 360 manufactured by Torr X-ray Corporation, a division of Phillips Electronics. This unit is rated for operation from 0 to 120 kv at either 3 or 5 ma, making it ideal for phenolic and carbon-carbon type materials. The unit incorporates certain characteristics that are essential for examination of low absorptive materials with high resolution and sensitivity. The focal spot size is 0.35 mm, and the X-ray tube window is 0.015-inch thick beryllium. A small focal spot size provides high sensitivity and distortion-free imaging of small discontinuities. Radiographic sensitivity using extra-fine grain film is within 1 percent (per MIL STD 453).

Operational and film development procedures were consistent with conventional good radiographic practices. For example, image sensitivity and contrast was enhanced by using minimum power settings for longer time periods. Sharp imaging was ensured by using extra-fine grain film (such as Eastman Type M) and by using a long focus to film distance (FFD) of up to 46-inches. Hand film processing in accordance to the film manufacturer's suggested procedure was used to assure maximum quality. Image quality was checked using penetrameters from similar material. Penetrameter hole sizes used were 1/2T, 1T and 2T (1T and 2T holes as defined by MIL-STD-453). Radiographs were inspected in a dark room using a high intensity (variable) spot illuminator.

ULTRASONICS - Basic apparatus used in the ultrasonic measurements of velocity and through-transmission are a Sperry UM721 Reflectoscope and a Tektronix 564 Oscilloscope. Velocity is evaluated using the through-transmission, elapsed-time technique. The Sperry UM721 is used as the pulser, and the Tektronix 564 complete with a 3B3 time base (precision of 1 percent) and a 3A3 vertical amplifier is used as the signal measuring device. Transmission measurements were made using the pulse through-transmission technique with an in-line attenuator to simulate the varying degrees of structural change. The basic apparatuses used were the Sperry UM721 as the signal pulser, the Tektronix 564 as the signal measuring device, and a Kay Model 20-0, 41-dB in-line attenuator for assessing relative structural change in the various specimens.

In using the through-transmission, elapsed-time technique for measuring acoustic velocity, a short pulse of longitudinal-mode sound is transmitted through the specimen. An electrical pulse originates in a pulse generator and is applied to a ceramic piezoelectric crystal (SFZ). The pulse generated by this crystal is transmitted through a short delay line and inserted into the specimen. The time of insertion of the leading edge of this sound beam is the reference point on the time base of the oscilloscope which is used as a high-speed stopwatch. When the leading edge of this pulse of energy reaches the other end of the specimen, it is displayed on the oscilloscope. The difference between the entrance and exit times is used with the specimen length in calculating ultrasonic velocity. A short Lucite delay line is used to allow time isolation of the sound wave from electrostatic coupling and to facilitate clear presentation of the leading edge of the entrant wave resulting in a more accurate "zero" for time.

Using 0.5/1.0 MHz transducers coupled with alcohol, the precision for this velocity measurement technique has been established for polygraphites such as ATJ-S as ±0.002 inch per microsecond for a 4-inch long by 1/2-inch diameter specimen and as ±0.010 inch per microsecond for a 1/4-inch long by 1/4-inch diameter specimen. High purity trimethylpentane was used as the coupling medium for these evaluations.

In using the through-transmission technique for detecting structural variations, Figure 6, sound is transmitted through the specimen and displayed by the oscilloscope. The gain of the oscilloscope is held constant and a calibrated step attenuator located in the input circuit is used to maintain the displayed wave-form at a constant amplitude. Values of transmission (called added-dB) relative to a reference material may be read from the step attenuator. Measurements are made in a bath (trimethylpentane for these evaluations) to minimize effects of contact coupling and near field effects. A suitable fixture is used to align the transducers and to hold the specimen squarely in the sound beam. When specimen geometry is such that part of the energy in the sound beam could by-pass the specimen, foam padding is used as a block to absorb this energy. The sensitivity of the calibrated attenuator is 1 dB with a minimum-maximum from 0 to 41 dB.

LIQUID PENETRANT INSPECTION - Volatile liquids are used on porous materials such as graphites, phenolic and carbon-carbon composites as a nondestructive test for surface discontinuities such as gross porosity, wide density variations, large inclusions and cracks. When a material is wetted with a volatile liquid, porous areas and cracks remain wet for a longer period of time than the surrounding material. This differential evaporation effect is discernible by visual observation. Although this technique is not quantitized (it probably could be), it is effective in revealing surface discontinuities.

The volatile liquid inspection procedure involves the following:

1. Application of a volatile liquid to surface of specimen usually for 5 to 10 seconds. This can be done by flooding, brushing, or immersing.

2. Inspection of specimen surface as the liquid evaporates. Porous areas will remain wetted while the surrounding smooth areas will dry. Cracks also will remain wetted depending primarily upon the depth and width of the crack.

3. Record is made of visual observations.

This technique is useful in revealing surface discontinuities. Other NDT methods of inspection such as ultrasonics and radiography can be used in conjunction with the penetrant inspection to determine the extent of the surface discontinuity internally. The volatile liquid used was high purity, 2, 2, 4-trimethylpentane.

NONDESTRUCTIVE MECHANICAL EVALUATIONS (NDM)

All rings receiving the full NDT evaluations also were given nondestructive mechanical evaluations. Two different methods were used before and after the underground exposure: first-ring flexure evaluation and second-hydrostatic compression evaluation. During these evaluations, the rings were loaded to no greater than 20 percent of the ultimate strength as defined by data from the Advanced Heatshield Program (AHP).

RING FLEXURE - A schematic drawing of the setup used for the ring flexure evaluations is shown as Figure 7. The ring was instrumented with four strain gages on the inside surface oriented in the circumferential direction. The ring to be evaluated was located between the crossheads of a Tinius-Olsen testing machine. Three dial indicators were located around the ring to measure radial deflections as shown in Figure 7. Strain was read using a Baldwin strain indicator. Load was read from an internal load cell in the testing machine. The ring was loaded incrementally and all dial indicator and strain gages read at each load increment. The ring was loaded to 20 percent or less of its ultimate strength. The sequence was repeated at least twice with the arbitrarily selected NDT zero orientation under the loading pad, rotated 45 degrees counterclockwise and at 90 degrees to the vertical. Modulus values were calculated using classical ring equations.

HYDROSTATIC COMPRESSION - The hydrostatic compression evaluation was run in a hydrostatic loading rig shown schematically in Figure 8. The loading medium was a thin wall rubber bladder which was connected to a hydraulic cylinder. The bladder was contained on the outside diameter by an outer closure ring and top and bottom closure plates. The bladder was contained on the inside diameter by the test ring and spacer

rings. The spacer rings were sized to give an assembled height with the test ring in place which was 0.005 inch less than the outer closure ring. The bladder was oversized for the cavity in the rig and this combined with its thin wall ensured that the bladder supported a negligible portion of the hydraulic loading. The hydraulic system was filled and bled. The hydraulic cylinder was loaded in a Tinius-Olsen testing machine. Load was measured by an internal load cell in the testing machine. This was was converted to hydraulic pressure and stresses were calculated using thick walled cylinder relationships.

$$\sigma = 2P \frac{R_2^2}{R_2^2 - R_1^2}$$

where

σ = Circumferential stress at I.D.

P = Hydraulic pressure

R_2 = Outside radius

R_1 = Inside radius

Strain was read using a Baldwin strain indicator. From the stress and strain values modulus was calculated using the Hook's Law relationship:

$$\sigma = E\varepsilon$$

SECTION IV

DATA AND RESULTS

NONDESTRUCTIVE TESTING AND MONITORS

AVCO R6300 - The NDT and monitor results on Rings 83301-305-1, 83301-305-4, and 83301-400 are presented in Table 2 and Figures 9 through 14. Material background and before and after-exposure variations as indicated by vision, X-ray, and liquid penetrants are also detailed in the table and figures.

Generally, the material background was similar to AHP R6300 material which was reported in "Thermal and Mechanical Properties of Advanced Heatshield Resinous (CP) and Carbonaceous (CC) Composites" No. AFML-TR-72-160. Variations considered typical for the rings were residual porosity to 20 mils, Figure 9a, and reinforcement wrinkling Figure 9b.

The following results were obtained for before and after-exposure values of density, axial velocity, radial velocity, and radial transmission. For Ring 83301-305-1, the respective values were 1.338 and 1.343 gm/cm^3, 0.129 and 0.130 in./μsec, 0.127 and 0.114 in./μsec, and 44 and 43 added-dB. Significant variations in radial velocity and transmission were measured in the exposed ring. For radial velocity, low values of 0.0887, 0.0996, and 0.1011 in./μsec were measured at 0°, 45°, and 315°. For transmission, low values of 34 and 35 added-dB were measured at exposure 0°. A slight variation in thickness was measured for the exposed ring. As shown in Figure 10, thickness varied from 0.4048-inch at 315° to 0.4132-inch at 90°. For Ring 83301-305-4, the respective values were 1.339 and 1.341 gm/cm^3, 0.128 and 0.130 in./μsec, 0.124 and 0.124 in./μsec, and 49 and 48 added-dB. There were no significant local variations in the data for the exposed ring, including thickness variations around the ring. For Ring 83301-400, the respective values were 1.340 and 1.343 gm/cm^3, 0.128 and 0.130 in./μsec, 0.124 and 0.123 in./μsec, and 48 and 47 added-dB. There were no significant local variations in the after-exposure data, and no significant thickness variation around the ring.

Visual, X-ray, and liquid penetrant inspections on the virgin rings revealed a single flaw in Ring 83301-305-1. A 20-mil low-absorptive area was indicated by axial X-ray close to the inner edge at 180°. The 0° orientation was designated to avoid this flaw.

Sketches summarizing the NDT and monitor inspection results on the virgin rings are given in Figures 11 through 13.

Some structural change was indicated in exposed Rings 83301-305-1 and 83301-400 by visual, X-ray, and liquid penetrant inspections. For 83301-305-1, the change was visually apparent matrix damage on the front face (outer surface) of the exposed area, Figure 14. Also, increased porosity to a depth of 100 mils on the rear face (inner surface) of the exposed zone was visually apparent. For 83301-400, the only change detected was increased porosity to a depth of 80 mils on the rear face (inner surface) of the exposed zone. No change was detected in Ring 83301-305-4.

AVCO 3DCP - NDT and monitor inspection results on virgin Rings 1, 2, 4, 8, 9, 11, 83301-200, 83301-202A, 83301-305-2, and 83301-305-3 are presented in Table 3 and Figures 15 through 25. Because of an unexpected failure in some 3DC/QP rings subjected to flyer plate testing at Kaman Sciences, work on some rings was stopped and application was redirected. The data presented include only the results from the virgin inspections.

The material background was generally similar to AHP 3DCP reported in AFML-TR-72-160. For Rings 1, 2, 4, 8, 9, and 11, the material had lower porosity and straighter circumferentials than the AHP material, Figure 15. For Rings 83301-200, 83301-202A, 83301-305-2, and 83301-305-3, the material had an extremely high residual porosity along the radials, Figure 16. The reinforcement in both sets of rings was workmanly placed.

The following results were obtained for virgin values of density, axial velocity, radial velocity, and radial transmission. For Ring 1, the respective values were 1.406 gm/cm^3, 0.371 in./μsec, 0.165 in./μsec, and 25 added-dB. For Ring 2, the respective values were 1.415 gm/cm^3, 0.367 in./μsec, 0.164 in./μsec, and 28 added-dB. For Rings 4 and 8, the work stoppage occurred before the velocity and transmission measurements were made. The respective densities of these two rings were 1.409 and 1.412 gm/cm^3. For Ring 9, the respective values of density, axial velocity, radial velocity, and radial transmission were 1.413, 0.366 in./μsec, 0.168 in./μsec, and 24 added-dB. For Ring 11, the respective values were 1.404 gm/cm^3, 0.370 in./μsec, 0.167 in./μsec, and 23 added-dB. For Ring 83301-200, the respective values were 1.316 gm/cm^3, 0.284 in./μsec, 0.193 in./μsec,

and 30.5 added-dB. For Ring 83301-202A, the respective values were 1.317 gm/cm^3, 0.284 in./μsec, 0.188 in./μsec, and 26.5 added-dB. For Ring 83301-305-2, the respective values were 1.316 gm/cm^3, 0.285 in./μsec, 0.190 in./μsec, and 26.5 added-dB. For Ring 83301-305-3, the respective values were 1.321 gm/cm^3, 0.281 in./μsec, 0.189 in./μsec, and 28 added-dB.

Visual, X-ray, and liquid penetrant inspection (except liquid penetrant on Rings 4 and 8) were completed on all designated rings before the work stoppage. No single flaws were revealed in Rings 1, 83301-200, 83301-202A, and 83301-305-3. For the other rings, flaws or anomalous material variations generally consisted of various indications of resin starved areas around radials by vision and low-absorptive alignments by axial X-ray. These and other variations are detailed in Table 3 and are depicted in Figures 17 through 19. Sketches summarizing the NDT and monitor inspection results on Rings 1, 2, 83301-200, 83301-202A, 83301-305-2, and 83301-305-3 are given in Figures 20 through 25.

AVCO 3DC/QP - NDT and monitor inspection results on virgin Rings 3, 83301-202B, and 83301-305-5 are presented in Table 4 and Figures 26 through 29. Again, because of the unexpected failure in some 3DC/QP rings subjected to flyer plate testing at Kaman Sciences, work on some rings was stopped, and their application was redirected. The data presented include only the results from the virgin inspections.

The material background was generally considered similar to AHP 3DC/QP material reported in AFML-TR-72-160. For Ring 3, the material had lower porosity and straighter circumferentials than the AHP material, Figure 26. For Rings 83301-202B and 83301-305-5, the material had an extremely high residual porosity along radials and between axials, Figure 27. Also, for these rings, missing pieces of axials and circumferentials from machined surfaces and residual porosity between radials and axials at the inner surface were typical of the material, Figures 26 and 27.

The following results were obtained for virgin values of density, axial velocity, radial velocity, and radial transmission. For Ring 3, the respective values were 1.476 gm/cm^3, 0.343 in./μsec, 0.166 in./μsec, and 30.5 added-dB. For Ring 83301-202B, the respective values were 1.343 gm/cm^3, 0.287 in./μsec, 0.192 in./μsec, and 21 added-dB. For Ring 83301-305-5, the respective values were 1.354 gm/cm^3, 0.284 in./μsec, 0.192 in./μsec, and 21.5 added-dB.

No single flaws were detected in the virgin rings by vision, X-ray, and liquid penetrant. Sketches summarizing the NDT and monitor inspection results on Rings 83301-202B and 83301-305-5 are given in Figures 28 and 29.

AVCO 3DCC - The NDT and monitor results on Rings 1109-35-2 and 1109-35-3 are presented in Table 5 and Figures 30 through 36. Material background and before and after-exposure variations indicated by vision, X-ray, and liquid penetrant are also detailed in Table 5 and Figures 30-36.

For background, the material was generally uniform, workmanlike, and similar to AHP 3DCC material which was reported in AFML-TR-73-160. The exception was that the delams (also called debond and matrix rich areas) along the circumferentials were more frequent than for the AHP material, Figure 30. These delams were uniformly distributed throughout the material. Also, missing radials in machined edges were also typical of the material.

The following results were obtained for before and after-exposure values of density, axial velocity, radial velocity, and radial transmission. For Ring 1109-35-2, the respective values were 1.638 and 1.636 gm/cm^3, 0.375 and 0.363 in./μsec, 0.244 and 0.218 in./μsec, and 18 and 22 added-dB. Systematic shifts were measured between the before and after data; however, no significant local variations were measured in the exposed ring. The variation in thickness around the exposed ring was only slight, Table 5. For Ring 1109-35-3, the respective values were 1.645 and 1.640 gm/cm^3, 0.377 and 0.356 in./μsec, 0.247 and 0.237 in./μsec, and 22 and 21.5 added-dB. Again, systematic shifts were measured between the before and after data, but no significant local variations were measured in the exposed ring. There was no significant variation in thickness around the ring, Table 5.

Visual, X-ray, and liquid penetrant inspections on the virgin rings revealed no single flaws. Sketches summarizing the NDT and monitor inspection results are given in Figures 31 and 32.

Structural change was visually apparent in both rings. Photographs showing the as-received rings are given in Figures 33 and 34. Generally, for both rings, the change consisted of raised or recessed and missing radials, cracking along local preexisting circumferential delams completely around the ring,

spalled sections of matrix and circumferential reinforcement (circs) over radials in edges, yarn lift from the front face, and discolorations (dark) on the front face. These and other changes are detailed in Table 5 and Figures 35 and 36. Absorption of trimethylpentane into edges of both exposed rings was higher in the exposed zone than out of the exposed zone. The only change indicated by axial X-ray was a 1-1/2-inch long circumferential low-absorptive alignment at 315°.

SANDIA FELT CC - The NDT and monitor results on Rings 9N-2 and 9P-2 are presented in Table 6 and Figures 37 through 43. Material background and before and after-exposure variations indicated by vision, X-ray, and liquid penetrant are also detailed in the table and figures. For background, the material was typical Sandia felt CC and was uniform throughout. Residual porosity was to approximately 12 mils, Figure 37.

The following results were obtained for before and after-exposure values of density, axial velocity, radial velocity, and radial transmission. For Ring 9N-2, the respective values were 1.813 and 1.814 gm/cm^3, 0.116 and 0.115 in./μsec, 0.119 and 0.117 in./μsec, and 51.5 and 49 added-dB. Local shifts in after-exposure radial velocity of 0.1117 at 0° and 0.1100 at 315° were significant variations. The variations in after-exposure axial velocity and radial transmission were systematic rather than local. A slight variation in thickness was measured around the ring. The thickness varied from approximately 0.497 inch at 0° to 0.499 inch at 90° and 270°; Table 6. For Ring 9P-2, the respective values were 1.830 and 1.830 gm/cm^3, 0.115 and 0.112 in./μsec, 0.117 and 0.118 in./μsec, and 52 and 50.5 added-dB. The only significant local variation was in the value of radial velocity of 0.1095 in./μsec at 315°. A variation in thickness similar to 9N-2 above was measured for 9P-2. The thickness varied from approximately 0.4975 inch at 0° to 0.499 inch at 90° and 270°; Table 6.

From the visual, X-ray, and liquid penetrant inspections on the before-exposure rings, only axial X-ray was effective in determining single flaws. For 9N-2, the single flaws revealed were a single skew low-absorptive alignment at 110 - 125° and a single 0.15-inch long radial low-absorptive alignment which extended inward from the outer surface at 255°. For 9P-2, the only single flaw revealed was a 1/4-inch by 1/2-inch low-absorptive area near the inner surface at 225°. Orientations were designated to avoid these flaws. Sketches summarizing the NDT and monitor results are given in Figures 38 and 39.

No really significant structural change such as cracking was detected in these two rings. Photographs showing the rings as-received are given in Figures 40 and 41. For 9N-2, the only changes or noteworthy observations were that the exposed-zone segment of the bottom edge was slightly more porous, Figure 42a, and the exposure-zone outer surface (front face) was slightly discolored (dark) and rougher in texture, Figure 42b and c. For 9P-2, change and noteworthy observations were discoloration (dark) on top edge, 80 mil chip in top outer edge at 315°, higher porosity in exposure-zone of bottom edge, 20-mil voids in bottom edge at 240 - 255° and 270°, and material removal and discoloration in exposure-zone front face. These changes are detailed in Table 6 and depicted in Figure 43. Axial X-ray and liquid penetrant inspection did not reveal any structural change in these rings.

NONDESTRUCTIVE MECHANICAL EVALUATIONS

The two 3DCC rings and two felt CC rings which were exposed in the underground event and one ring of each material which had received flyer plate testing at Kaman Sciences (called Kaman equivalents) were all disassembled at Southern Research. Table 7 summarizes diameter measurements at various stages of assembly and disassembly. It is interesting to note that the out-of-roundness figures indicate that the Kaman hit rings were more distorted than the station 4, underground exposure rings which were supposed to have had similar energy inputs.

Table 8 contains the results of all bulk modulus evaluations on the rings of the underground exposure program plus the two rings which had received flyer plate testing at Kaman Sciences. From the results several conclusions may be drawn.

1. The modulus values of the 3D materials calculated from deflection measurements from ring flexure are generally lower than for the other evaluation methods. (The more homogeneous materials, felt CC and R6300, do not show this result.) One possible explanation for the low modulus values could be the shear deflections which are probably increased for the 3D materials over the more homogeneous materials by the numerous small circumferential delaminations which seem to be more prevalent in them.

2. The moduli values of these rings seem to be similar to those measured in the AHP program on coupon specimens. See the last four columns of Table 8 for the AHP data range.

3. The 3DCC station 4 ring and Kaman ring seem to have similar retained moduli.

4. The felt CC station 4 ring and Kaman ring seem to have similar retained moduli, but this conclusion is not quite as evident as for the 3DCC rings.

SECTION V

IMPROVED METHODOLOGY

As this program on underground exposure rings proceeded, other Air Force programs had been developing, such as the Carbon-Carbon Design Program (CCDP), where other arcs and rings were being hit above ground by mag fliers and high explosive. It became apparent that the underground rings should not be subjected to further tests and certainly not destructed until additional tests could be developed using both nondestructive energies (NDT) and nondestructive (low stress) types of mechanical tests (NDM) that would not further damage the materials. Therefore, the work on the underground rings was stopped and this program was directed toward improving those needed additional tests including eddy current (NDT), circumferential velocity (NDT), turntable X-ray (NDT), curved coupon compression (NDM), ring segment tension (NDM), and ring segment compression (NDM). All of the NDM tests may be used to fracture if desired. Recall that only the two carbon materials are now available for further evaluations.

EDDY CURRENT

The use of eddy current evaluation on the two carbon materials involved the application of an old technology in a new way. In eddy current testing, a transducer (coil or double coil) is held close to a material and couples to the workpiece by the impedance resulting from the resistance and reactanace of the material. Normally, an operating mode is selected so that the measurement is sensitive to the surface of the work and surface anomalies, such as small cracks. However, it is possible to operate the equipment in null-reject and at a frequency such that it monitors primarily the resistance of the material in depth or nearly through the thickness of a ring. This latter mode was chosen so that in-depth damage to a ring (from shock loading) would be related to instrument output. Indeed, an extremely tight correlation has been found on arcs and rings for output versus impact level. This inspection method will be used on the carbon-carbon underground rings.

CIRCUMFERENTIAL SEGMENT VELOCITY

Another NDT method was found that correlates the damage in the rings quite well-circumferential segment velocity. In this technique, the normal instruments for measuring sonic velocity are used, but the longitudinal wave is introduced into the ring over a circumferential segment about 3-1/4 inches long. On shorter 2-inch arcs, the technique was not successful and so was discarded; however, at the longer segment lengths, good correlations are being found with damage. This technique also is now being employed on the underground rings.

TURNTABLE X-RAY

In earlier work, axial X-rays were made on groups of arcs and on rings with the X-ray aperture at (and above) the geometric center of the general field of view. This has been altered so that, in case of a ring, it is rotated under the aperture providing a direct path through areas (or cracks) concentrically positioned in the ring and on to the film in a normal, or 90°, approach. Since the ring is rotated under the aperture, the method is called turntable X-ray (TTX). The X-rays are sharp and a picture of the entire ring can be presented in perfect geometric reproduction for overlay comparison between virgin and damaged material.

CURVED COUPON COMPRESSION

Circumferential compression coupon testing historically has been accomplished using a straight specimen. This method yields good results on an homogeneous material; however, if the material is a composite with curved elements in the circumferential direction, results from straight specimens do not give the best results. Moreover, the outer fibers of a material can not be tested using a straight specimen.

Testing a curved specimen has always given poor ultimate strengths and poor estimates of other properties due to bending, which has invariably been associated with this type test. To obtain good results from a curved specimen, the bending stresses must be controlled.

The technique developed at SoRI for compression consists of testing a curved specimen with fixed ends and the option of restraining lateral motion in order to achieve 100 percent uniaxial (P/A) stress. The apparatus used is shown in Figure 44. The specimen is rigidly fixed in the grips so there is no motion of the specimen ends relative to the grips. The grips are inserted in a close fitting sleeve which allows only axial motion; therefore, load to the specimen is applied only axially. This basic setup would still allow bending in the specimen and could not achieve pure compression. To restrain the specimen from bending a lateral support at midspan is used.

This apparatus allows the lateral load to be varied during a run; therefore, the capability exists of running compression tests at any given ratio of P/A stress to bending stress that is desired. Some stress-strain curves for curved compression are shown in Figures 45 through 47 and 54. Strains on Figures 45 through 47 and 54 were measured with clip-on extensometers located on the edges of the specimen so that the output was an average strain across the specimen. Figure 48 summarizes the results obtained in the test fixture on the influence of repeated cycling on the initial modulus of curved 3DCC specimens. Figure 49 shows the results of a run on a 3DQP specimen with strain data measurements from independent strain gages on the two curved surfaces. This run illustrates the close agreement possible between the two strain outputs (100 percent P/A) by using the lateral support.

Typical results shown in Tables 9 through 11 illustrate the difference in strengths for curved specimens which were unsupported and supported. The supported runs were run at approximately 60 percent P/A. (This value was determined on a later test).

The results obtained at 100 percent P/A are in good agreement with strengths obtained from ring testing.

RING SEGMENT TESTING

Ring segment testing was developed to yield improved estimates of the elastic modulus of selected sections of virgin and degraded rings in a controlled stress field and without introducing further degradation. Methods used in the early portion of this program were ring flexure and hydrostatic compression or tension. Ring flexure evaluations provide a stress field that is essentially bending and require assumptions about the distribution of the modulus of the ring

since the entire ring is stressed. Hydrostatic compression and tension evaluations are somewhat sensitive to geometric and material imperfections or nonuniformity and tend to give an average of the entire ring. By isolating the segment of the ring under test from the remainder of the ring, the new evaluation method eliminates the need for distribution assumptions and simplifies the data reduction methods.

Basically, as shown in the sketch in Figure 50, the entire ring, except for a small arc on each side, is completely fixed in the fixture. When evaluated without lateral supports, the major portion of the stress in the gage sections is bending. When properly applied lateral supports are used, the bending stresses are reduced, thus giving a more uniform stress field. By using strain gages on the inside and outside surfaces, the ratio of P/A to total stress may be determined and controlled. If the support is just firmly applied before testing, the resulting stress distribution is approximately 50 percent P/A. By adjusting the supports during a run, the ratio of P/A to total stress may be maintained at any level desired. Figure 51 shows the results of tests for varying percentages of P/A.

RING SEGMENT COMPRESSION (RSC) - This test is run using the above philosophy. The outside support is used during a compressive run to maintain the percentage P/A desired. It is important that support adjustments be made continuously during a run and that they be removed continuously during unload in order not to crack the ring due to side loading or bending stresses.

RING SEGMENT TENSION (RST) - This test is run essentially the same as RSC, the main difference is that the inside surface supports are adjusted to control the percentage P/A.

RING SEGMENT RESULTS - Some of the results from initial evaluations with the fixture are shown in Figures 52 and 53. Two cycles of a compressive load/unload run on a felt CC ring are shown in Figure 52. This run was made at 100 percent P/A. This figure shows that permanent deformations may be induced and the effects on properties for subsequent loadings or the cumulative effects studied. Figure 53 shows the results of load/unload in tension/compression on a felt CC ring. Again, the runs were made at 100 percent P/A.

COMPARISON OF RING TESTS - Two 3DQP rings were used for this comparison. These rings were nondestructively tested by ring flexure, hydrostatic tension and compression, and ring segment tension and compression. The resulting MOEs found are shown in Table 12. It can be seen from this table that the agreement of hydrostatic (pure) tests and ring segment tests is good.

SECTION VI

ADDITIONAL EVALUATIONS

The experimental techniques (NDT and NDM) described in the previous section have now been demonstrated and are operable. Under CCDP additional data on the two 3DCC rings and two felt CC rings from the underground exposure program plus the rings of each material from the AHCA program will be generated. The full program to be run on these rings is shown below and will provide the final analysis to this program. Of course a portion of this work has already been accomplished and some of those results are included in this report. It is extremely fortunate that the underground exposure program permitted these refinements and, thus, a better, eventual analysis of the results of underground nuclear exposure.

MATRIX FOR 3DCC AND FELT CC UNDERGROUND EXPOSURE AND KAMAN SCIENCES EQUIVALENT RINGS

A. Nondestructive Testing (NDT): density, turntable X-ray, eddy current, circumferential velocity, radial velocity, and radial attenuation.

B. Nondestructive Mechanical Evaluations (NDM).

   1. Ring flexure.
   2. Ring hydraulic compression (buckle measurements).
   3. Ring hydraulic tension.
   4. Ring segment compression at 40 percent and 100 percent P/A.
   5. EME (Kaman test).

C. Cut to three subrings: 0.6 inch height, about 0.35 inch height, and about 0.35 inch height; remove edge.

D. Prime NDT on each of three subrings.

E. NDM on each of three subrings.

   1. Ring flexure.
   2. Ring hydraulic compression (buckle measurements).
   3. Ring hydraulic tension.
   4. Ring segment compression at 40 percent and 100 percent P/A.
   5. EME (Kaman test).

F. Slice three subrings to in/out: 0.150-inch in and 0.150 inch outer.

G. Prime NDT on three subrings in/out.

H. NDM on each of in/out of each subring.

1. Ring flexure.
2. Ring hydraulic compression (buckle measurements).
3. Ring hydraulic tension.
4. Ring segment compression at 40 percent and 100 percent P/A.
5. EME (Kaman test).

I. Destructive evaluations on center subring (may add a hard test).

1. Inner: hydraulic tension.
2. Outer: ring segment compression or hydraulic compression.

J. Destructive evaluations on end subrings.

1. Inner: hydraulic tension or ring segment tension.

2. Outer: ring segment compression or hydraulic compression.

K. NDT of remnants.

Notes:

1. Key rings to arcs per other work before step I.
2. Key end point tests are on "center" rings; "edge" rings for additional information if uniformity all right.

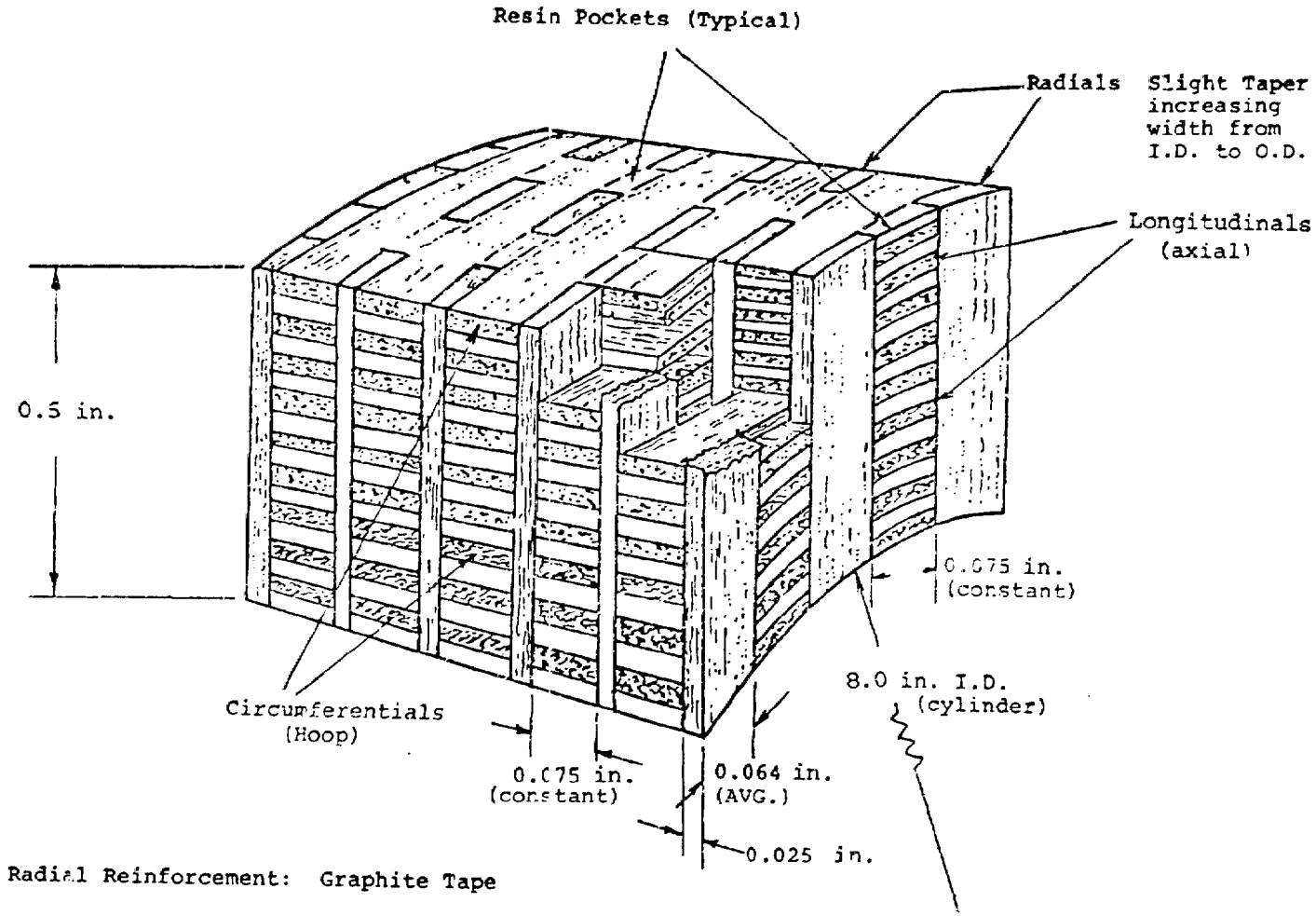

Radial Reinforcement: Graphite Tape

Circumferential and
Axial Reinforcement: Thornel-50 Tape

Figure 1. AVCO Orthogonal 3D Carbon-Carbon - Material 8

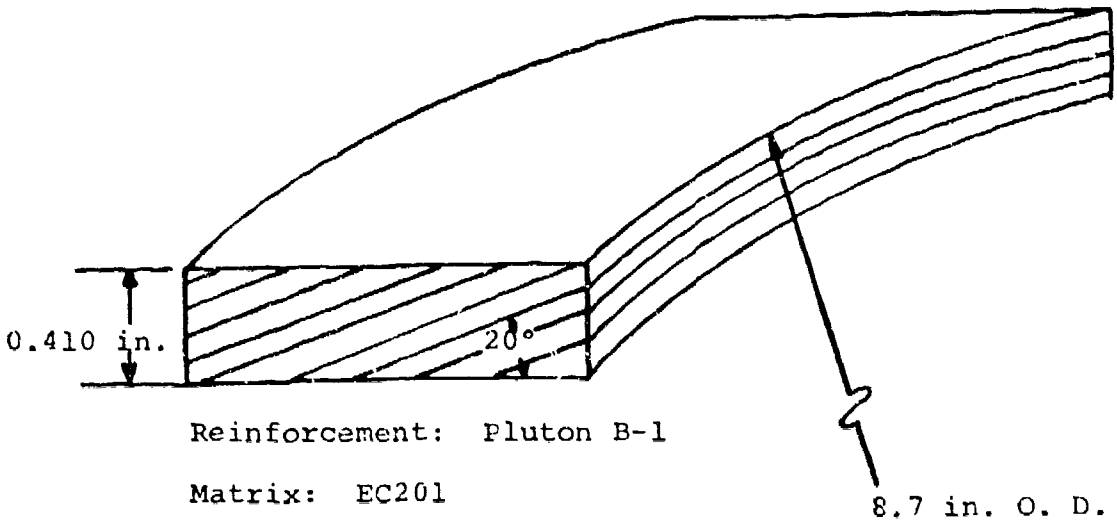

Figure 2. AVCO R6300 - Single-Phase, 2D, 20-Degree Angle Tape-Wrapped, Carbon Phenolic

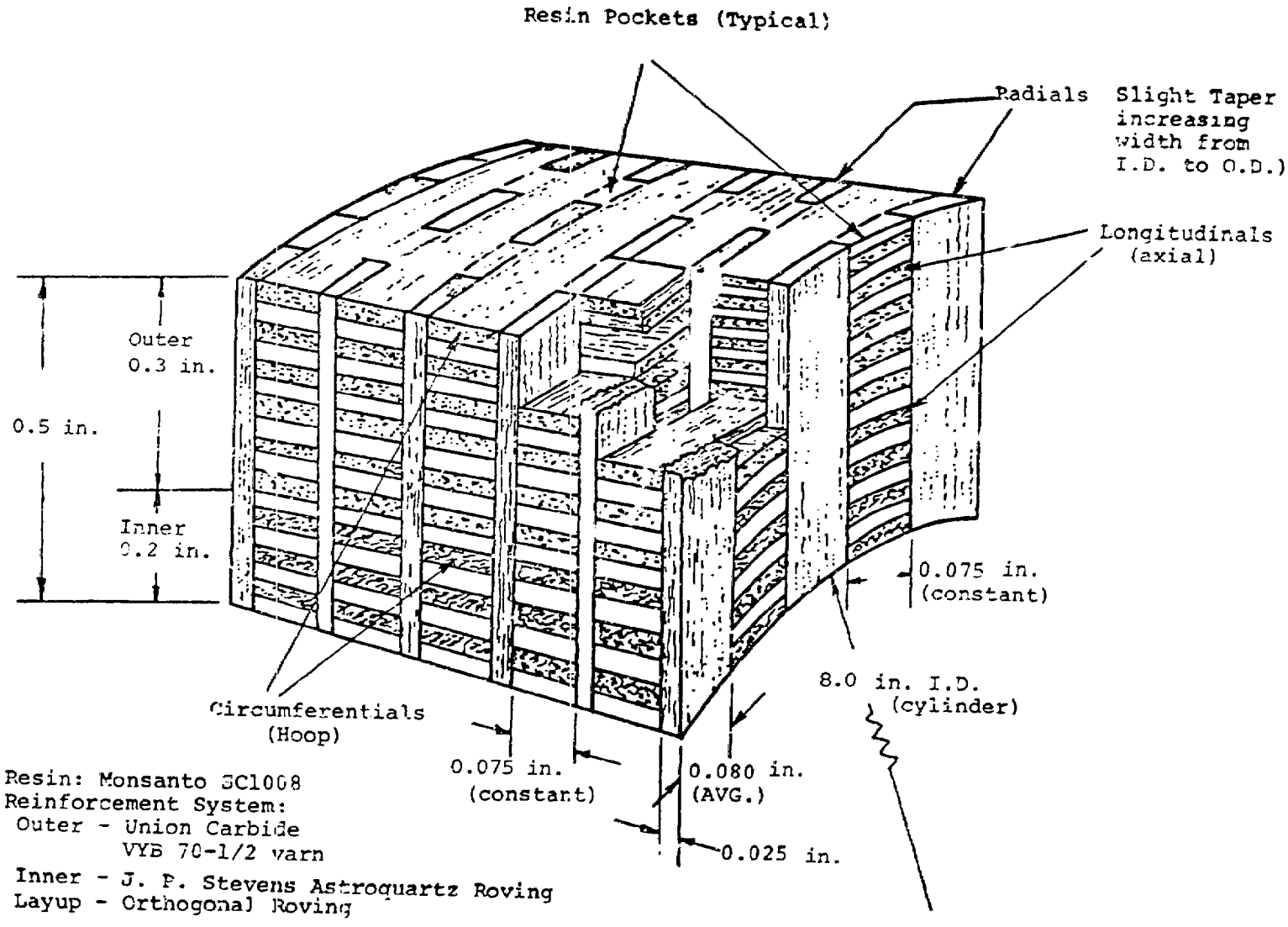

Figure 3. AVCO Two-Phase, 3D, Orthogonal, Carbon/Quartz-Phenolic - Material #15

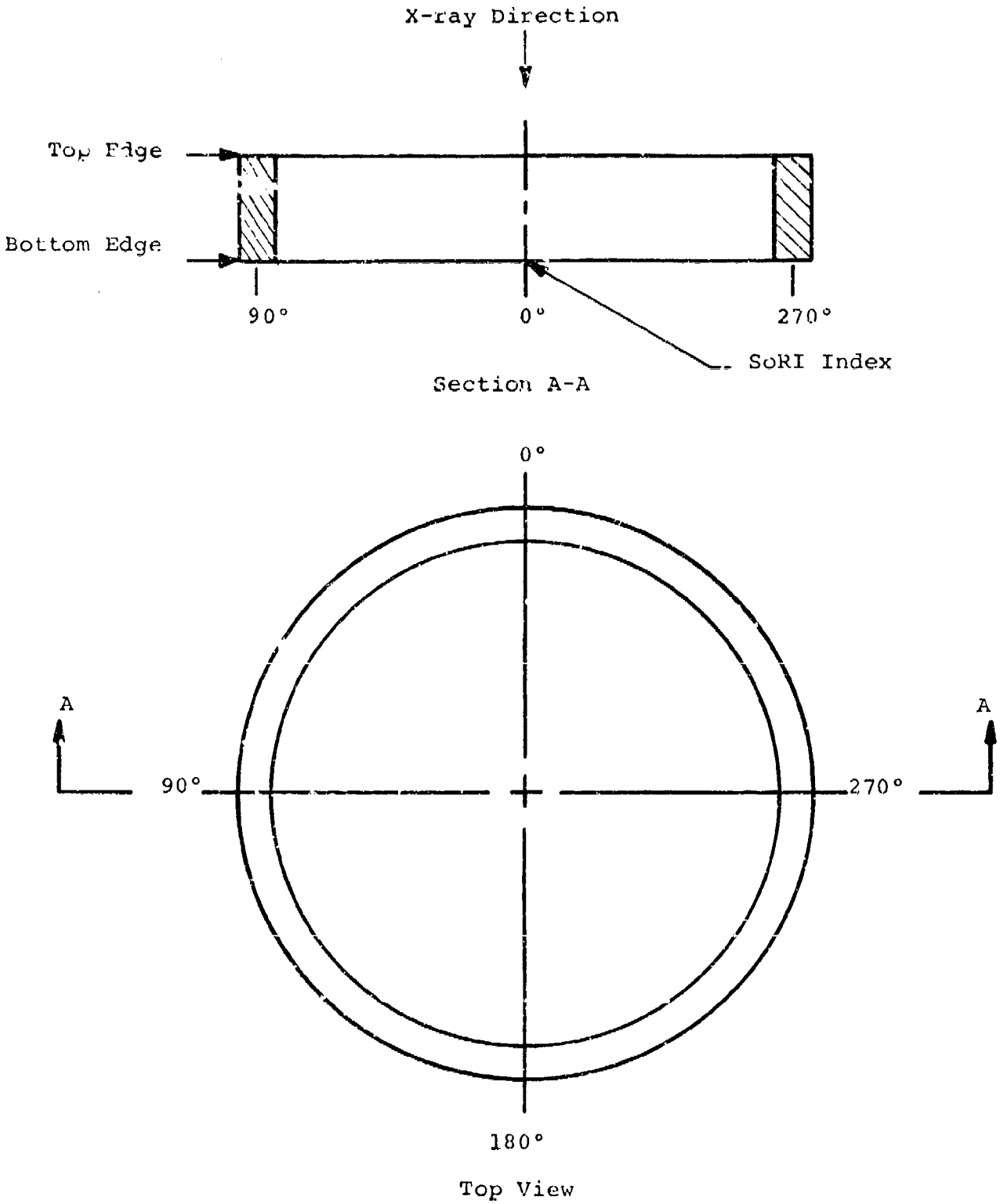

Figure 4. SoRI Indexing and Orientation System for Rings

Rear Delam

Bulk Delam

Mid Delam

Rear Lift

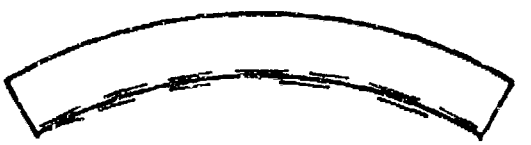

Front Face Crack

Front Radial Recession
(Bulk Expansion of Laterals
Toward Front Face)

Rear Radial Recession
(Bulk Expansion of Laterals
Toward Rear Face)

Front Yarn Lift — Raised or Missing Yarn From Front Face

Rear Yarn Lift — Raised or Missing Yarn From Rear Face

Front Crush

Matrix Spall

Figure 5. Definition of Structure-Change Terms

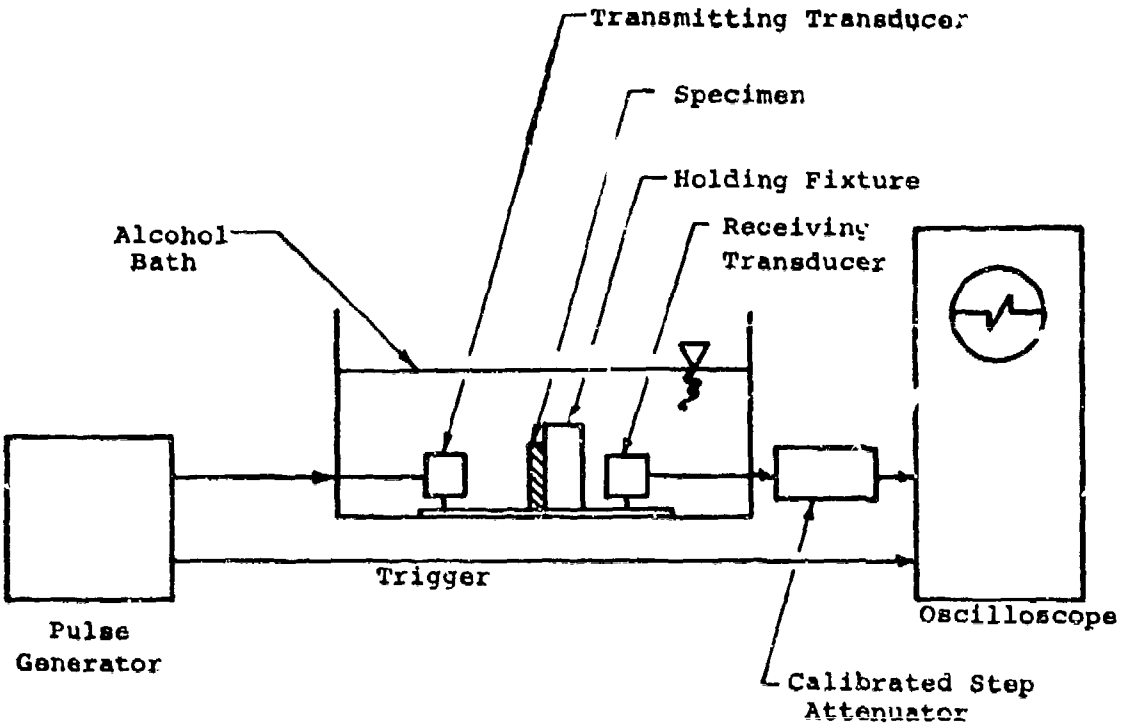

Figure 6. Ultrasonic Attenuation Setup Using the Pulsed Through-Transmission Technique

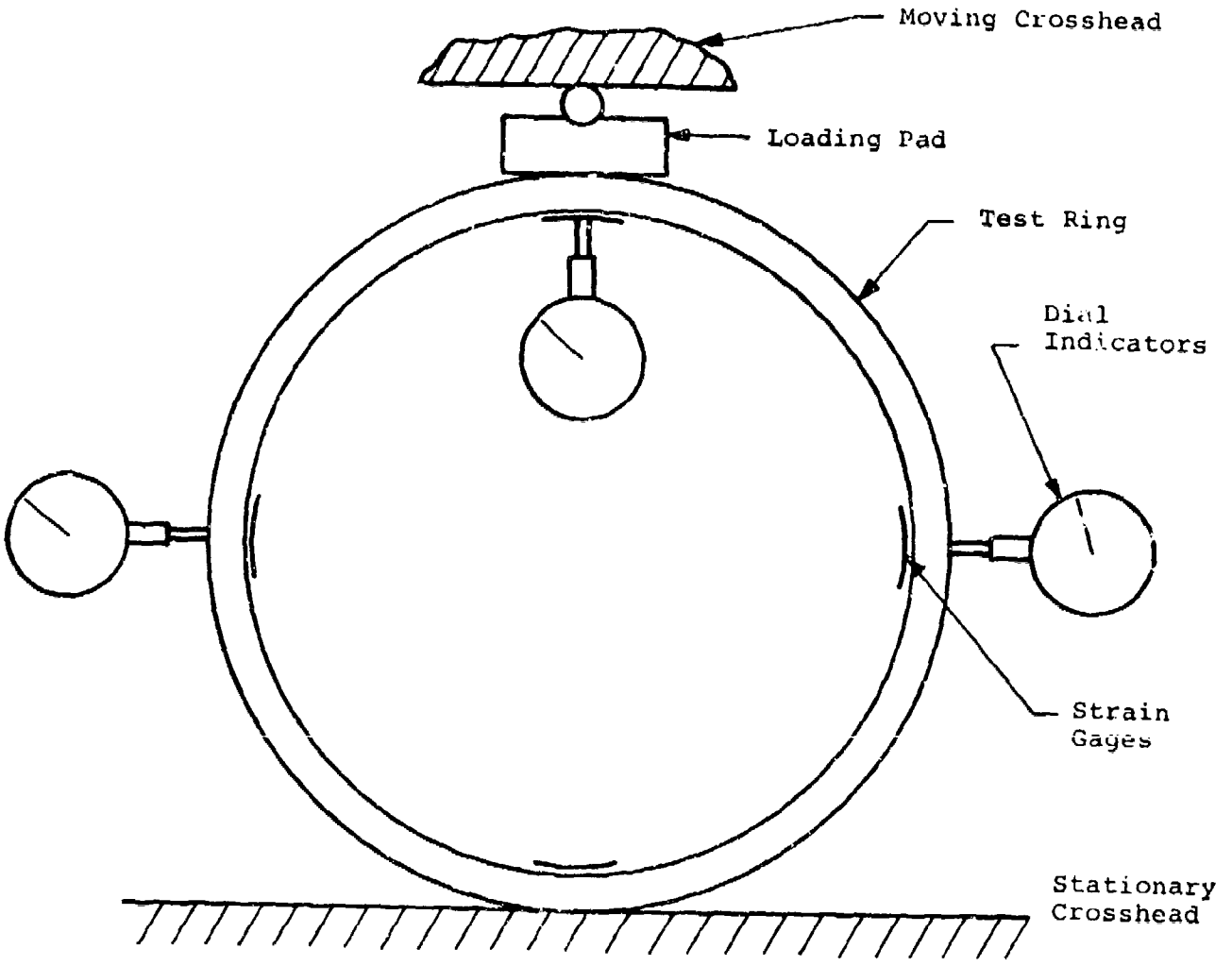

Figure 7. Schematic of Ring Flexure Setup Used For Modulus of Elasticity in Flexure (MOE) Evaluations

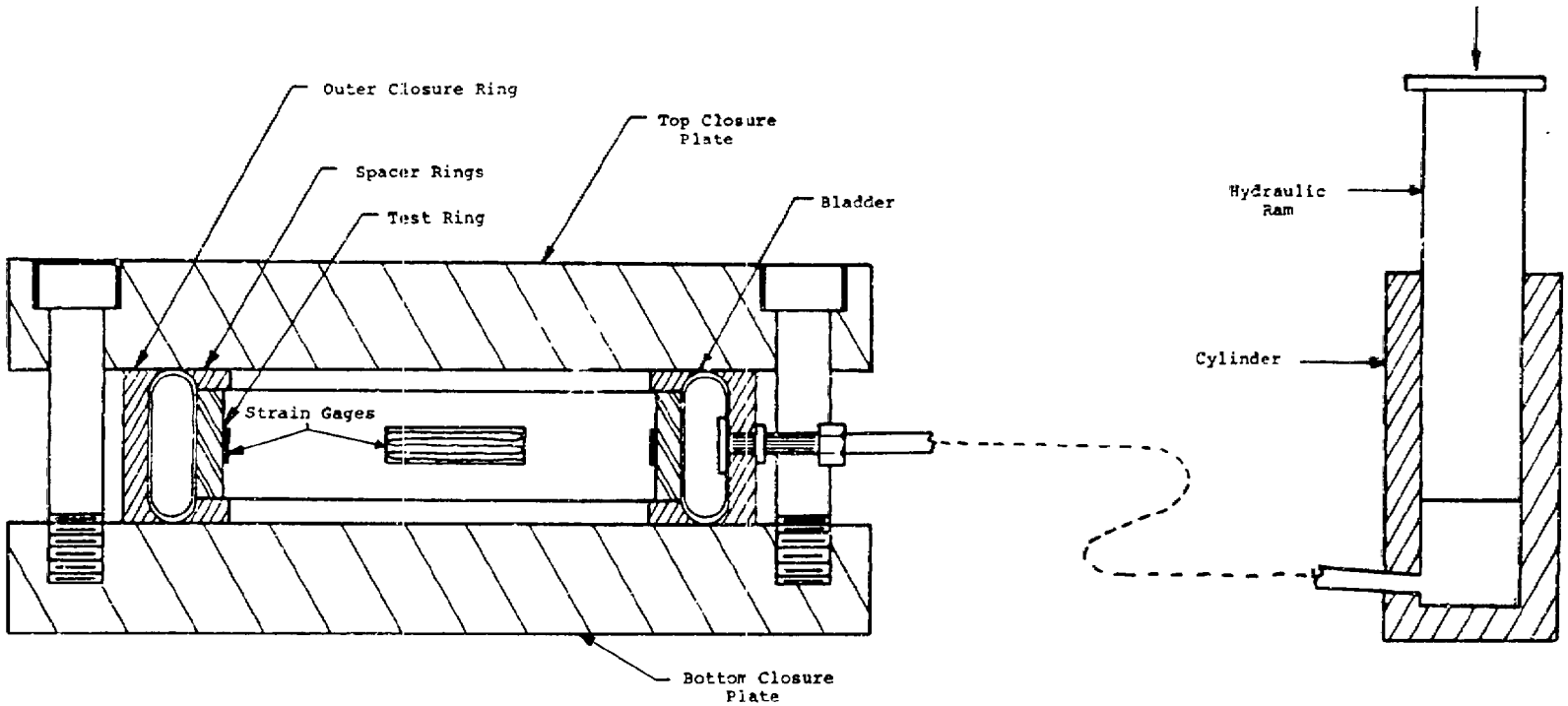

Figure 8. Schematic of Hydrostatic Ring Evaluation Setup Used for Compressive Modulus Evaluation

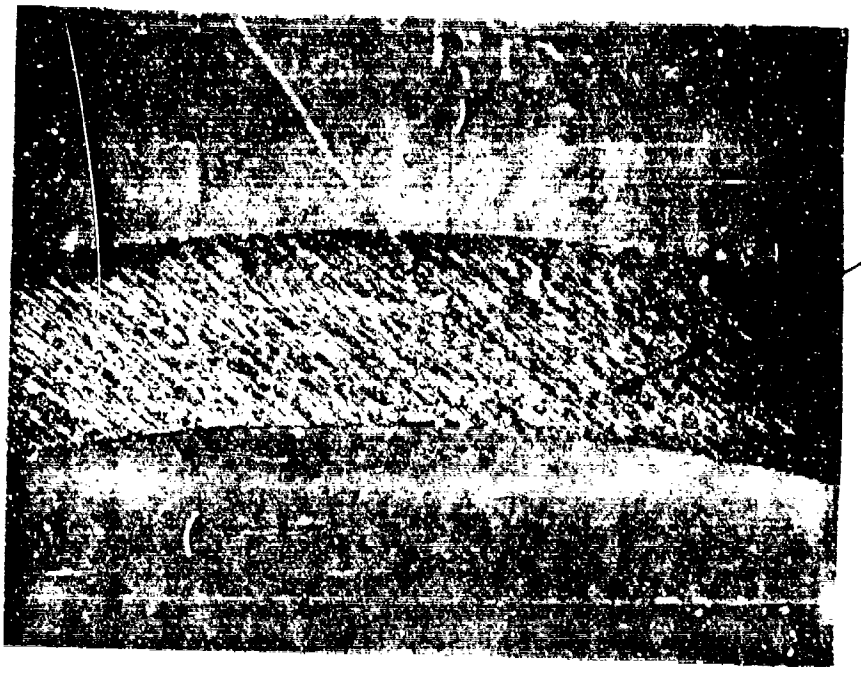

a. Axial View of Edge
(2.7X)

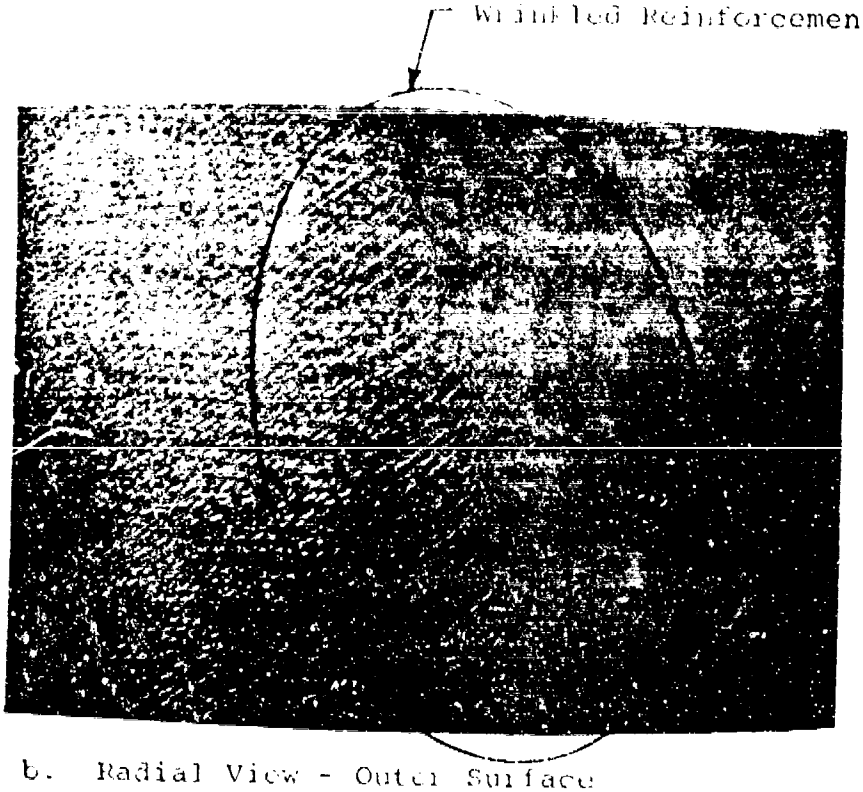

b. Radial View - Outer Surface
(1.5X)

Figure 9. Photographs Showing Typical AVCO R6300

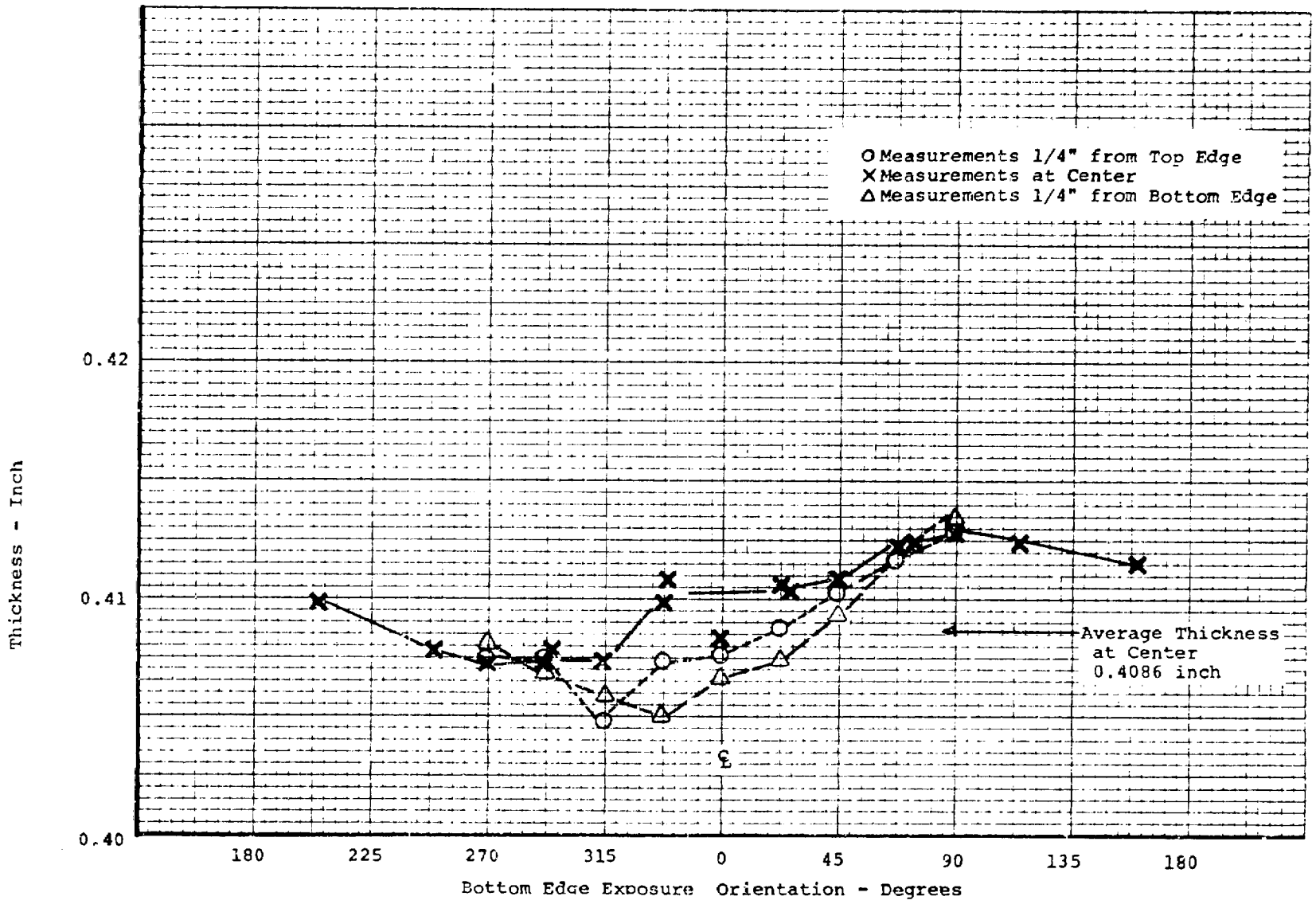

Figure 10. Thickness Variation for Ring 83301-305-1 from AVCO R6300

General Notes

1. ⬡ Radial Velocity in in./μsec
   (Relative Radial Transmission in added-dB)-Higher readings correlate lower attenuative material
2. + Axial Velocity in in./μsec
3. Visual and penetrant inspection revealed no flaws
4. Radiography revealed uniform material with no single flaws
5. Density = 1.340 gm/cm³

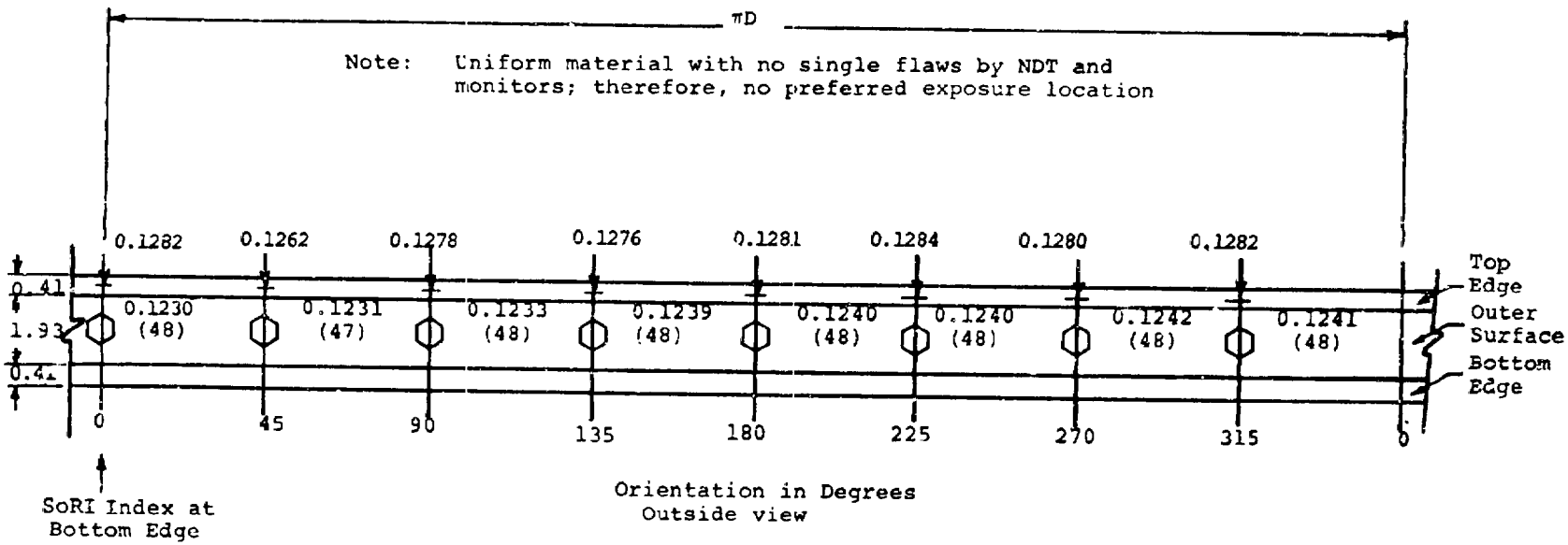

Figure 11. Sketch Showing Inspection Results on Ring 83301-400 from AVCO R6300

General Notes

1. ⬡ Radial Velocity in in./μsec
   (Relative Radial Transmission in added dB)-Higher readings correlate lower attenuative material
2. ↓ Axial Velocity in in./μsec
3. Visual and penetrant inspection revealed no flaws
4. Radiography revealed uniform material with no single flaws
5. Density - 1.339 gm/cm³

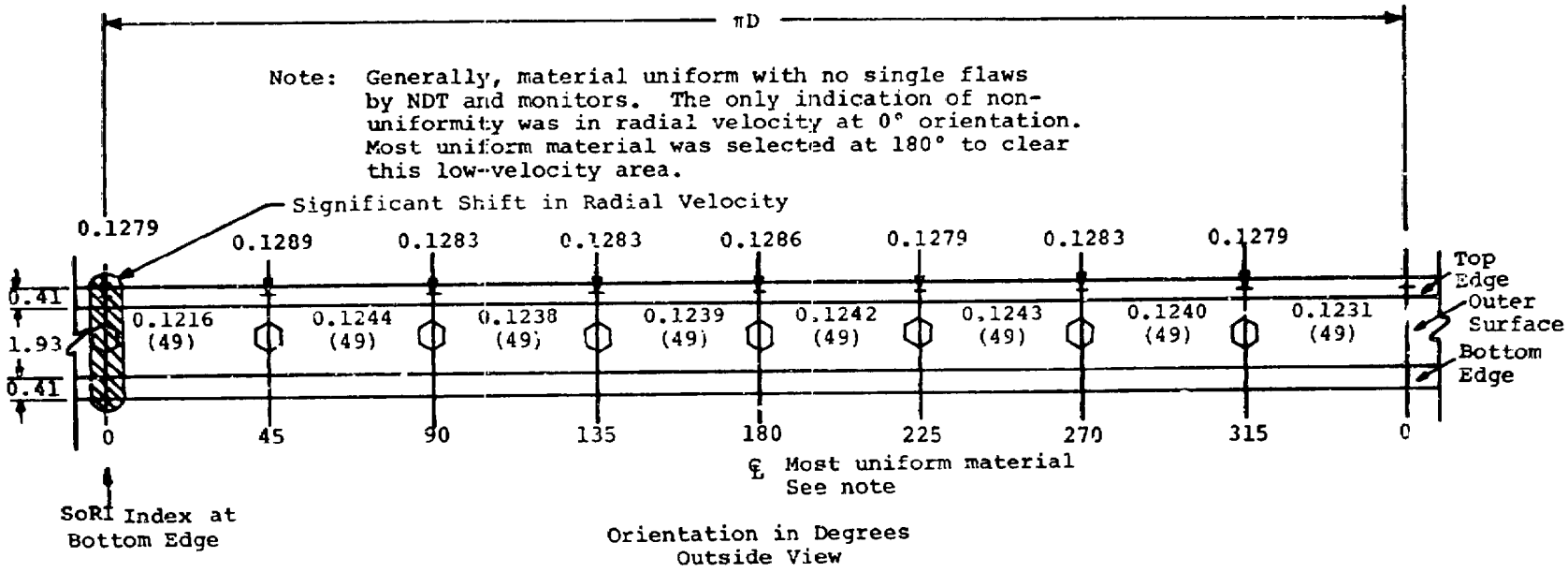

Figure 12. Sketch Showing Inspection Results on Ring 83301-305-4 from AVCO R6300

Notes

1. ⬡ Radial velocity in in./μsec
   (Relative radial transmission in added dB) - First Run
   (Relative radial transmission in added dB) - Second Run
   } Higher attenuation readings correlate lower attenuative material
2. ↓ Axial velocity in in./μsec
3. Visual inspection results - no single flaws
4. Penetrant inspection on edges using 2, 2, 4 - Trimethylpentane - no single flaws

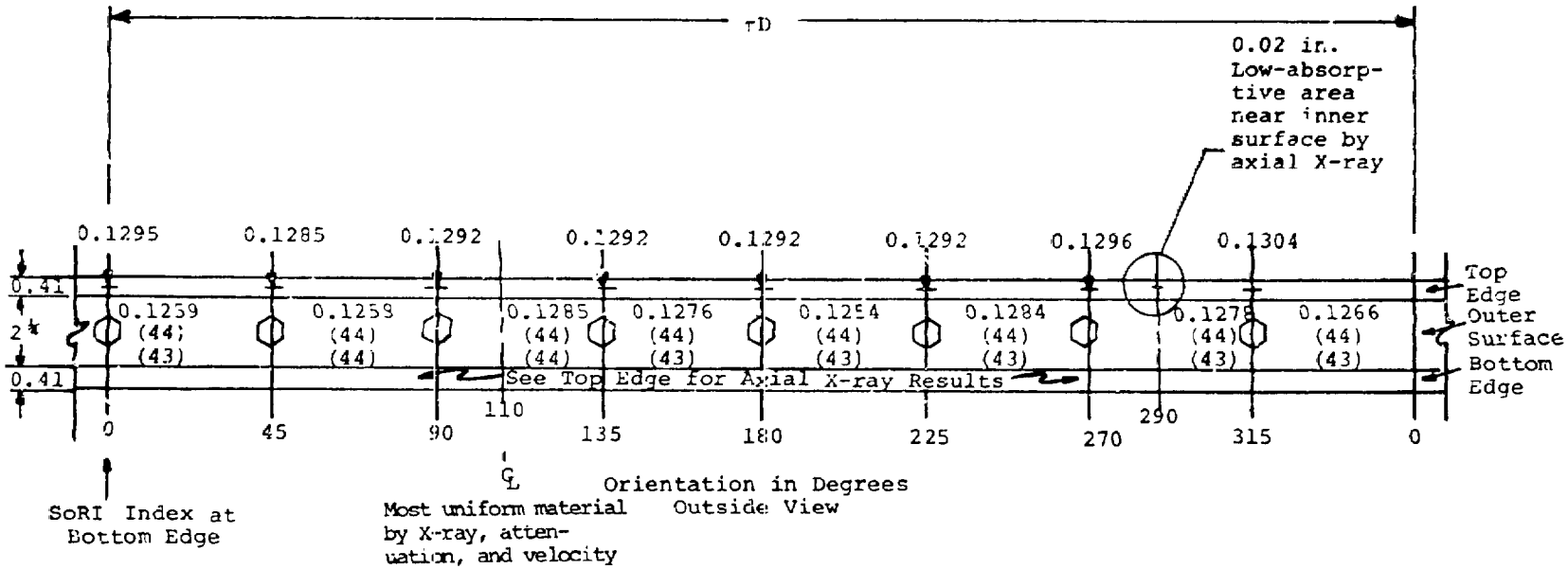

Figure 13. Sketch Showing Inspection Results on Ring 83301-305-1 from AVCO R6300

Note: Matrix eroded and/or melted 270-0-75°

Radial View of Outer Surface at 0°
(2X)

Figure 14. Photograph Showing Outer Surface of Exposed Ring 83301-305-1 from AVCO R6300

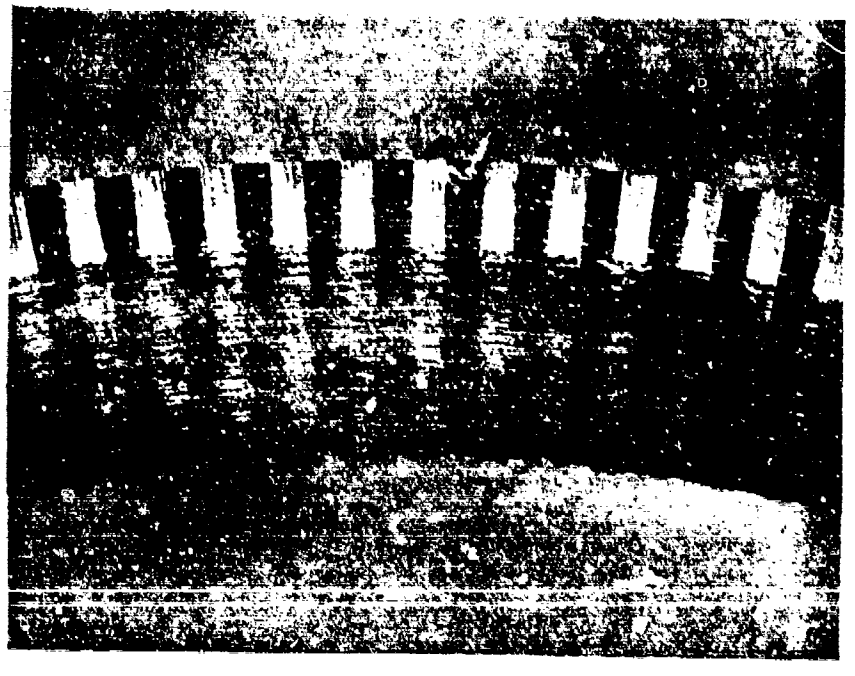

Edge View
(5X)

Note: Circumferentials straighter and residual porosity lower than previous AHP material

Figure 15. Photograph Showing Typical AVCO 3DCP for Rings 1, 2, 4, 8, 9, and 11

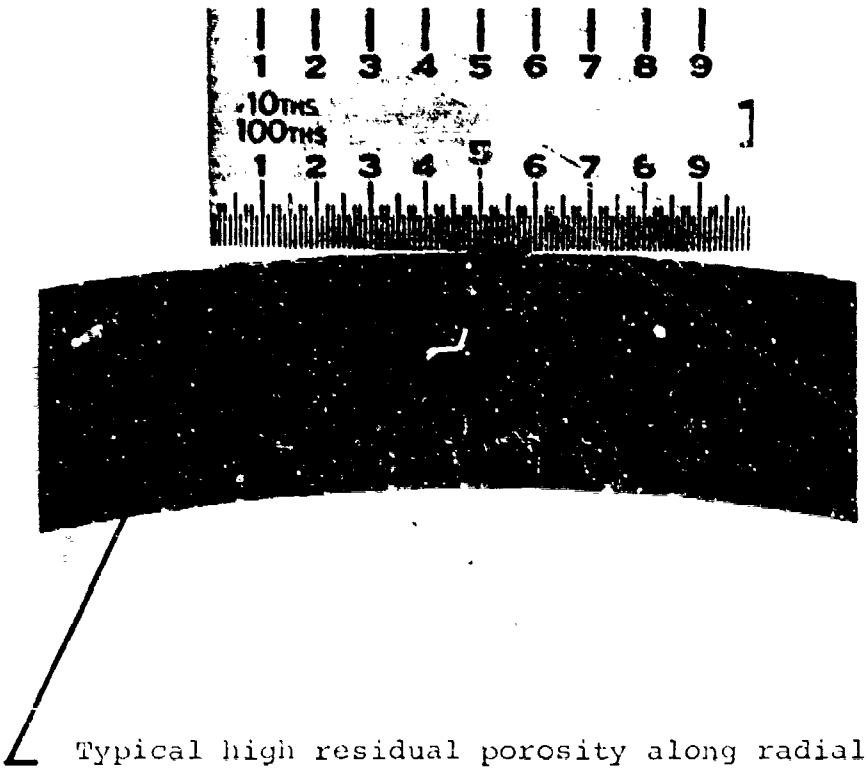

Typical high residual porosity along radials

Axial View - Edge
(3X)

Figure 16. Photograph Showing Typical AVCO 3DCP for Rings 83301-200, 83301-202A, 83301-305-2, and 83301-305-3

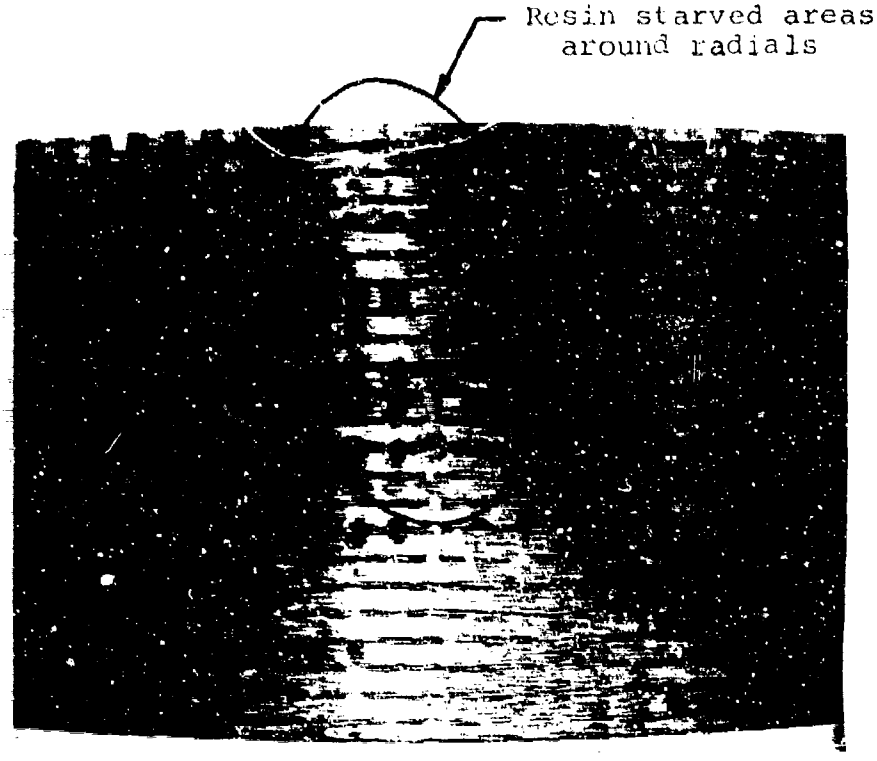

Radial View - Outer Surface
(1.5X)

Figure 17. Photograph Showing Visual Resin-Starved Areas Around Radials in Ring 2 from AVCO 3DCP

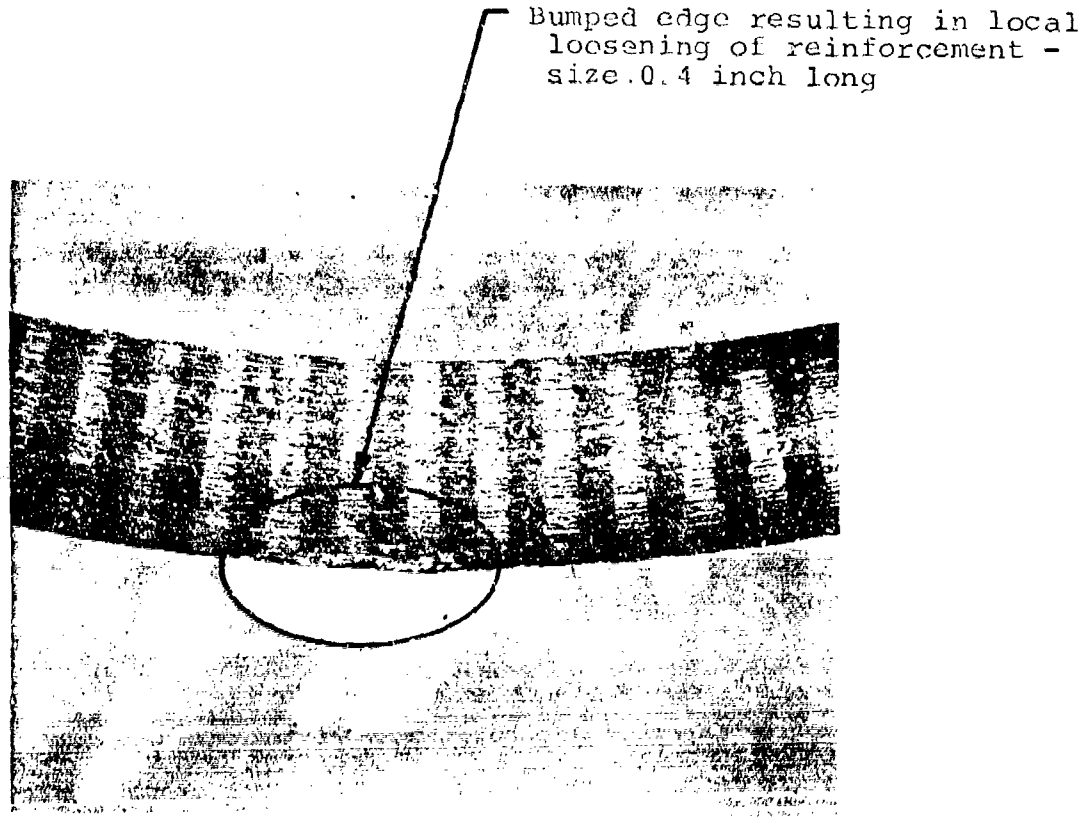

Axial View - Top Edge
(2.9X)

Figure 18. Photograph Showing Bumped Outer Edge on Ring 2 from AVCO 3DCP

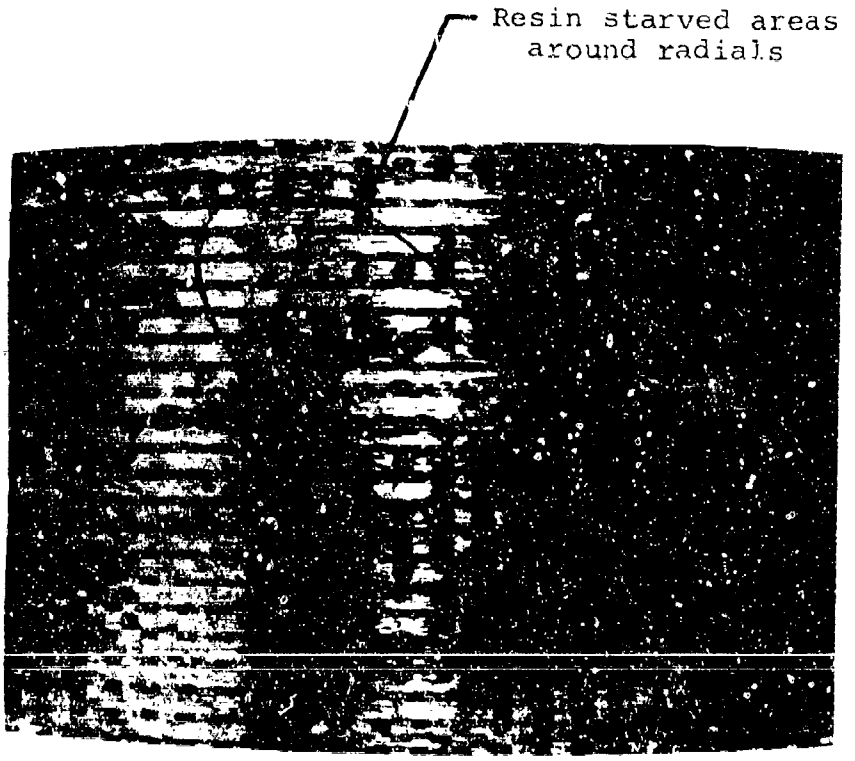

Radial View - Outer Surfac
(1.5X)

Figure 19. Photograph Showing Visual Resin-Starved Areas Around Radials in Ring 8 from AVCO 3DCP

General Notes

1. ⬡ Radial Velocity in in./μsec
   (Average for two runs-relative radial transmission in added-dB)-Higher readings correlate lower material attenuation)
2. ↓ Axial velocity in in./μsec
3. Visual and penetrant (2, 2, 4-Trimethylpentane) revealed no single flaws
4. Radiography was not revealing of any single flaws
5. Density = 1.406 gm/cm^3
6. Most uniform material ℄ - Any orientation--note lowest radial transmission orientation

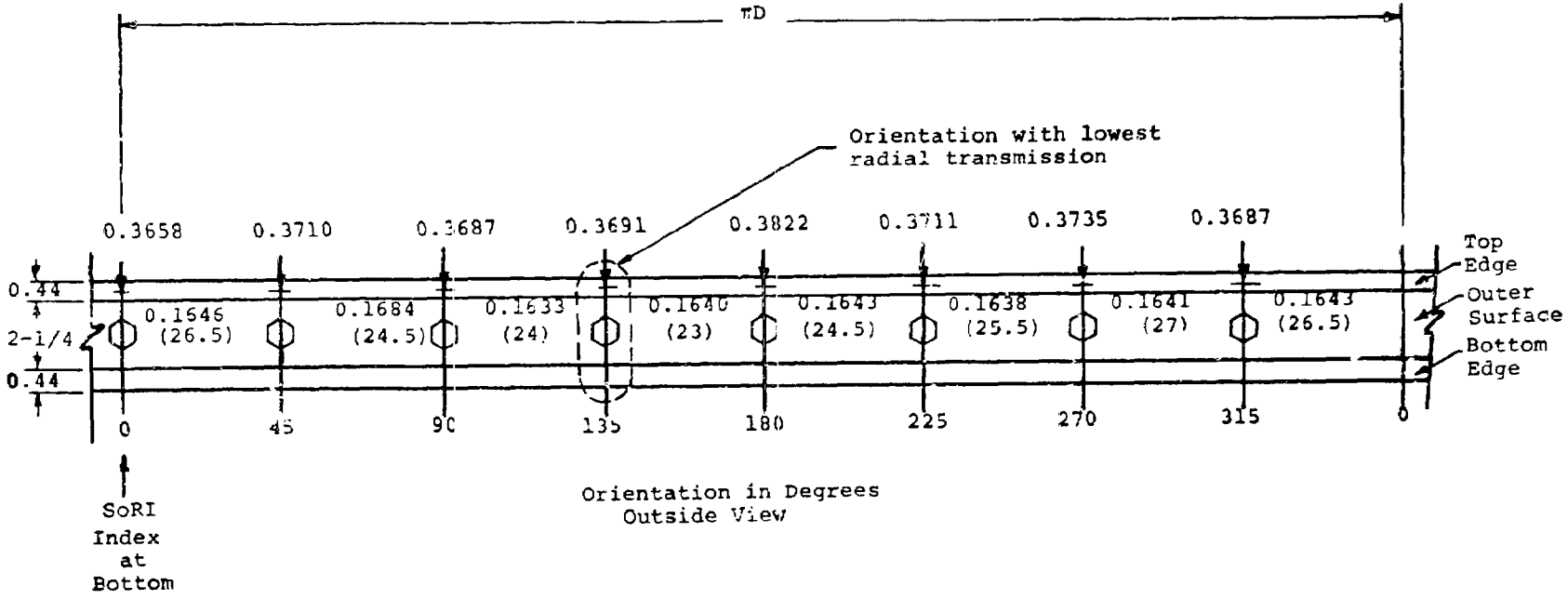

Figure 20. Sketch Showing Inspection Results on Ring 1 from AVCO 3DCP

General Notes:

1. ⬡ Radial Velocity in in./μsec
   (Average for two runs-Relative Radial transmission in added-dB)-Higher readings correlate lower material attenuation.
2. ↓ Axial Velocity in in./μsec
3. Penetrant (2,2,4- Trimethylpentane) not revealing
4. Density = 1.415 gm/cm³
5. Most uniform material ℄ at 270°

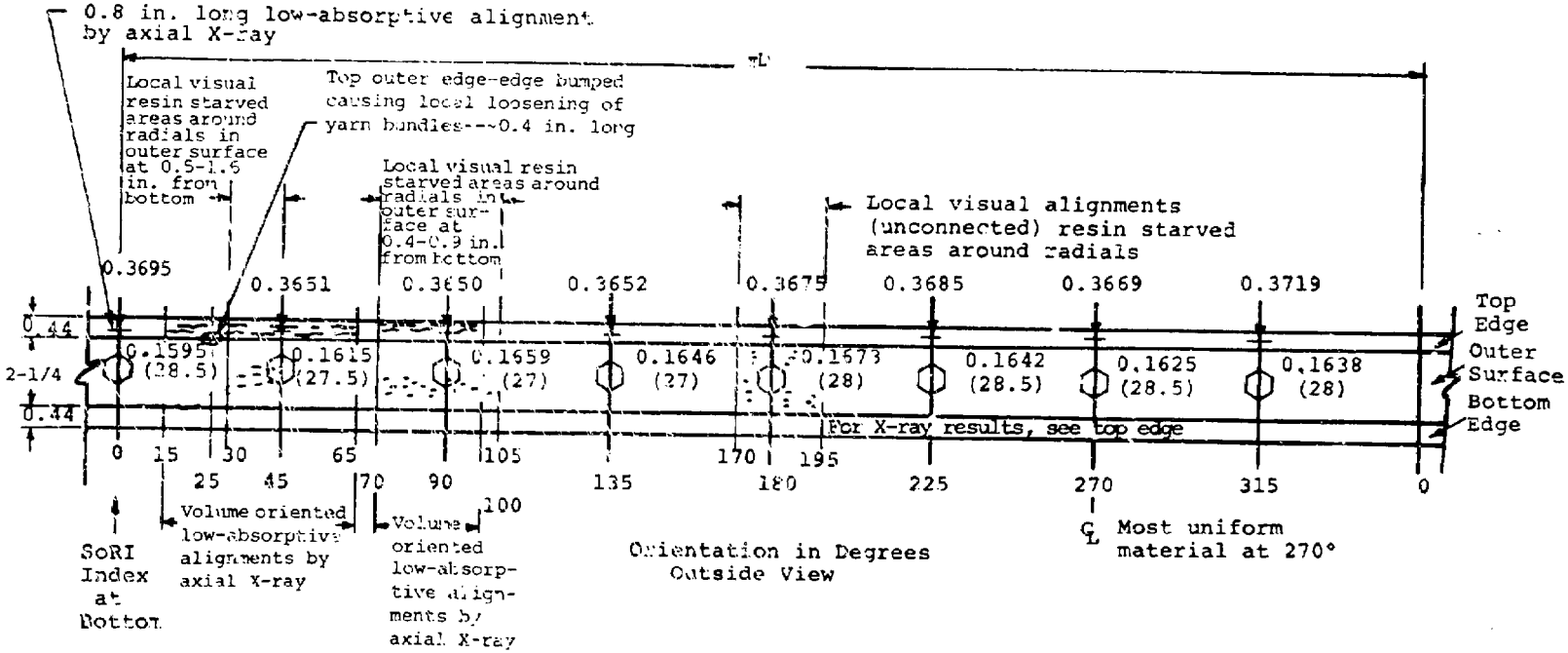

Figure 21. Sketch Showing Inspection Results on Ring 2 from AVCO 3DCP

General Notes

1. ⬡ Radial Velocity in in./usec
(Average relative radial transmission in added-dB)-Higher readings correlate lower material attenuation
2. ↓ Axial Velocity in in./μsec
3. Visual and penetrant inspection revealed no single flaws
4. Radiography revealed no single flaws
5. Density = 1.316 gm/cm³

} see Background note

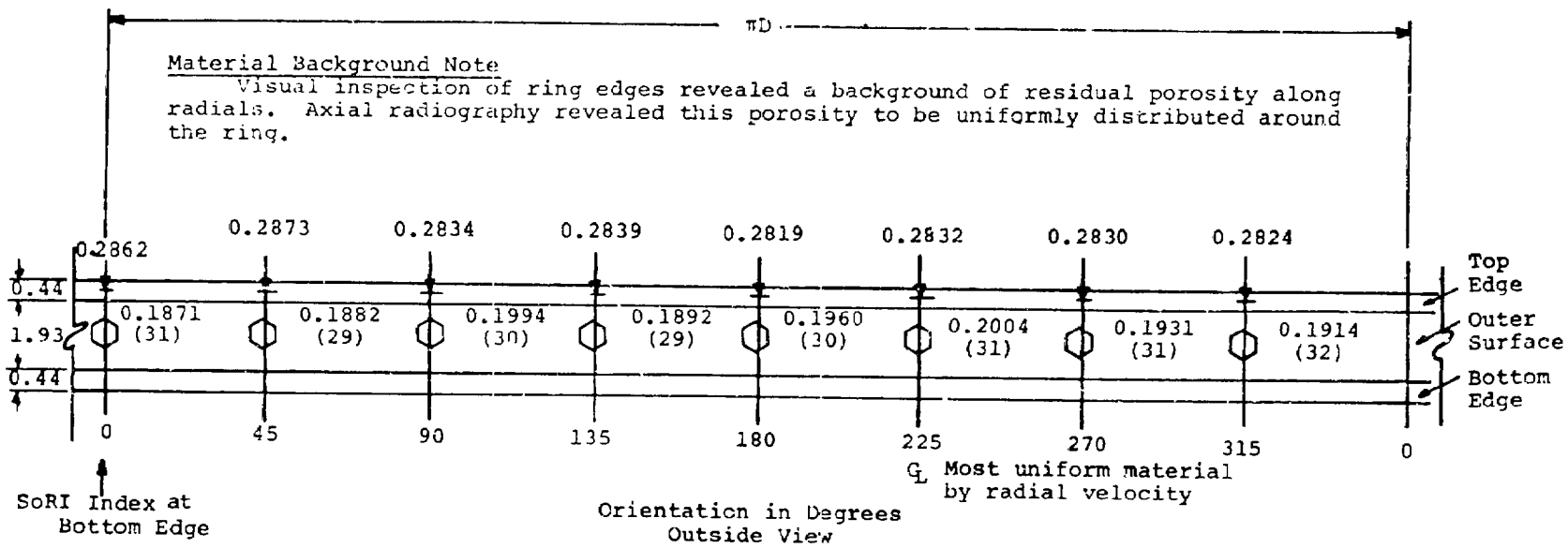

Figure 22. Sketch Showing Inspection Results on Ring 83301-200 from AVCO 3DCP

General Notes

1. ⬡ Radial Velocity in in./μsec
   (Average relative radial transmission in added-dB)-Higher readings correlate lower material attenuation
2. ↓ Axial Velocity in in./μsec
3. Visual and Penetrant inspection revealed no single flaws
4. Radiography revealed no single flaws-most uniform material at 225° (first choice) and 90° (second choice)
5. Density = 1.317 gm/cm³

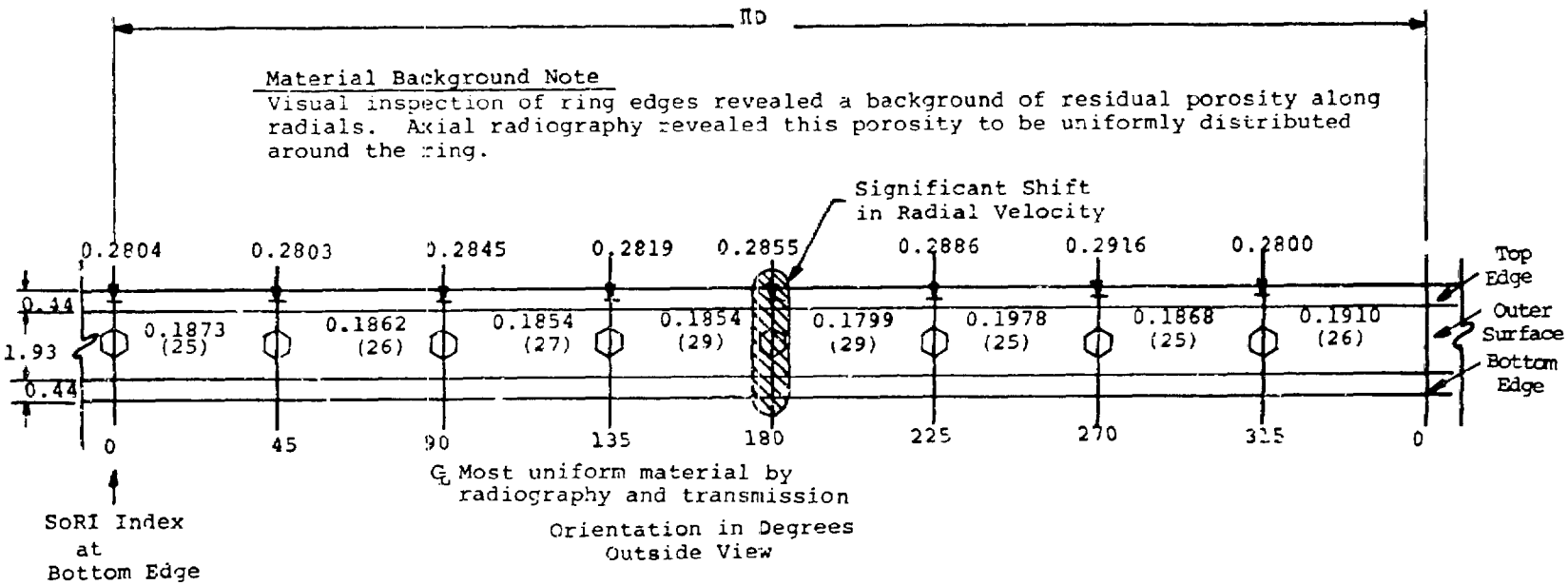

Figure 23. Sketch Showing Inspection Results on Ring 83301-202A from AVCO 3DCP

General Notes

1. ⬡ Radial Velocity in in./μsec
   (Average relative radial transmission in added-dB)-Higher readings correlate lower material attenuation
2. + Axial Velocity in in./μsec
3. Visual and penetrant inspection revealed no single flaws
4. Density = 1.316 gm/cm³

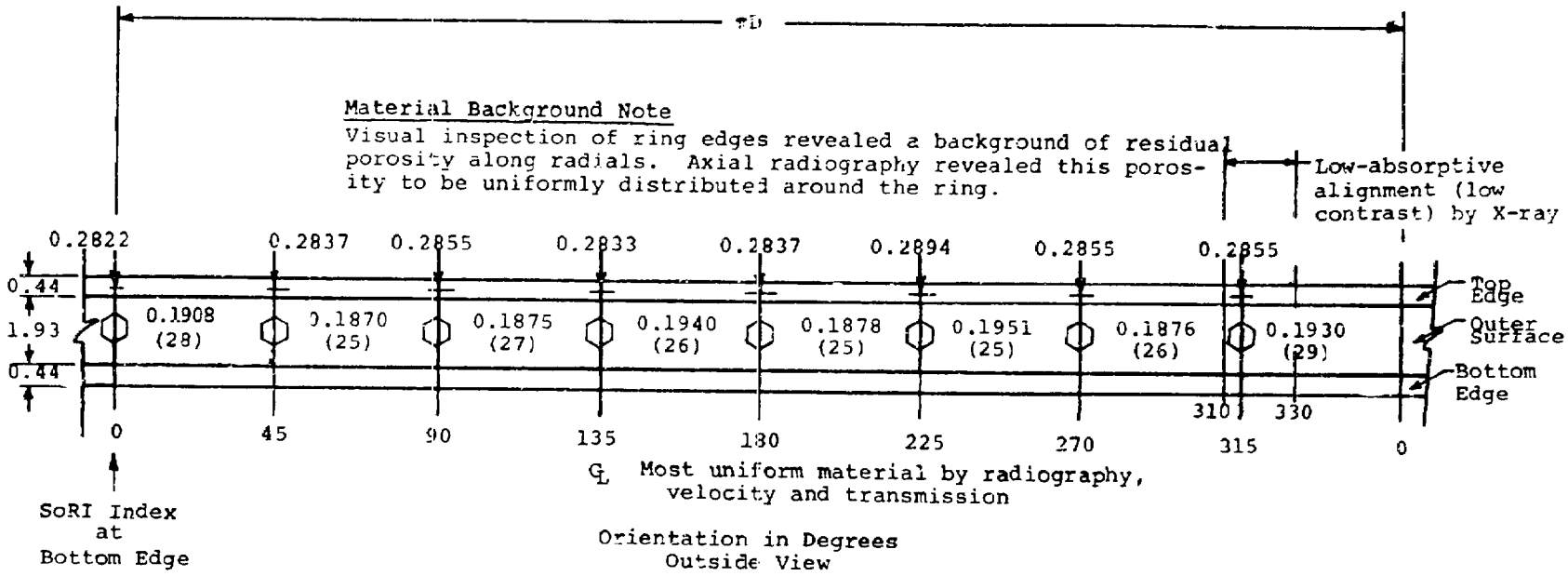

Figure 24. Sketch Showing Inspection Results on Ring 83301-305-2 from AVCO 3DCP

General Notes

1. ⬡ Radial Velocity in in./μsec
   (Average relative radial transmission in added-dB)-Higher readings correlate lower material attenuation
2. + Axial Velocity in in./μsec
3. Visual and penetrant inspection revealed no single flaws
4. Radiography revealed no single flaws - most uniform material at 90° and 180° orientation
5. Density = 1.321 gm/cm^3

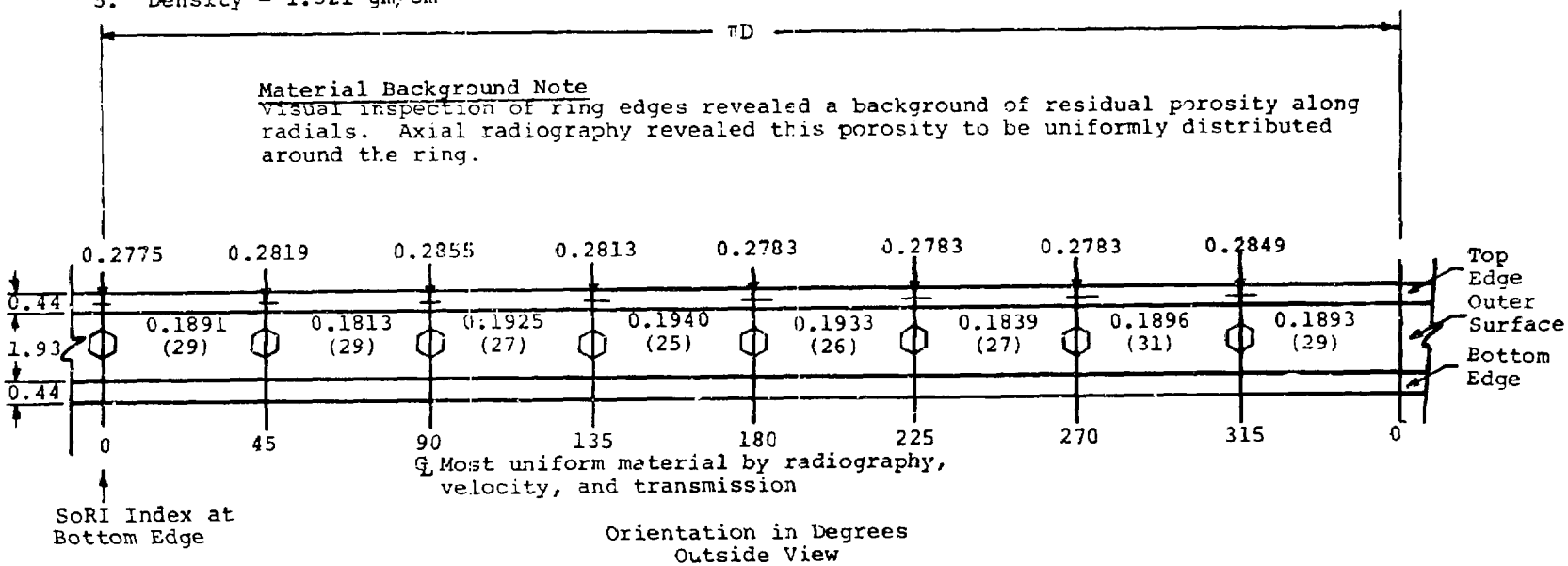

Figure 25. Sketch Showing Inspection Results on Ring 83301-305-3 from AVCO 3DCP

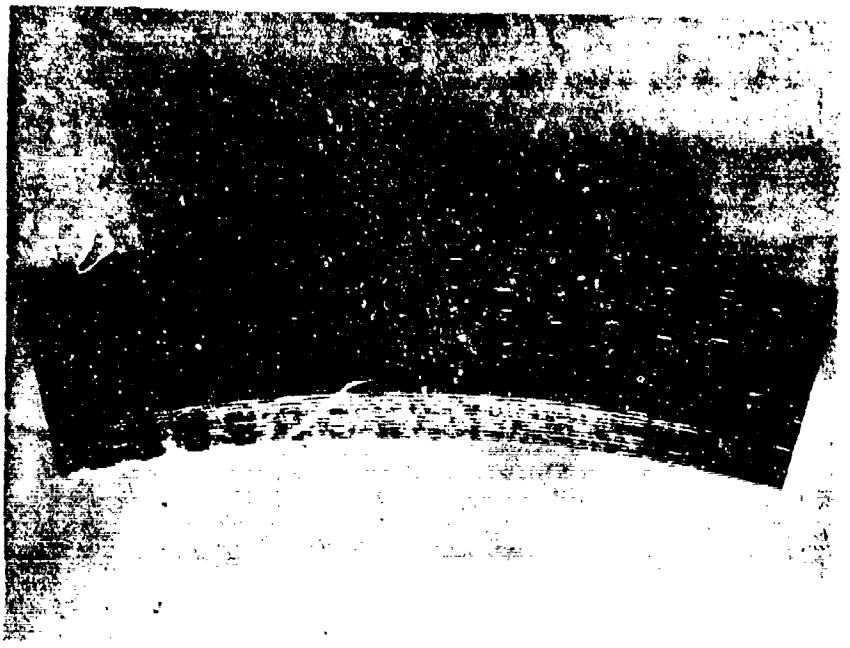

Note: Workmanlike material similar to AHP 3DC/QP except residual porosity and waviness in circs were less for this material

a. Axial View (2.1X)

Local area showing maximum porosity

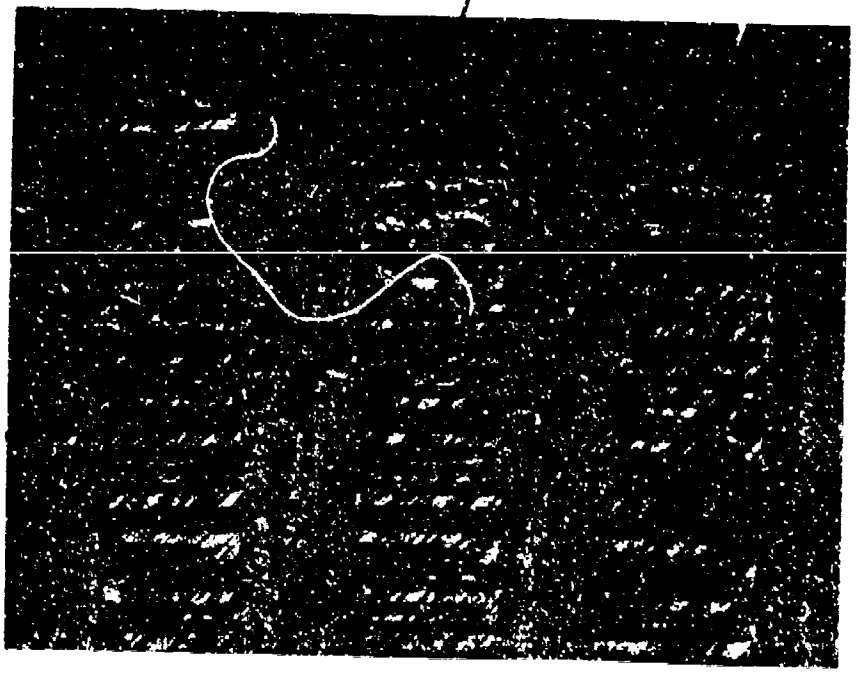

b. Axial View (10X)

Figure 26. Photograph Showing Typical AVCO 3DC/QP for Ring 3

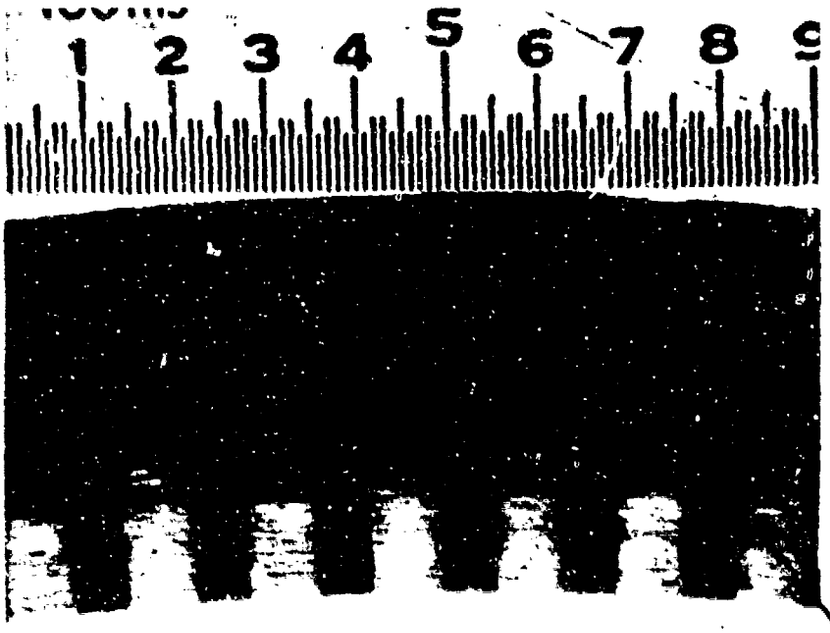

Axial View
(5X)

a.

Extremely high
residual porosity
along radials and
between axials

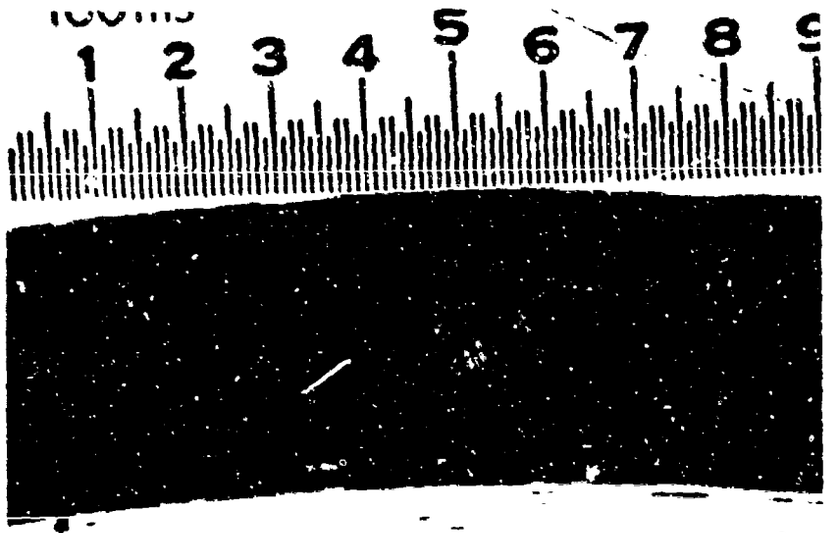

Axial View
(5X)

b.

Extremely high residual porosity
along radials and between axials

Figure 27. Photograph Showing Typical AVCO 3DC/QP in Rings 83301-202B and 83301-305-5

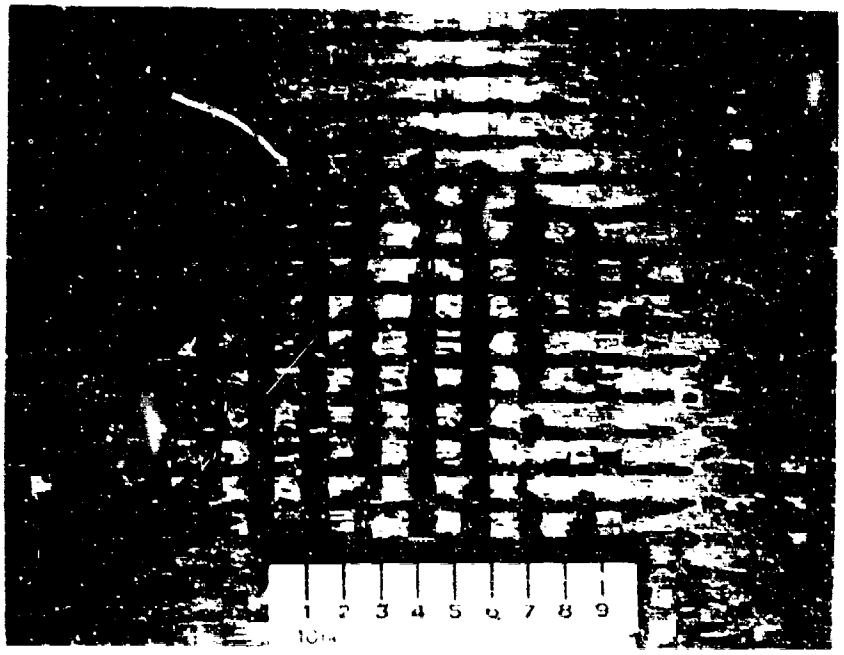

Note: Missing pieces of axials and circumferentials typical on outer and inner surfaces

c. Radial View - Outer Surface (2X)

Residual Porosity Between One Side of Radial and Axial-Typical for Inner Surface

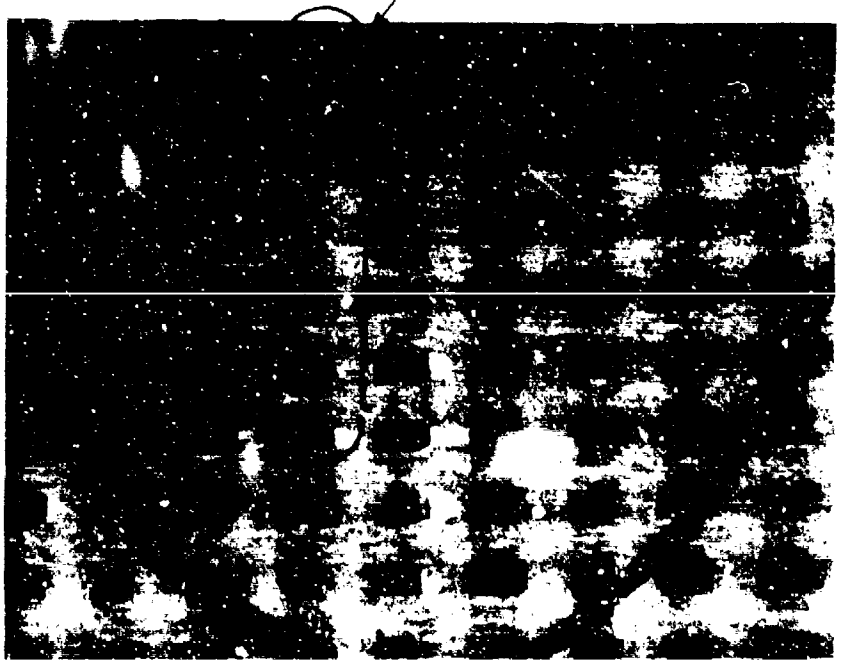

d. Radial View - Inner Surface (No Scale)

Figure 27 Continued.

General Notes

1. ⬡ Radial velocity in in./μsec
   (Relative radial transmission in added-dB)-Higher readings correlate lower material attenuation
2. ↓ Axial velocity in in./μsec
3. Visual and penetrant inspection revealed no single flaws
4. Radiography revealed uniform material with no single flaws
5. Density = 1.343 gm/cm³

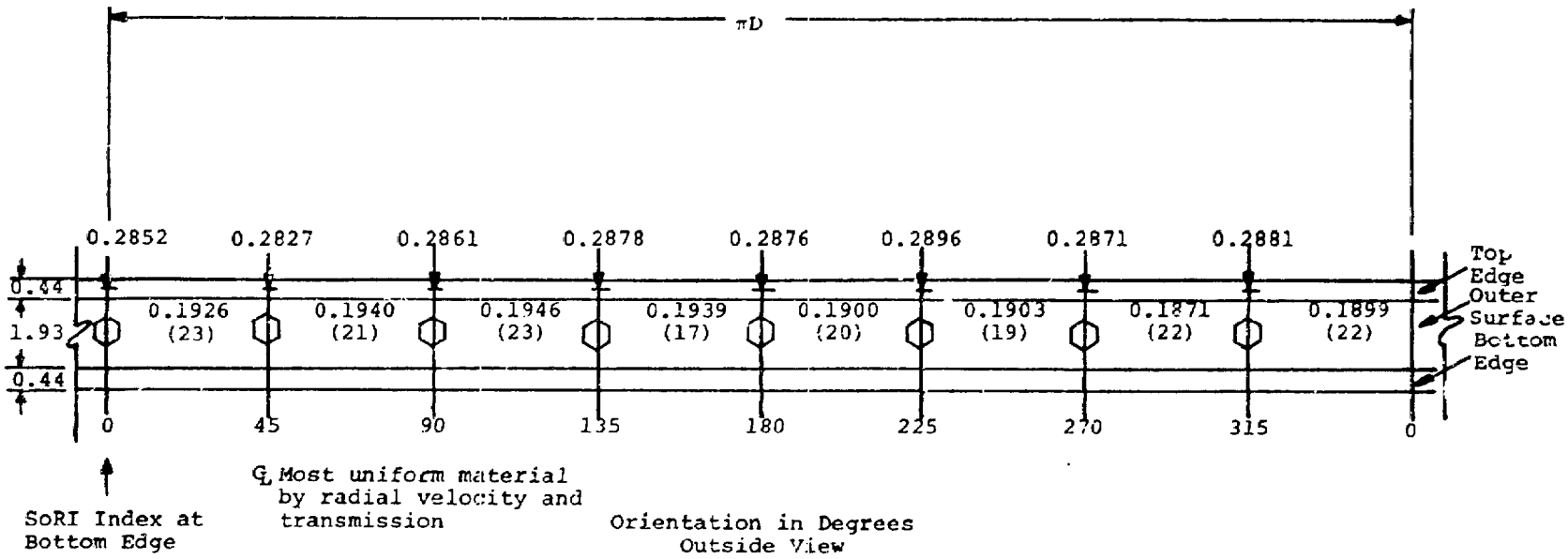

Figure 28. Sketch Showing Inspection Results on Ring 83301-202B from AVCO 3DCP/QP

General Notes

1. ⬡ Radial velocity in in./μsec
   (Relative radial transmission in added-dB)-Higher readings correlate lower material attenuation
2. ↓ Axial velocity in in./μsec
3. Visual and penetrant inspection revealed no single flaws
4. Radiography revealed uniform material with no single flaws
5. Density = 1.354 gm/cm³

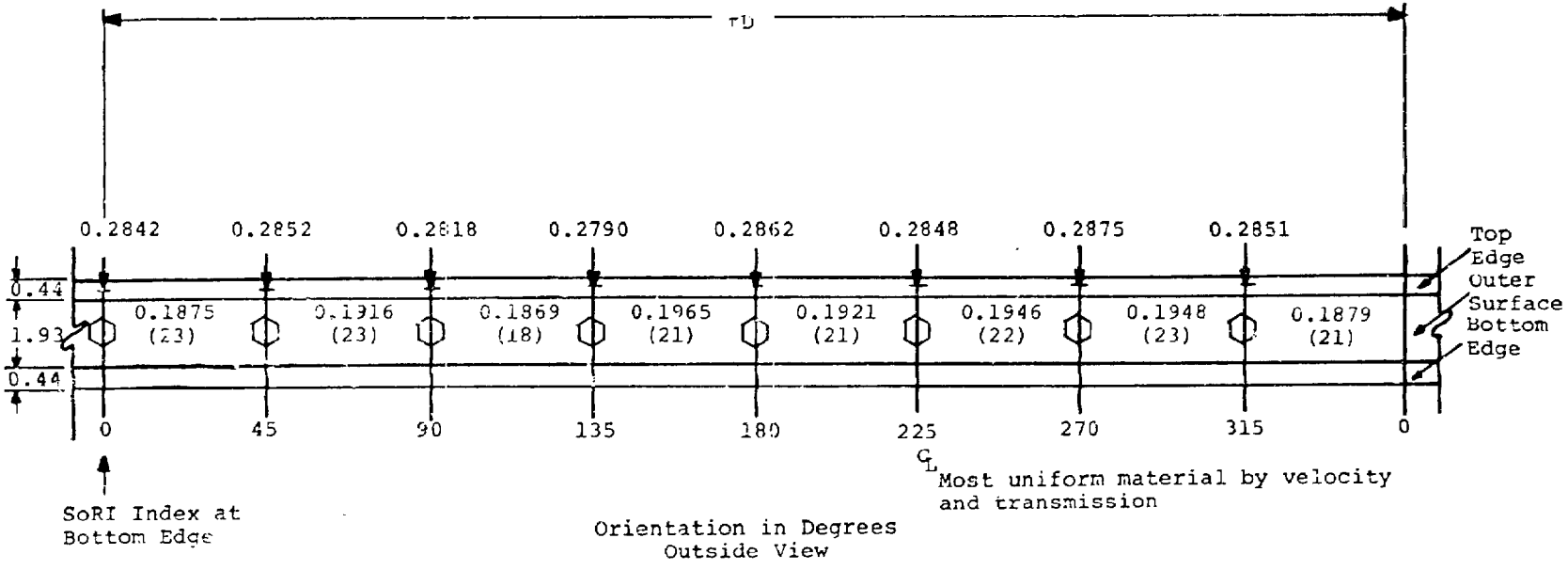

Figure 29. Sketch Showing Inspection Results on Ring 83301-305-5 from AVCO 3DCP/QP

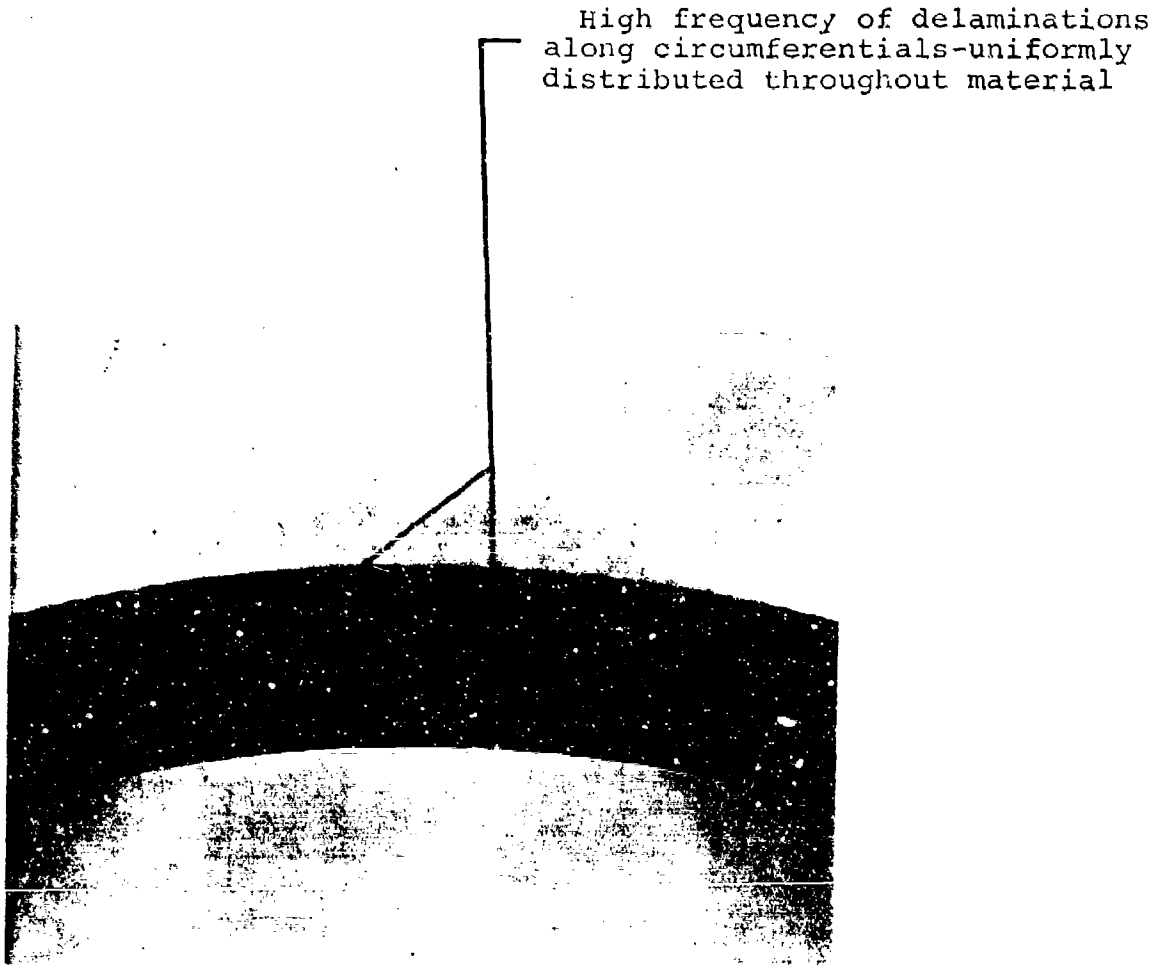

Figure 30. Photograph Showing Typical AVCO 3DCC

General Notes

1. ⬡ Radial Velocity in in./μsec
   (Radial ultrasonic transmission in added-dB)-First Run } Higher transmission readings correlate
   (Radial ultrasonic transmission in added-dB)-Second Run } lower attenuative material
2. ↓ Axial Velocity in in./μsec
3. Visual inspection results - no single flaws
4. Penetrant inspection on edges using 2,2,4 Trimethylpentane-no single flaws.
5. This material had a visual background delaminations extending across radials in the axial and circumferential directions. Occurrence was frequent
6. Bulk density = 1.638 gm/cm³

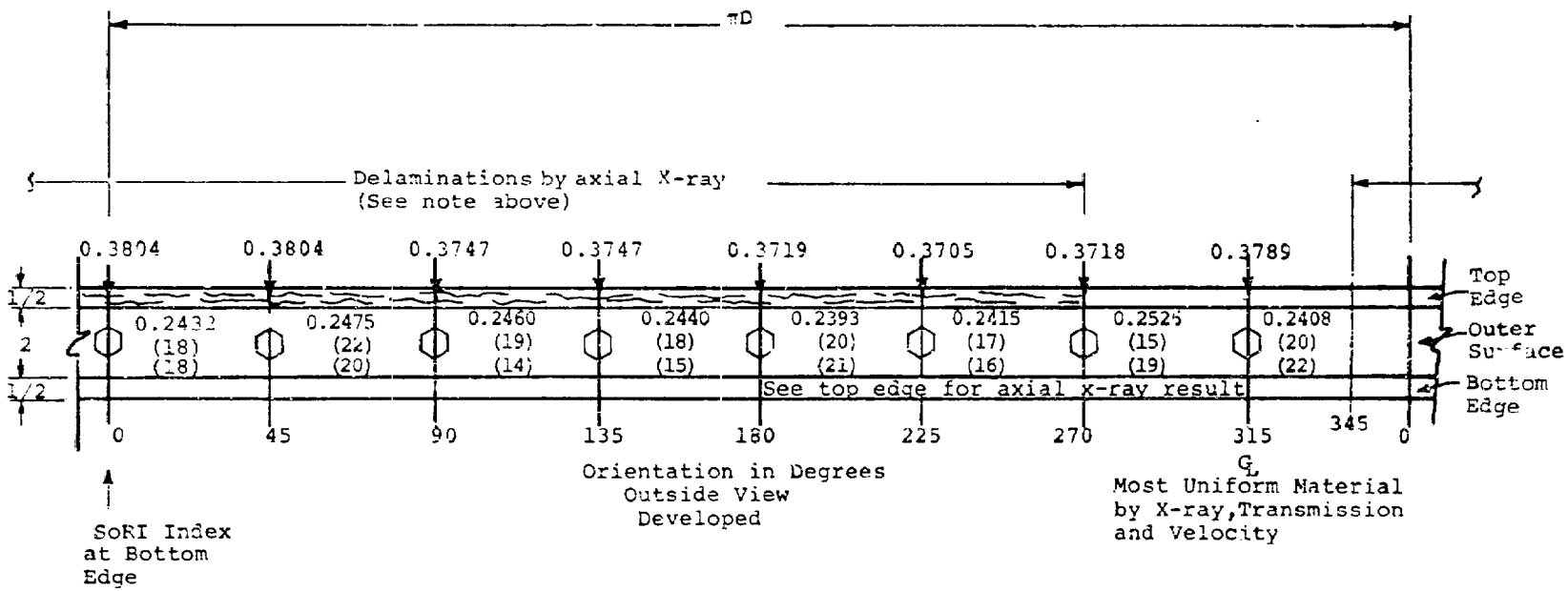

Figure 31. Sketch Showing Inspection Results on Ring 1109-35-2 from AVCO 3DCC

General Notes:

1. ⬡ Radial velocity in in./μsec
   (Radial Ultrasonic transmission in added-dB)-First Run } Higher transmission readings correlate
   (Radial Ultrasonic transmission in added-dB)-Second Run } lower attenuative material.
2. ↓ Axial velocity in in./μsec
3. Visual inspection results-no single flaws
4. Penetrant inspection on edges using 2,2,4 Trimethylpentane-no single flaws
5. This material had a high frequency of background circumferential delaminations extending across radials in the axial and circumferential directions by vision.
6. Bulk density = 1.645 gm/cm³

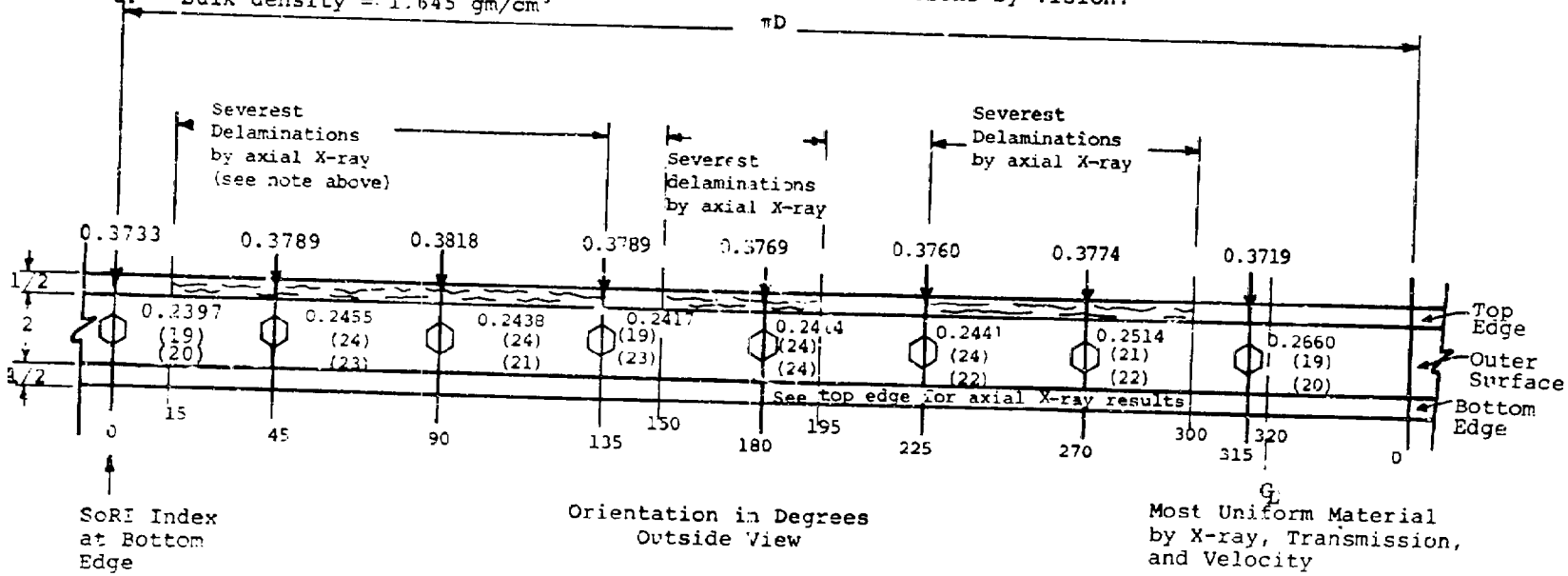

Figure 32. Sketch Showing Inspection Results on Ring 1109-35-3 from AVCO 3DCC

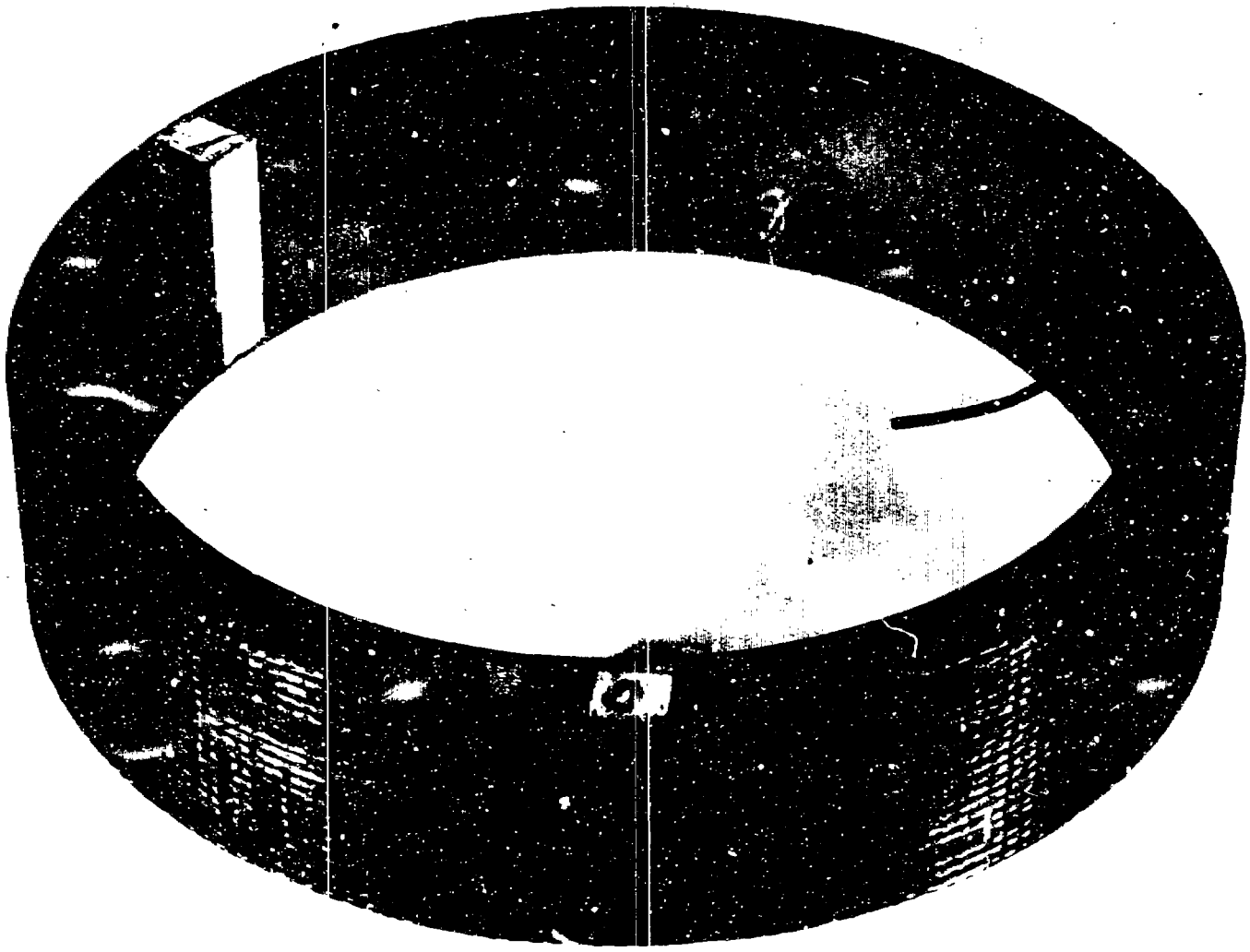

(No Scale)

a.

Figure 33. Photographs Showing As-Received Ring 1109-35-2 from AVCO 3DCC After Exposure

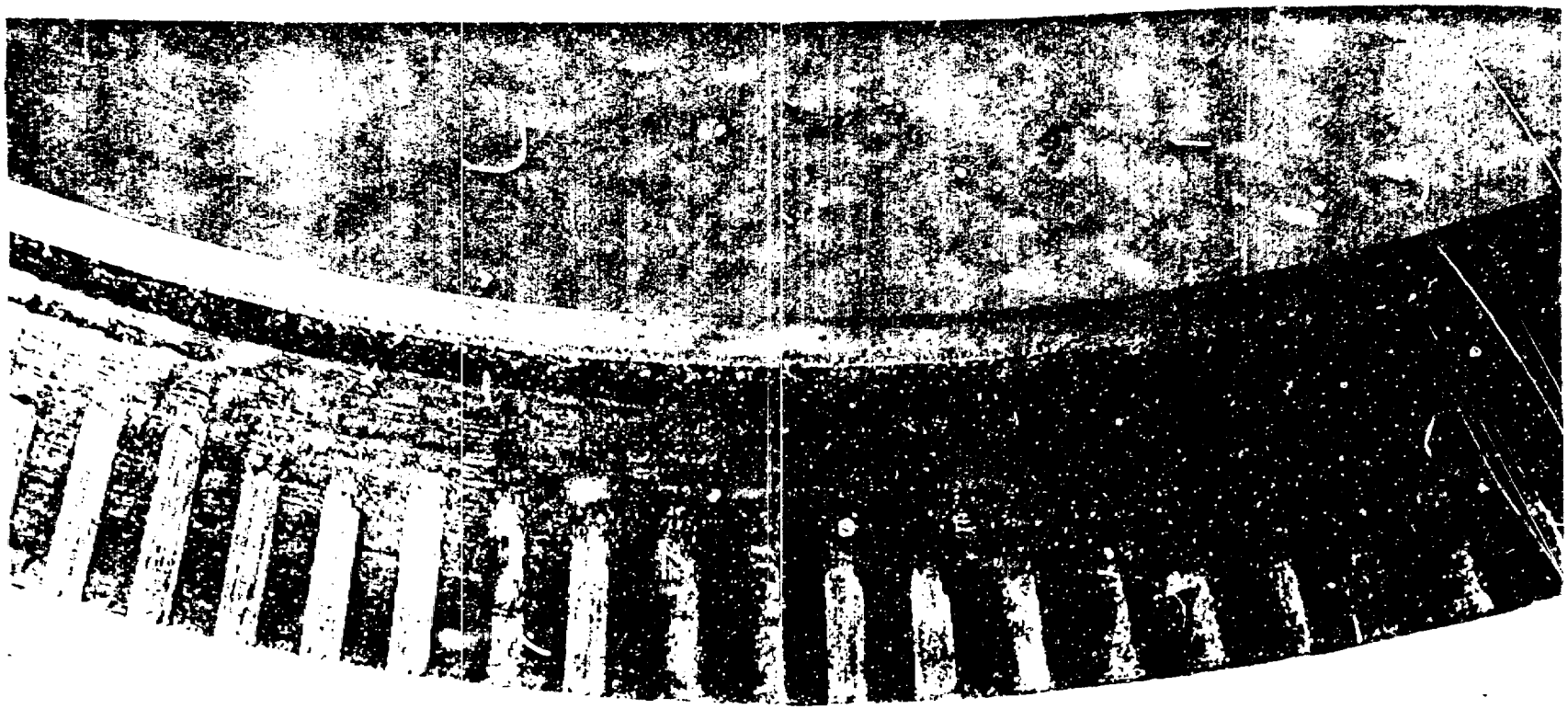

b. Axial View - Top Edge at 10°
(No Scale)

Figure 33 Continued.

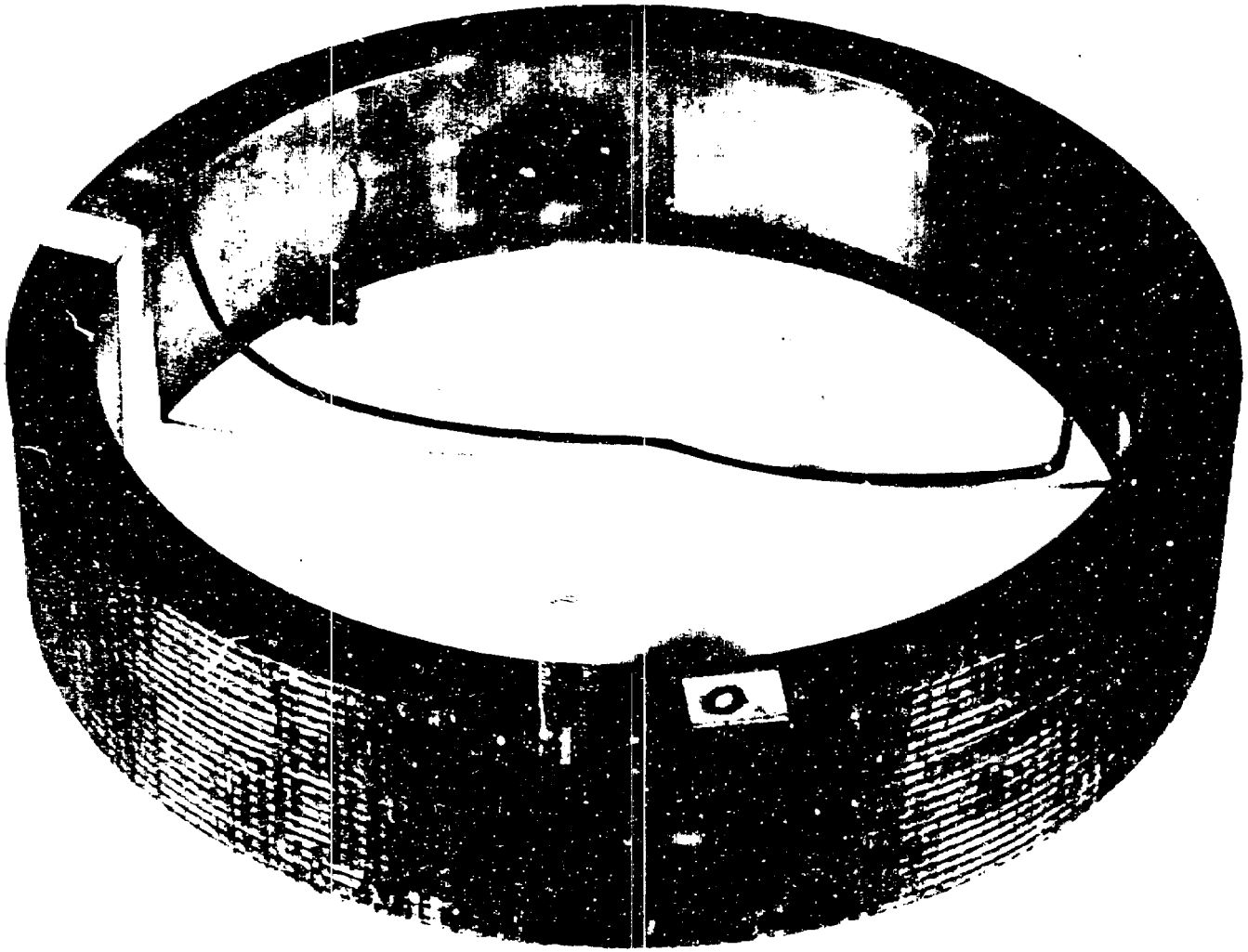

a. (No Scale)

Figure 34. Photographs Showing As-Received Ring 1109-35-3 from AVCO 3DCC After Exposure

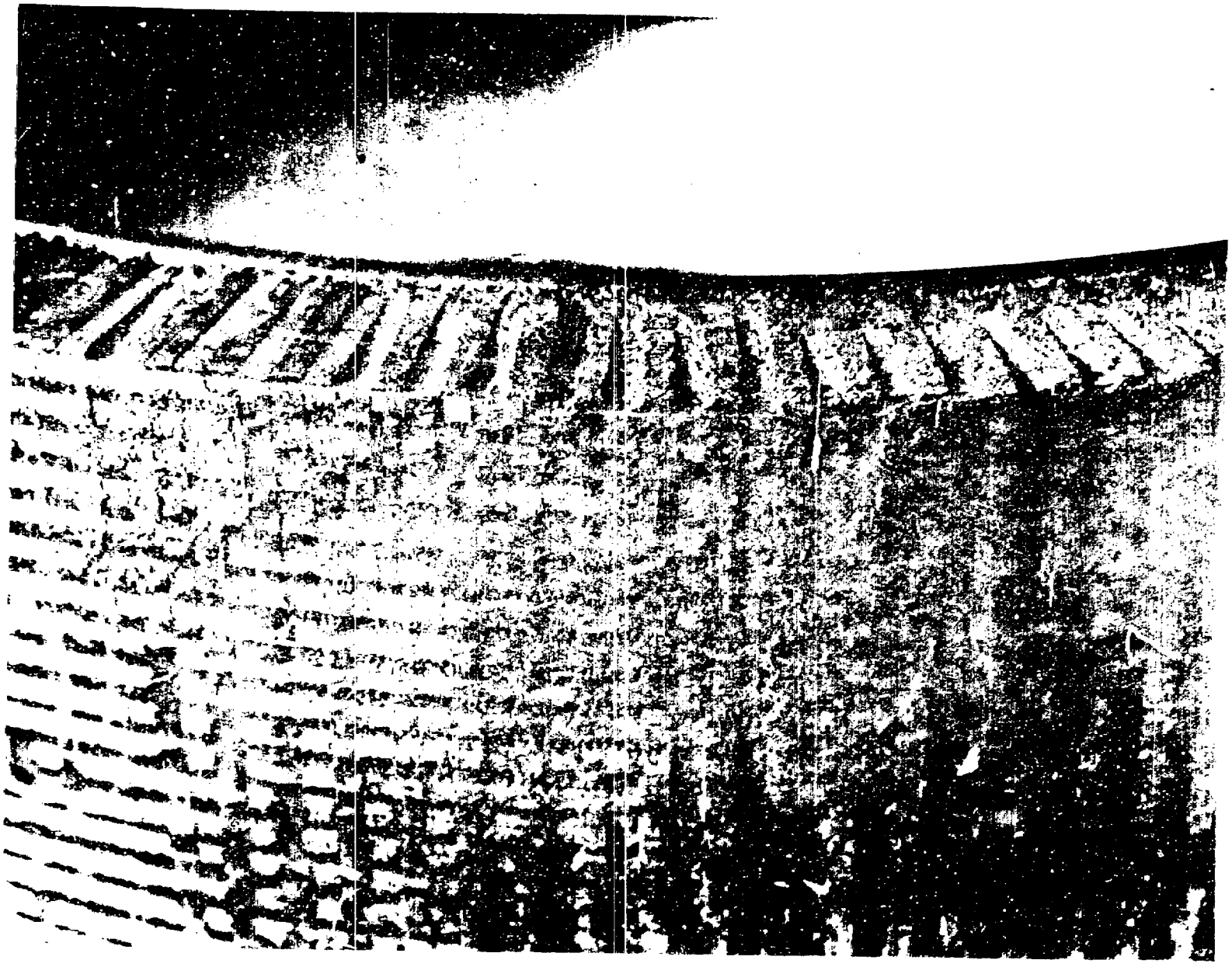

b. Exposed Zone
(No Scale)

Figure 34 Continued.

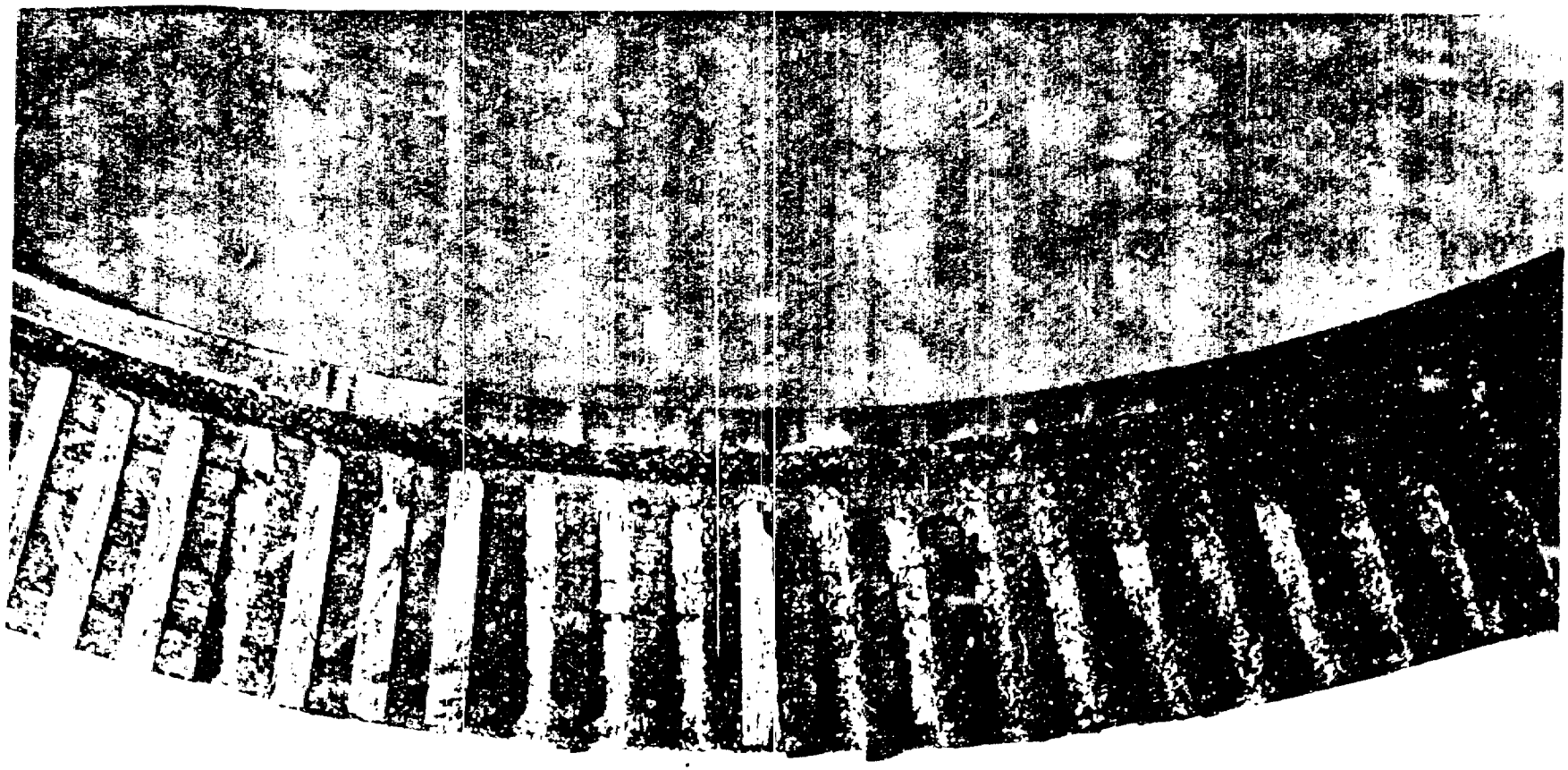

c. Axial View - Top Edge
Exposed Zone
(No Scale)

Figure 34 Continued.

Missing and raised radials located 285-0-15°

a. Axial View - Bottom Edge
(2.5X)

Missing sections of matrix and circumferentials over radials located 60-150° in bottom edge

b. Axial View - Bottom Edge
(2.5X)

Figure 35. Photographs Showing Structural Change After Exposure in Ring 1109-35-2 from AVCO 3DCC

Single 0.34 in. long circumferential crack located in bottom edge 0.25 in. from inner edge and at at 60-65°

c. Axial View - Bottom Edge (2.5X)

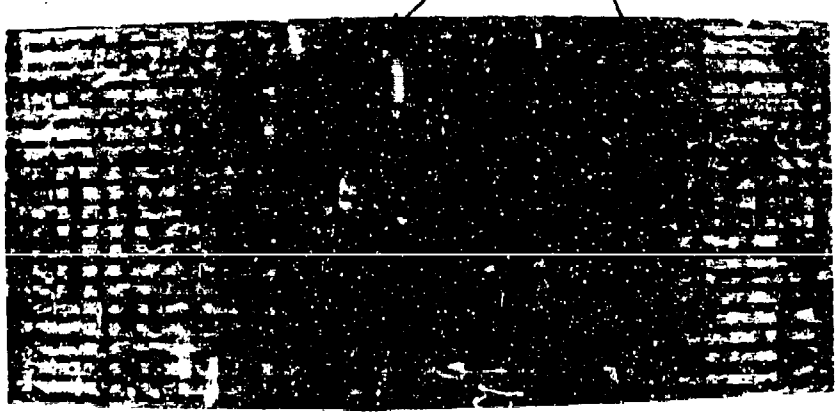

Front Yarn Lift Located at 300-45°

d. Radial View - Outer Surface at 0° (1X)

Figure 35 Continued.

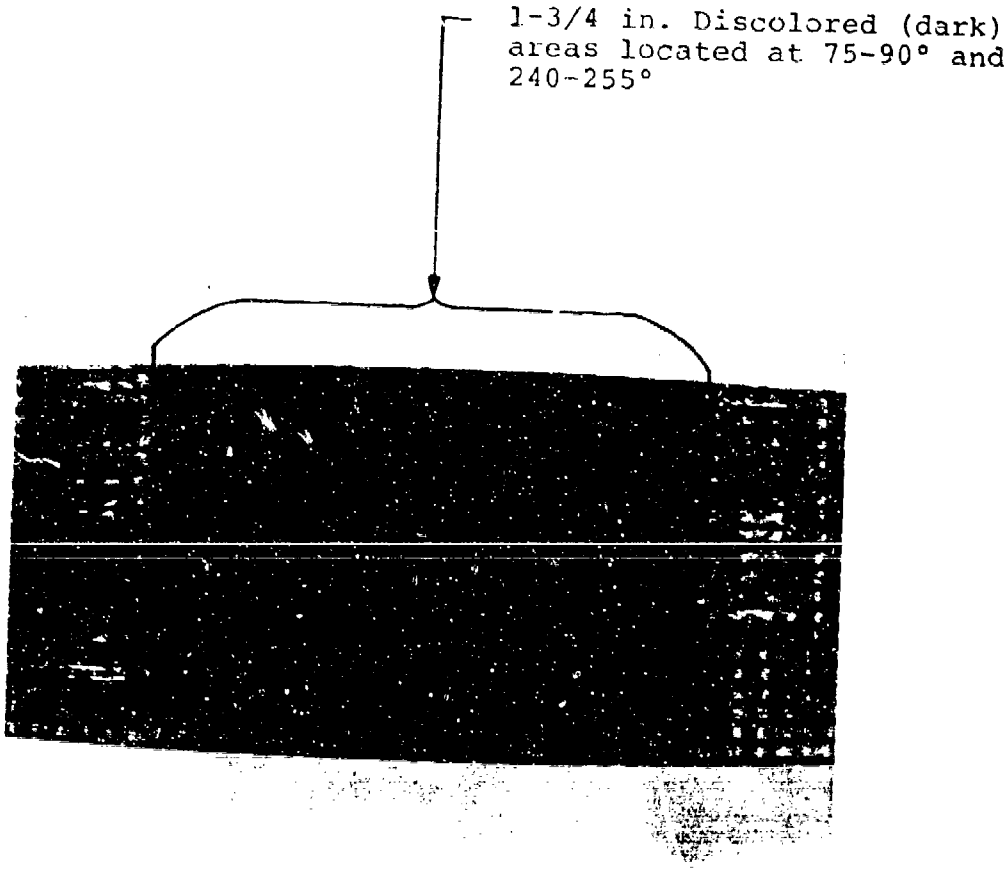

e. Radial View - Outer Surface

Figure 35 Continued.

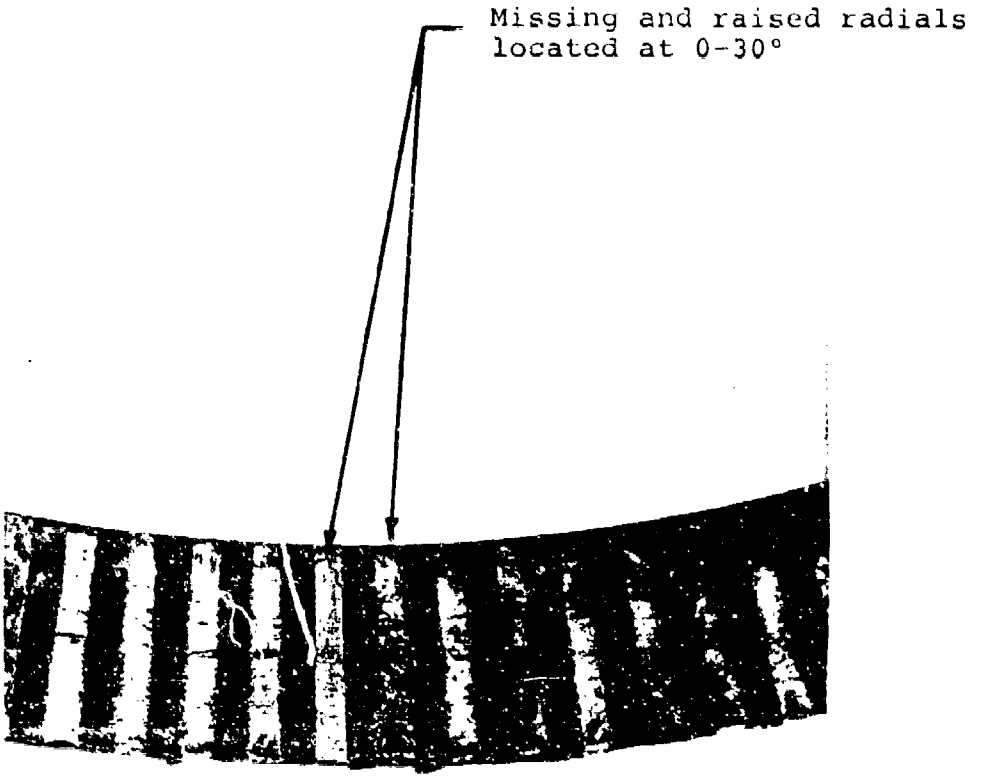

a. Axial View - Bottom Edge
(2.5X)

Figure 36. Photographs Showing Structural Change After Exposure in Ring 1109 -35-3 from AVCO 3DCC

b. 90°

Cracking Along Pre-existing Circumferential Delaminations

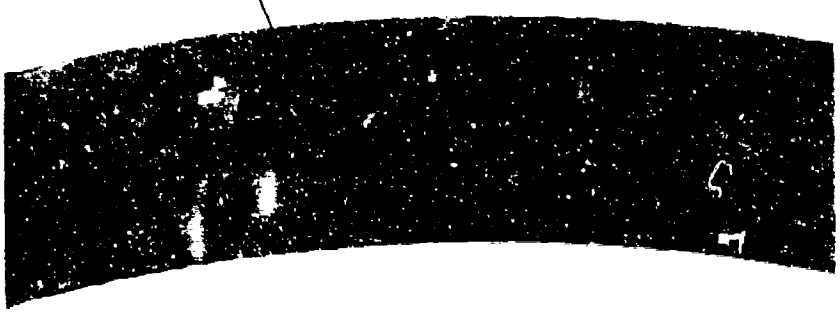

c. 180°

Axial View - Bottom Edge
(2.5X)

Figure 36 Continued.

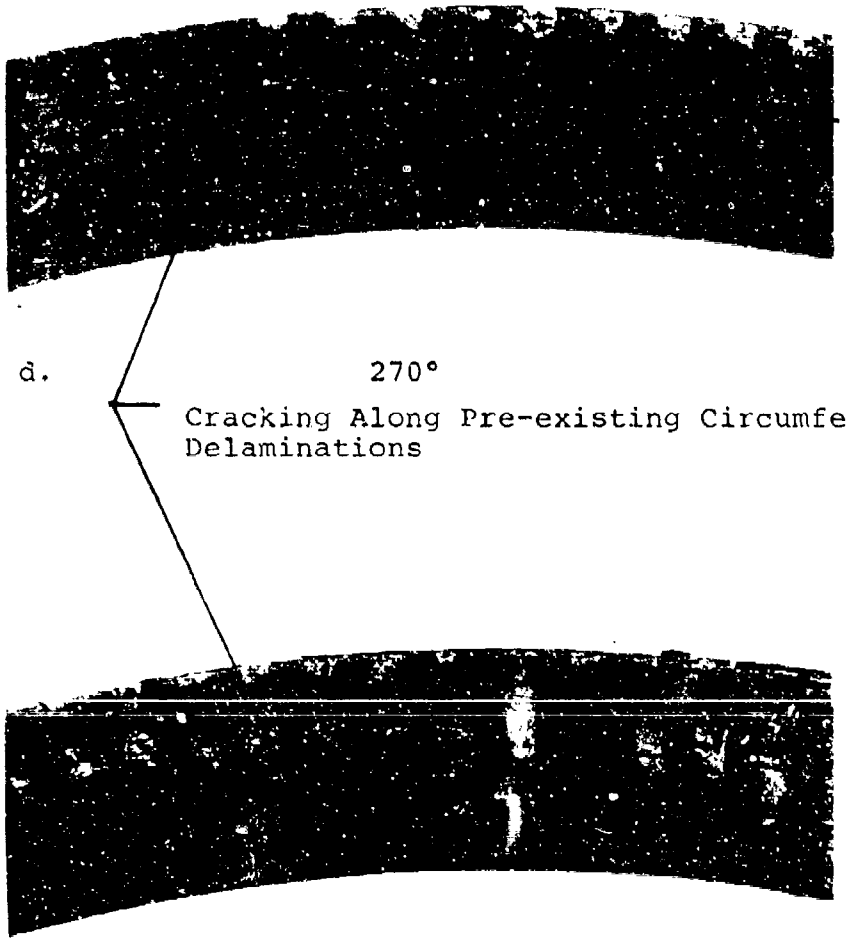

d. 270°

Cracking Along Pre-existing Circumferential Delaminations

e. 315°

Axial View-Bottom Edge
(2.5X)

Figure 36 Continued.

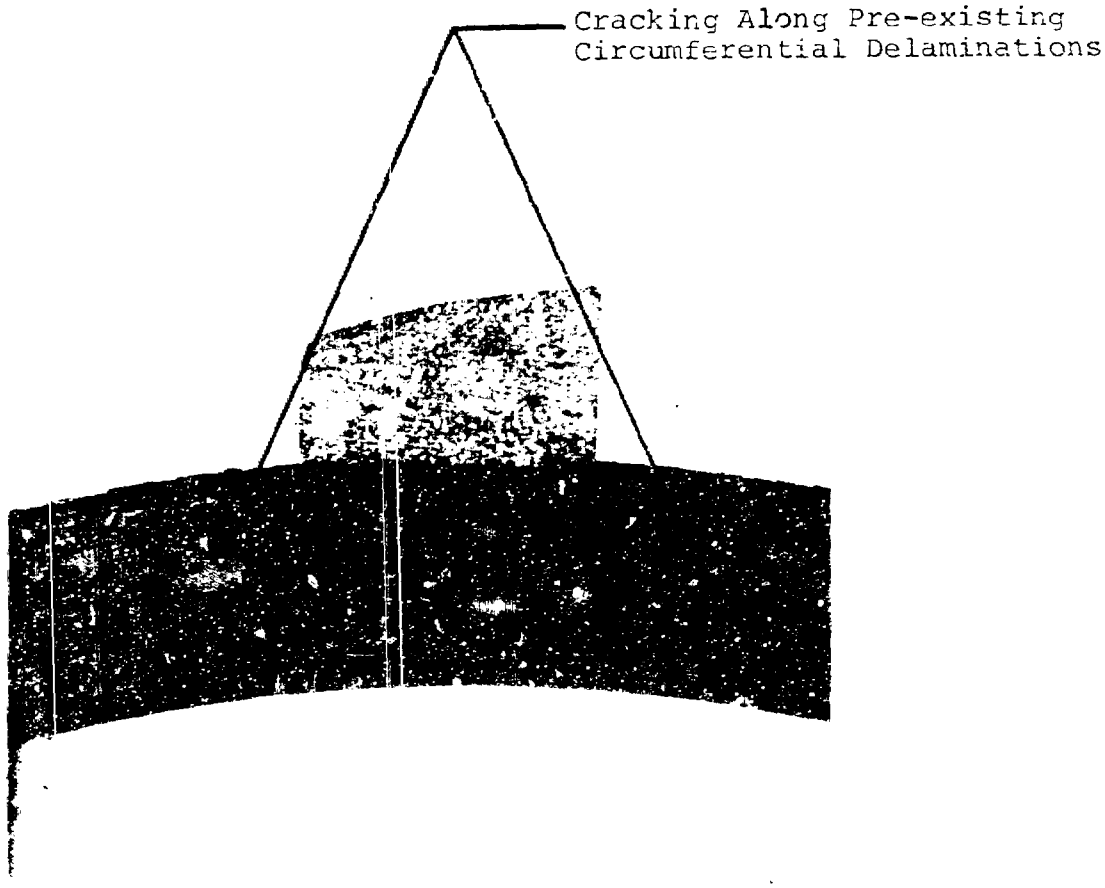

f. 0°
Axial View - Top Edge
(2.5X)

Figure 36 Continued.

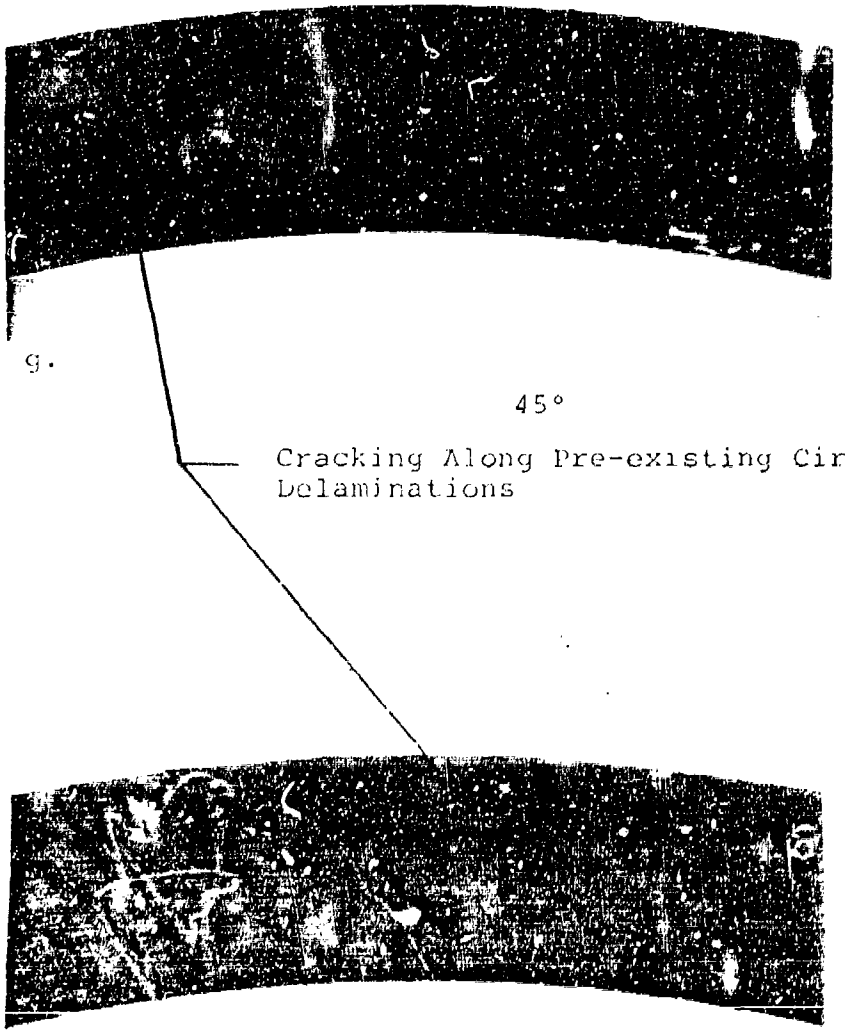

Axial View-Top Edge
(2.5X)

Figure 36 Continued.

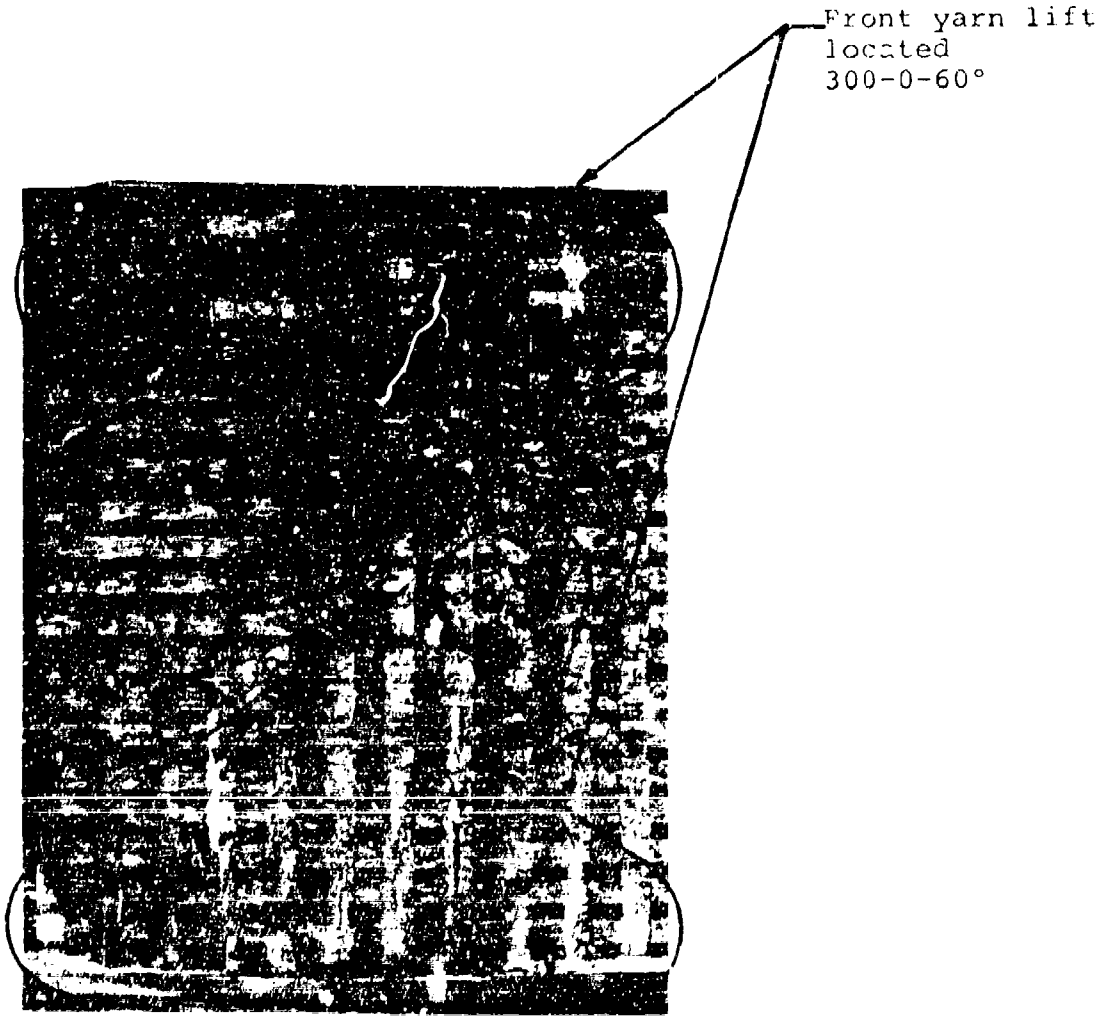

i. 0°

Radial View - Outer Surface

Figure 36 Continued.

a. Axial View
(5X)

Note:
Residual
Porosity
to about
12 mils

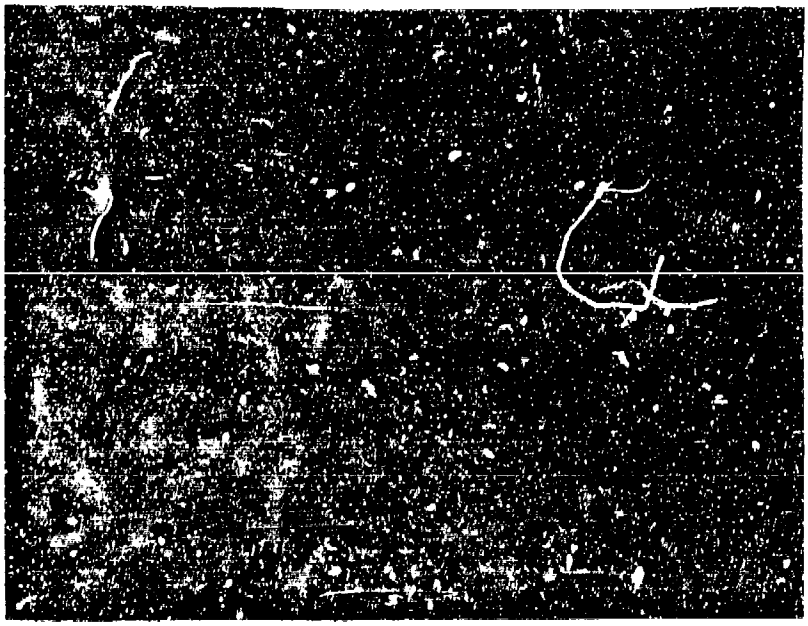

b. Radial View
(5X)

Figure 37. Photographs Showing Typical Sandia Felt CC

Notes

1. ⬡ Radial velocity in in./μsec
   (Relative radial transmission in added-dB) - First Run } Higher transmission readings correlate
   (Relative radial transmission in added-dB) - Second Run } lower attenuative material
2. ↓ Axial velocity in in./μsec
3. Visual inspection results - no single flaws
4. Penetrant inspection on edges using 2, 2, 4-Trimethylpentane - no single flaws

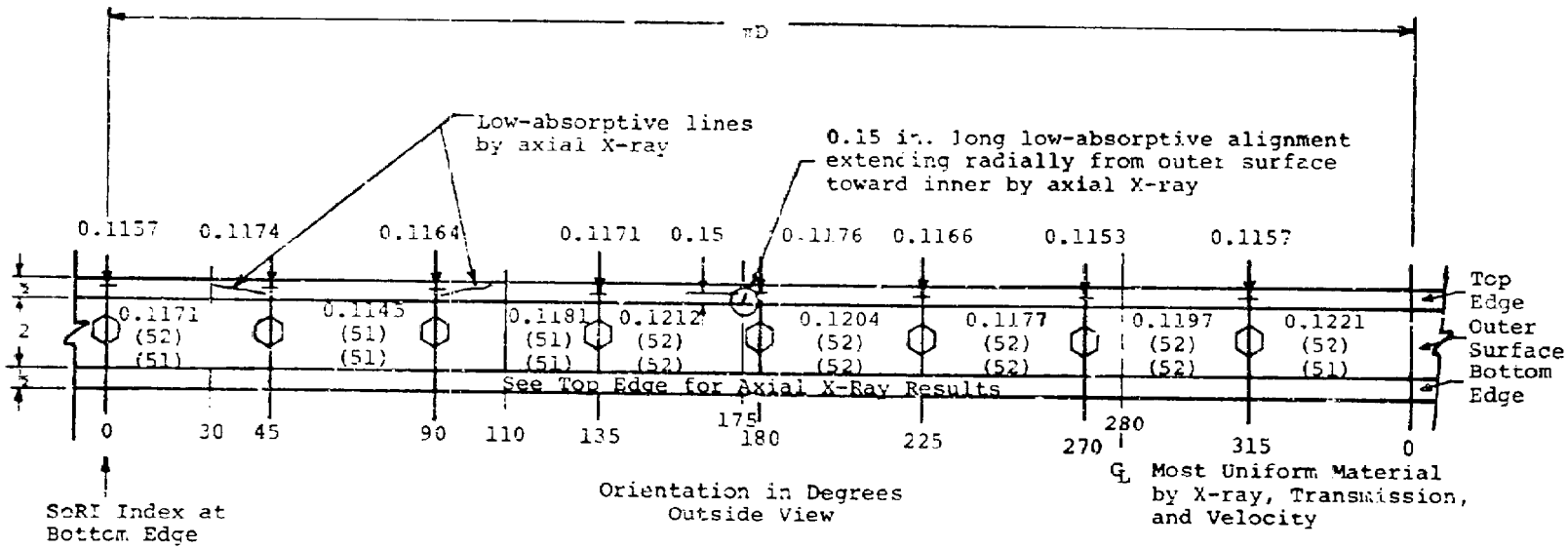

Figure 38. Sketch Showing Inspection Results on Ring 9N-2 from Sandia Felt CC

Notes

1. ⬡ Radial Velocity in in./μsec
   (Relative radial transmission in added-dB) - 1st Run } Higher transmission
   (Relative radial transmission in added-dB) - 2nd Run } readings correlate lower attenuative material
2. + Axial velocity in in./μsec
3. Visual inspection results - no single flaws
4. Penetrant inspection on edges using 2, 2, 4-Trimethylpentane - no single flaws

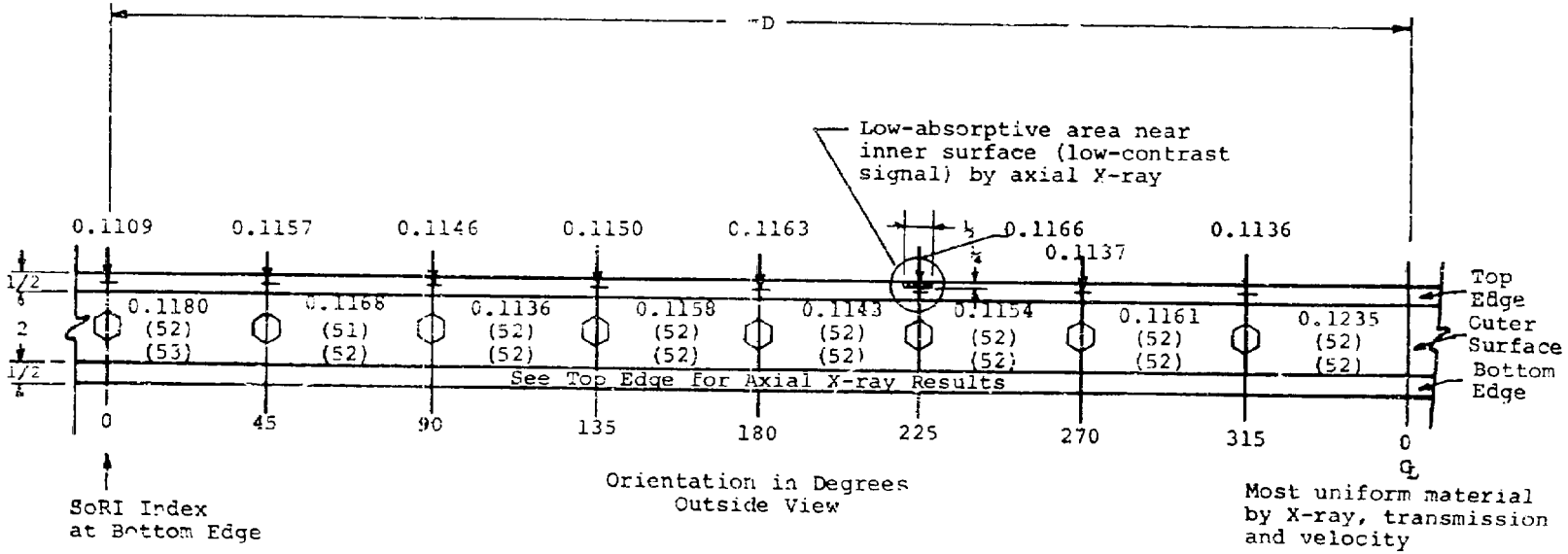

Figure 39. Sketch Showing Inspection Results on Ring 9P-2 from Sandia Felt CC

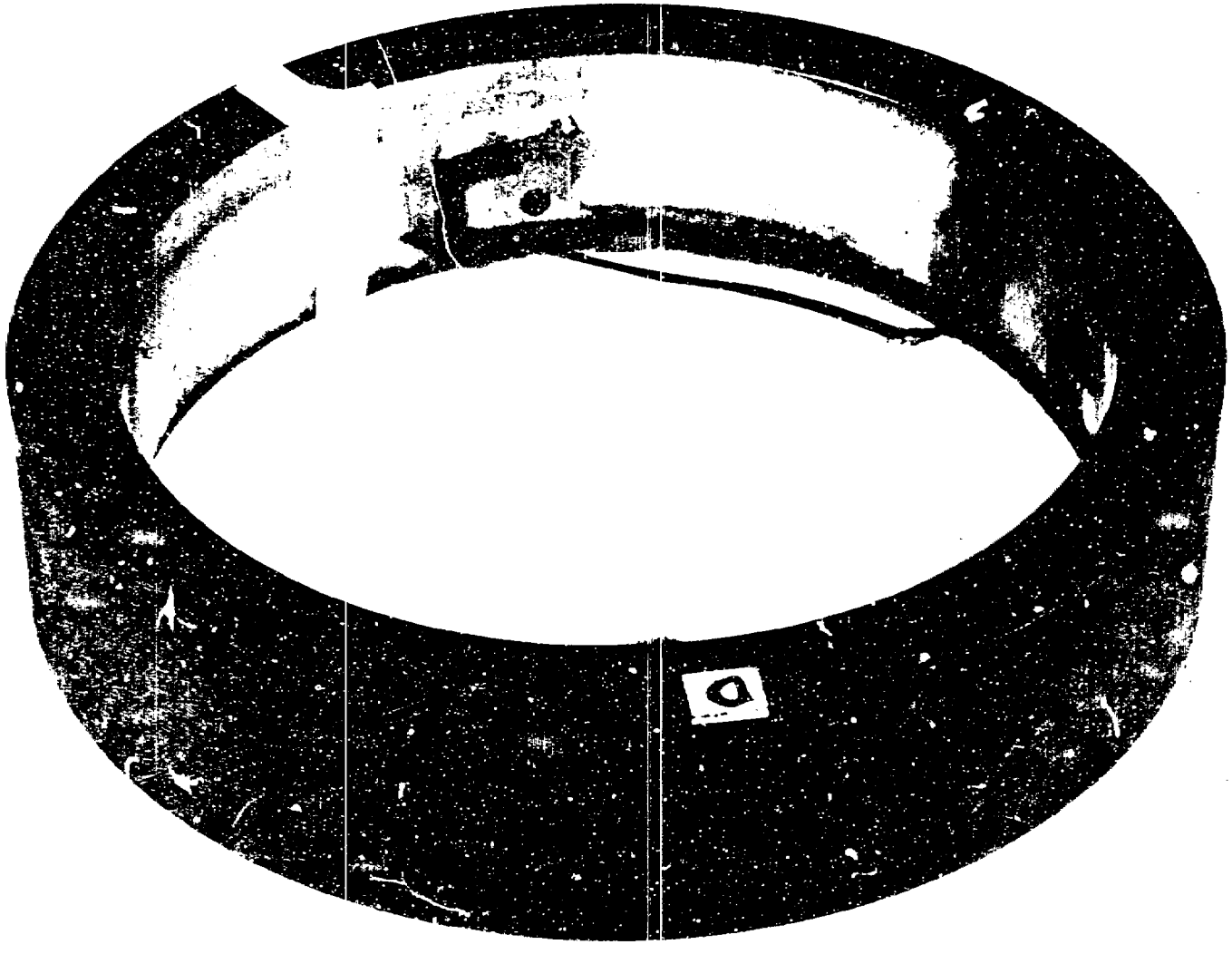

a. (No Scale)

Figure 40. Photographs Showing As-Received Ring 9N-2 from Sandia Felt CC After Exposure

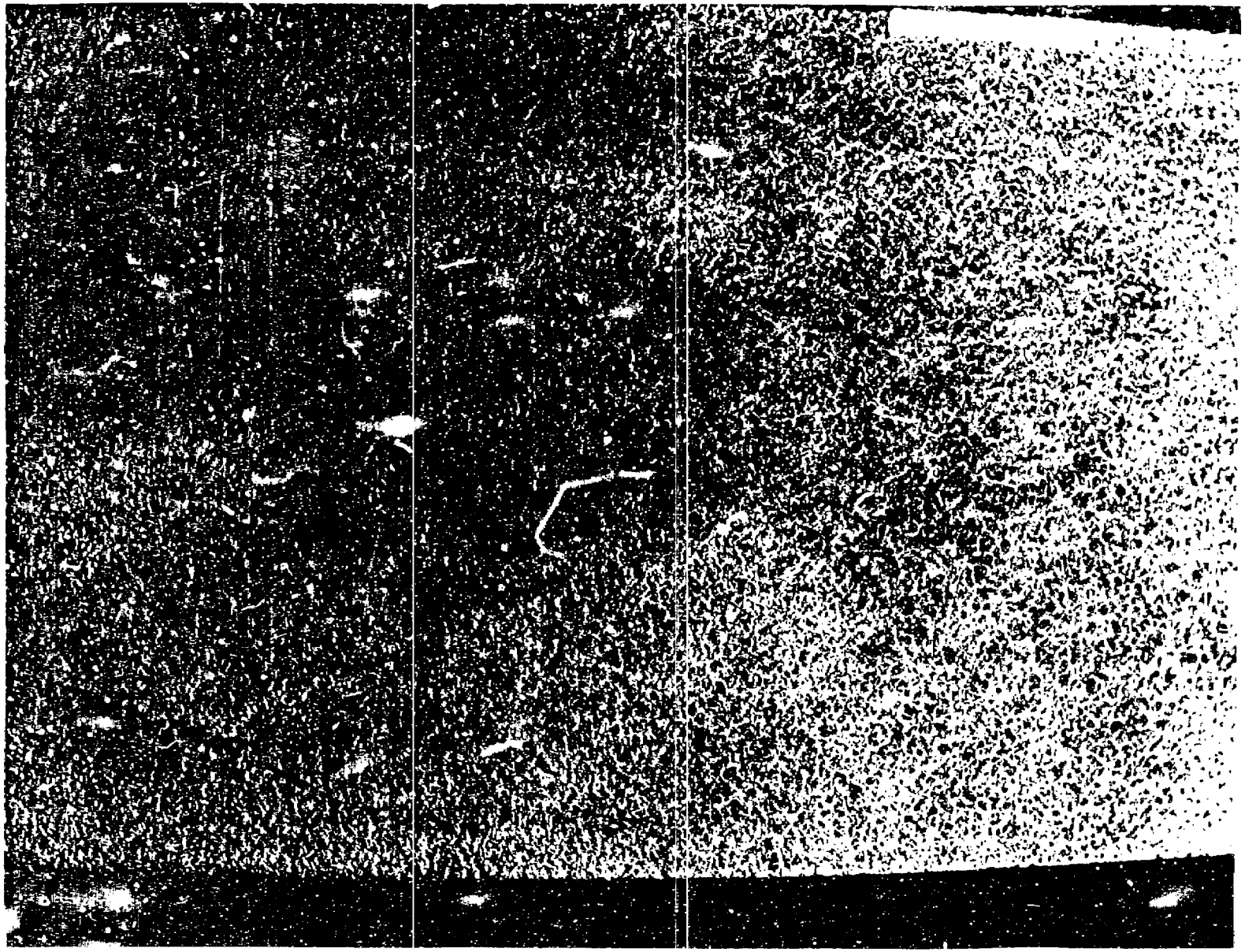

b.

(No Scale)
Radial View - Outer Surface Near 0°

Figure 40 Continued.

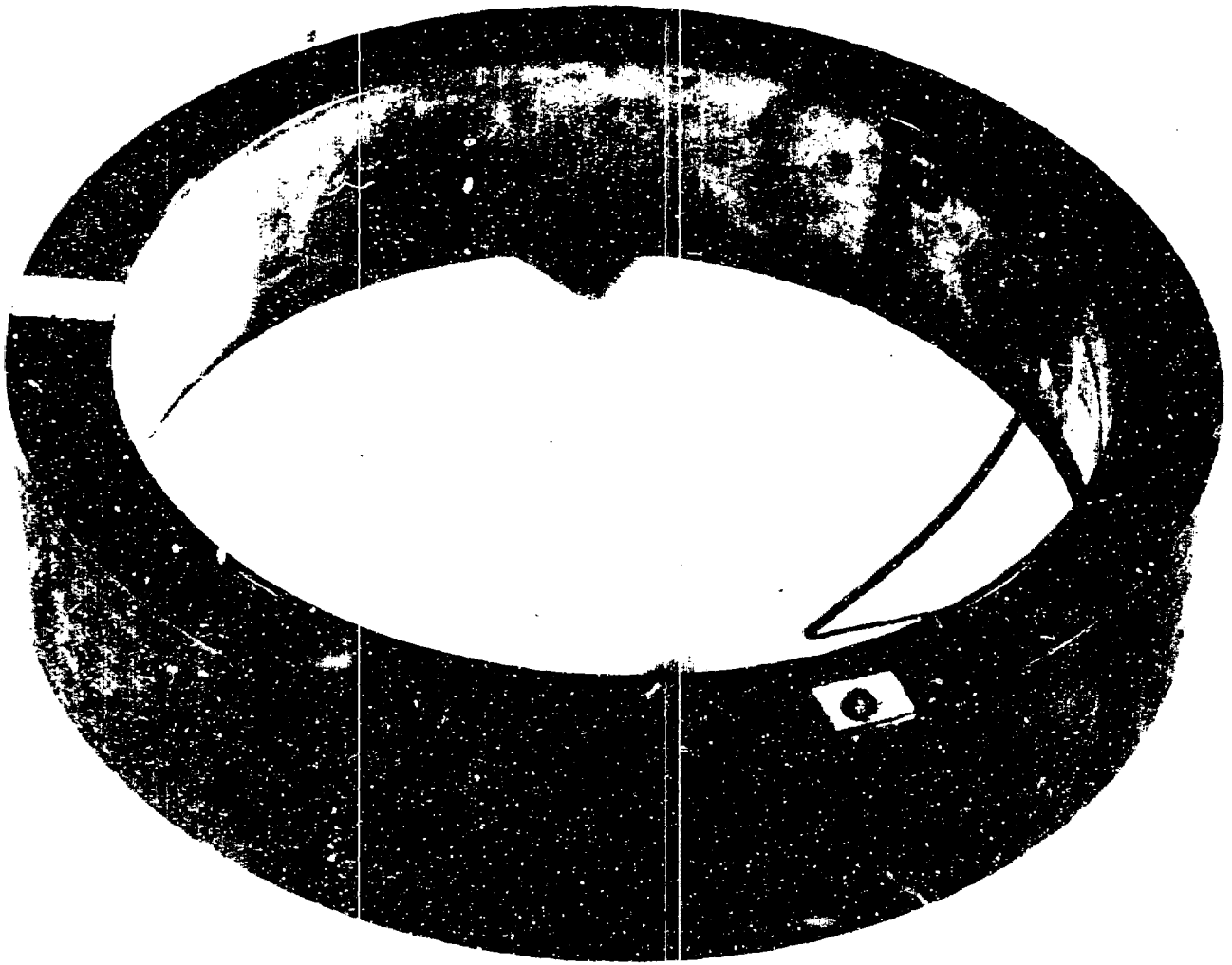

a. (No Scale)

Figure 41. Photograph Showing As-Received Ring 9P-2 from Sandia Felt CC After Exposure

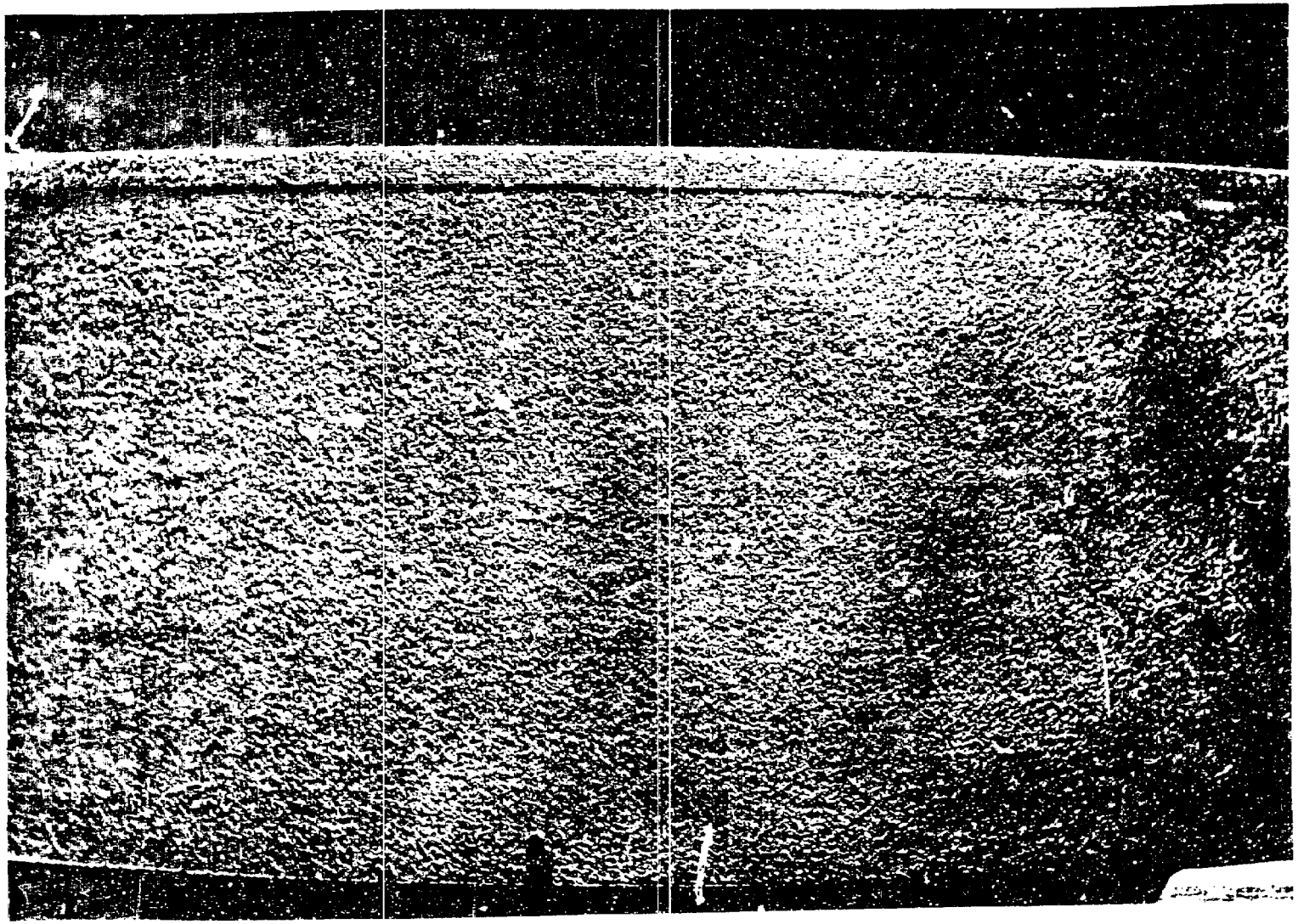

b. (No Scale)
Radial View - Outer Surface in Exposed Zone

Figure 41 Continued.

Note: Bottom edge was slightly more porous at 275-0-45° location.

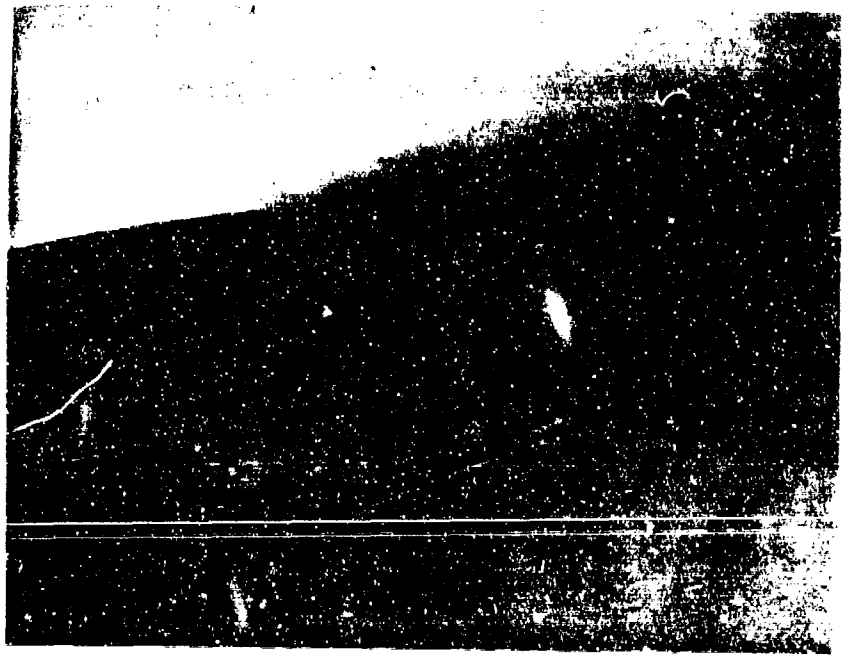

a. 0°

Axial View - Bottom Edge
(2.5X)

Figure 42. Photographs Showing Structural Change After Exposure in Ring 9N-2 from Sandia Felt CC

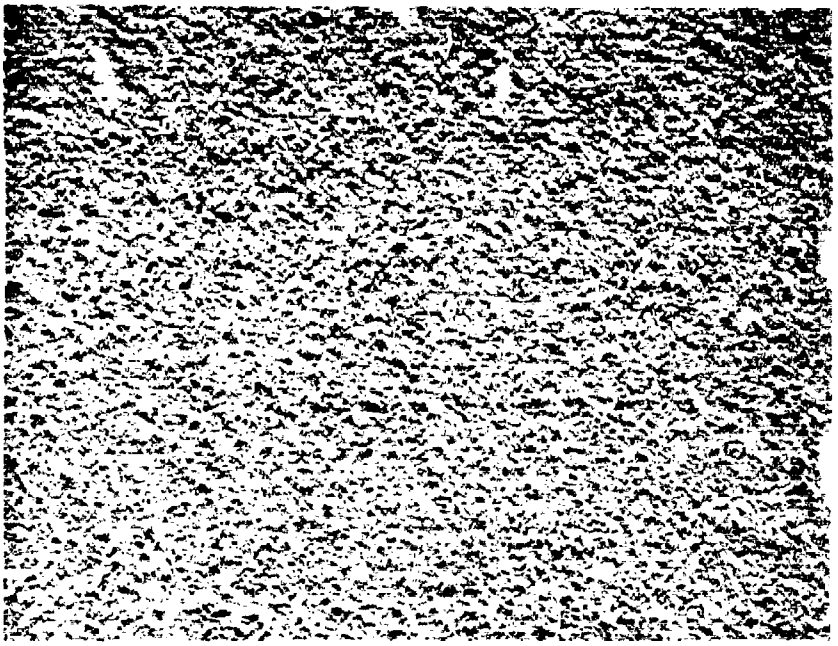

b. 0°
(Centered)
Radial View-Outer Surface (5X)

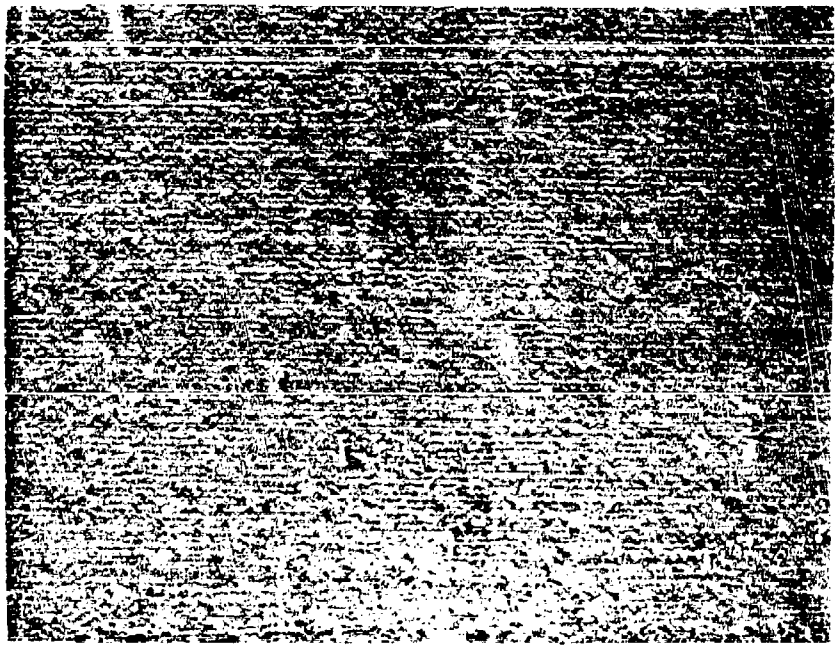

c. 180°
Radial View-Outer Surface (5X)

Note: Material in Outer Surface at 270-0-90° was slightly discolored (dark), and texture was rougher.

Figure 42 Continued.

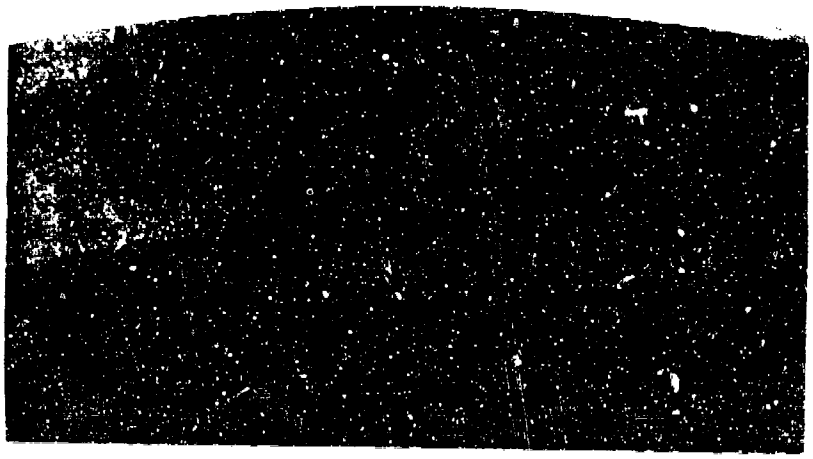

Note: No significant structural change such as cracking.

a. 0°
Axial View - Bottom Edge
(2.5X)

20 mil voids in surface located 240-255° and 270°

b. Axial View - Bottom Edge
(5X)

Figure 43. Photographs Showing Structural Change After Exposure in Ring 9P-2 from Sandia Felt CC

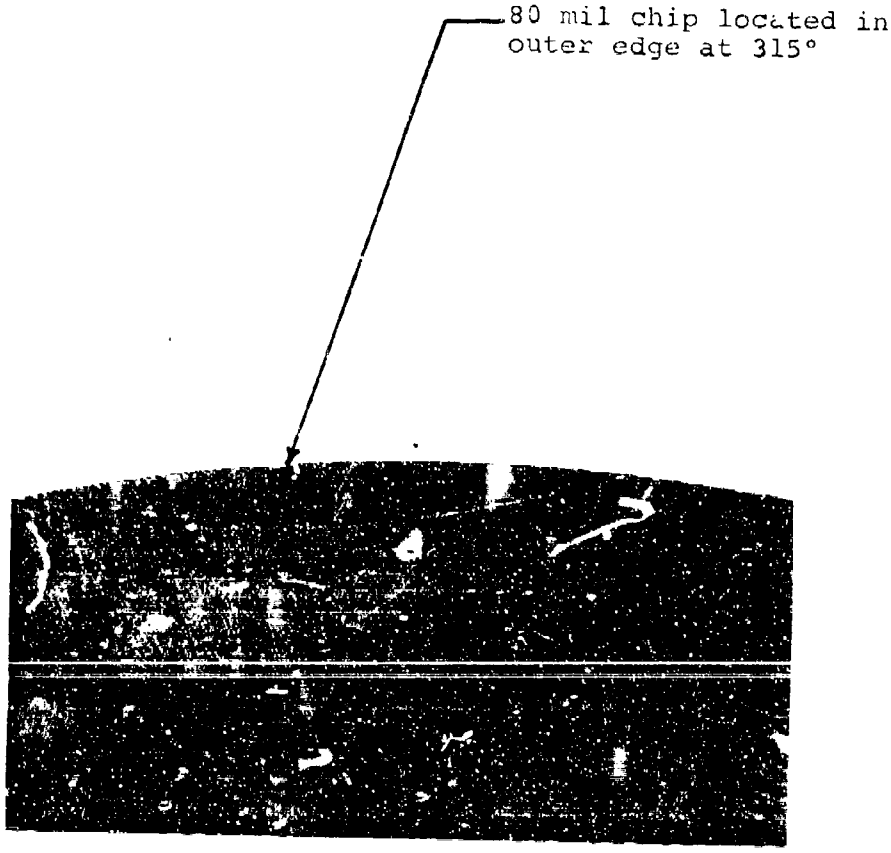

c. 315°
Axial View - Top Edge
(2.5X)

Figure 43 Continued.

Material removal and discoloration in exposed zone located approximately 270-0-90°. Porosity and surface texture near normal.

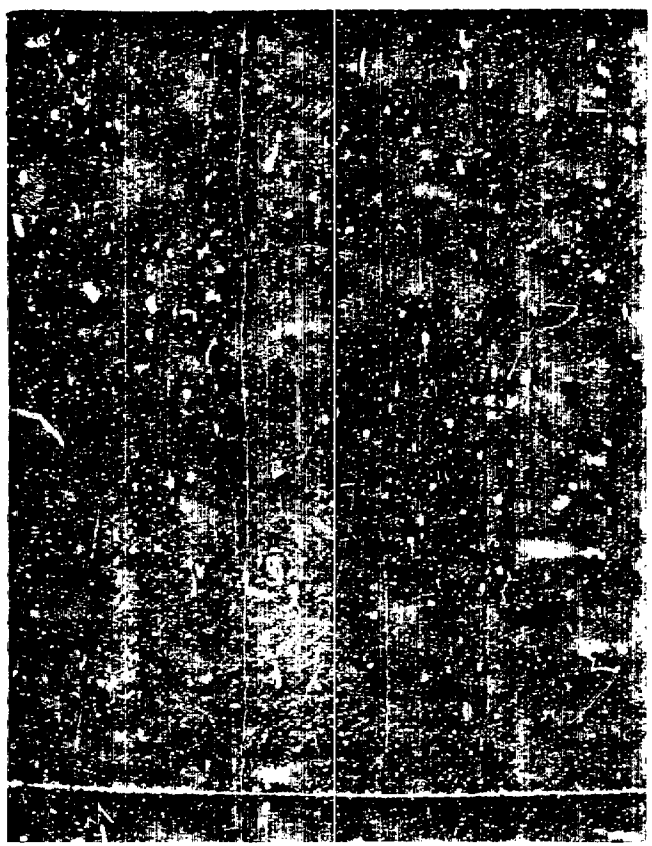

d. 270°

e. 0°

Radial View - Outer Surface
(2.2X)

Figure 43 Continued.

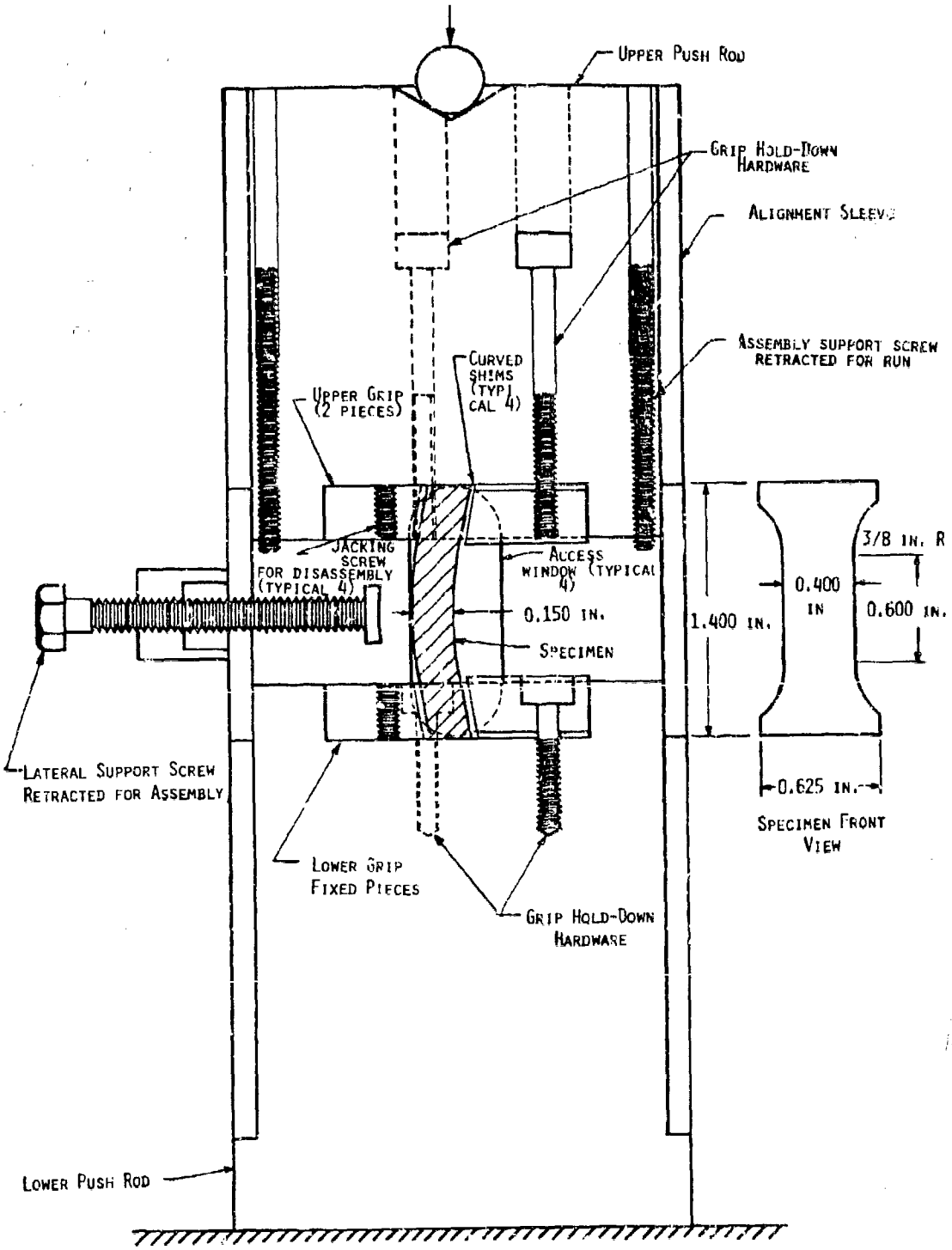

FIGURE 44. CURVED SPECIMEN COMPRESSION TEST FIXTURE

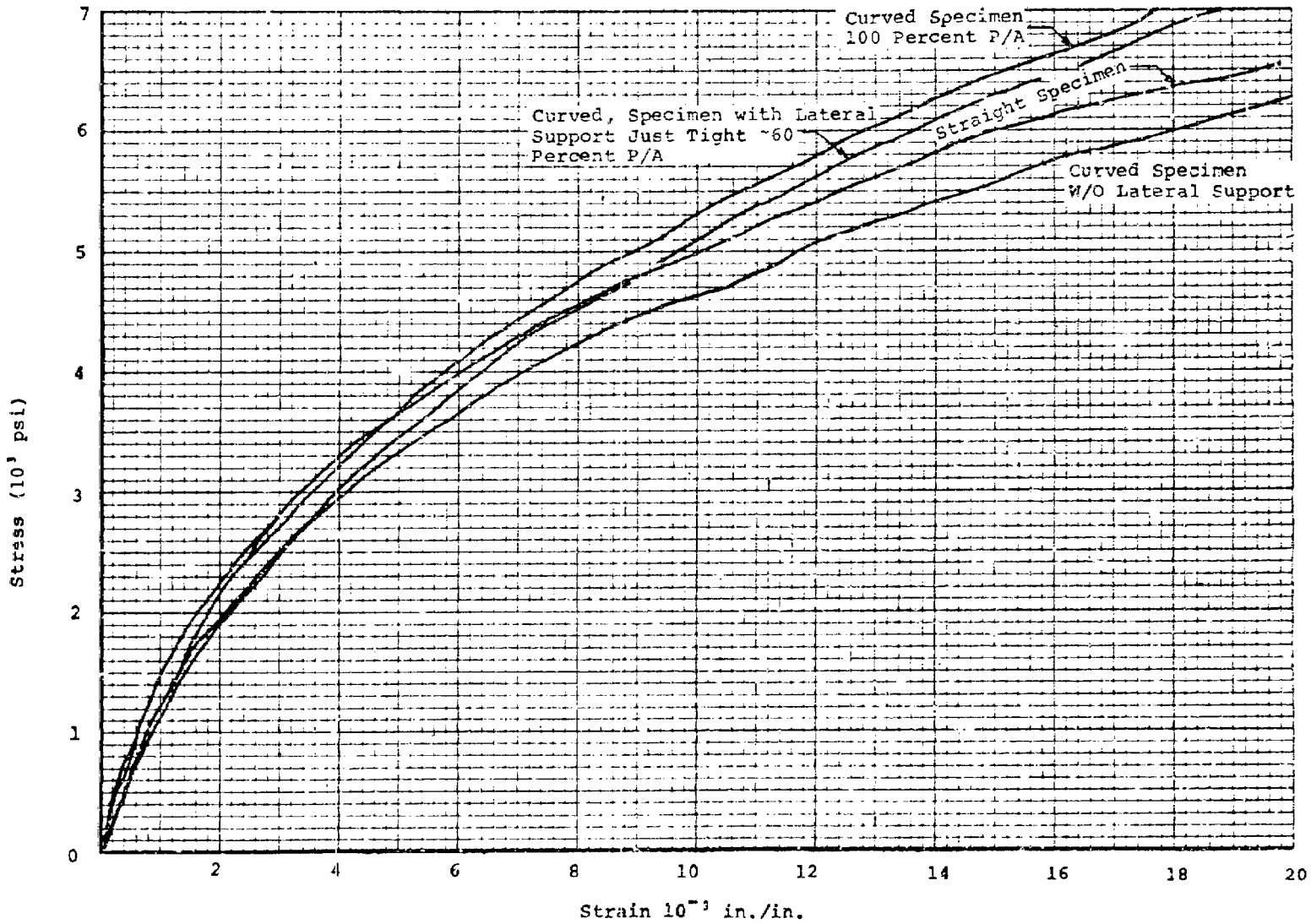

Figure 45. Comparison of Initial Portions of Stress-Strain Curves of Several Compressive Evaluation Methods on Felt CC Material

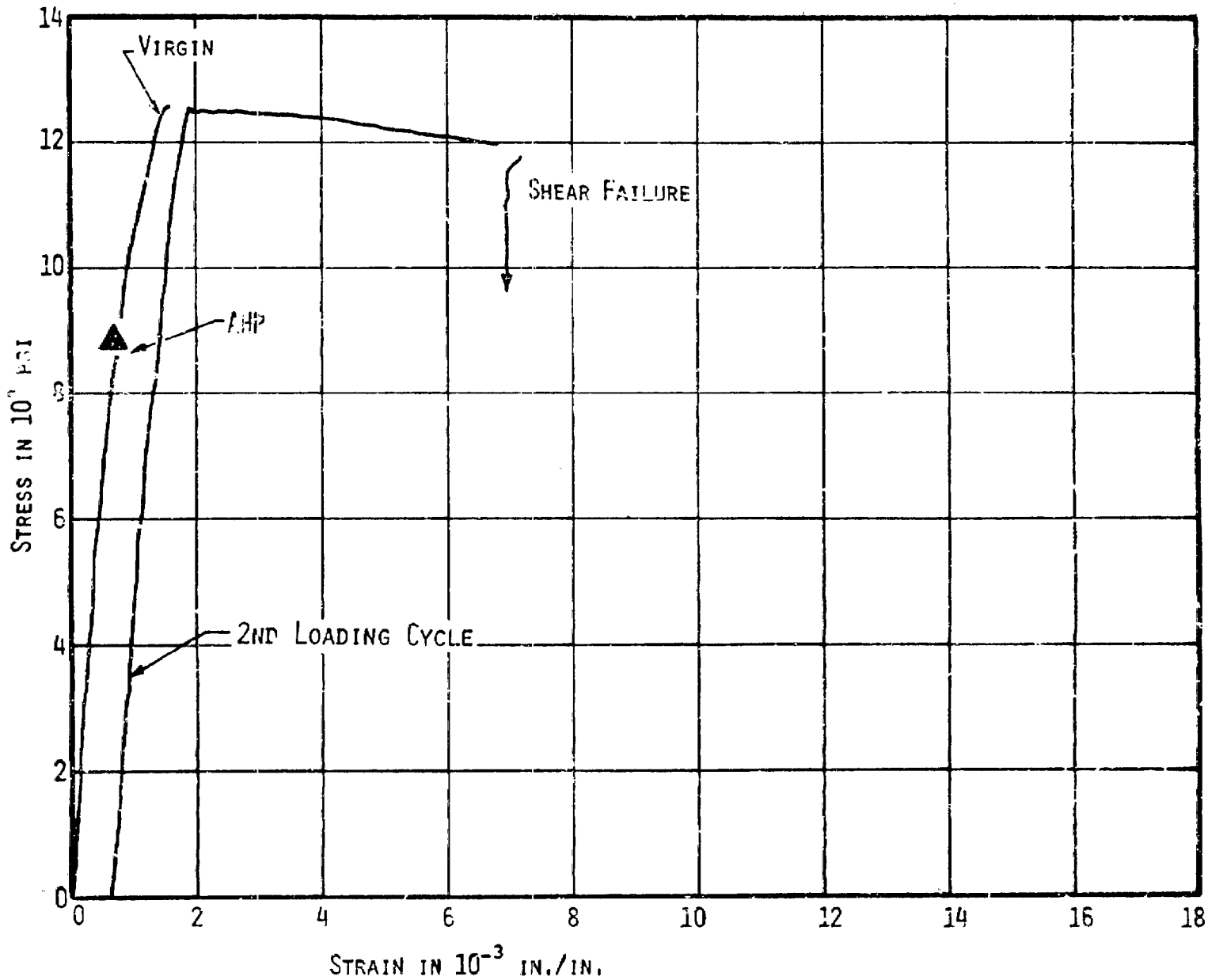

FIGURE 46. CIRCUMFERENTIAL COMPRESSION 3DCC CURVED SPECIMEN 5-0 SUPPORTED LATERALLY

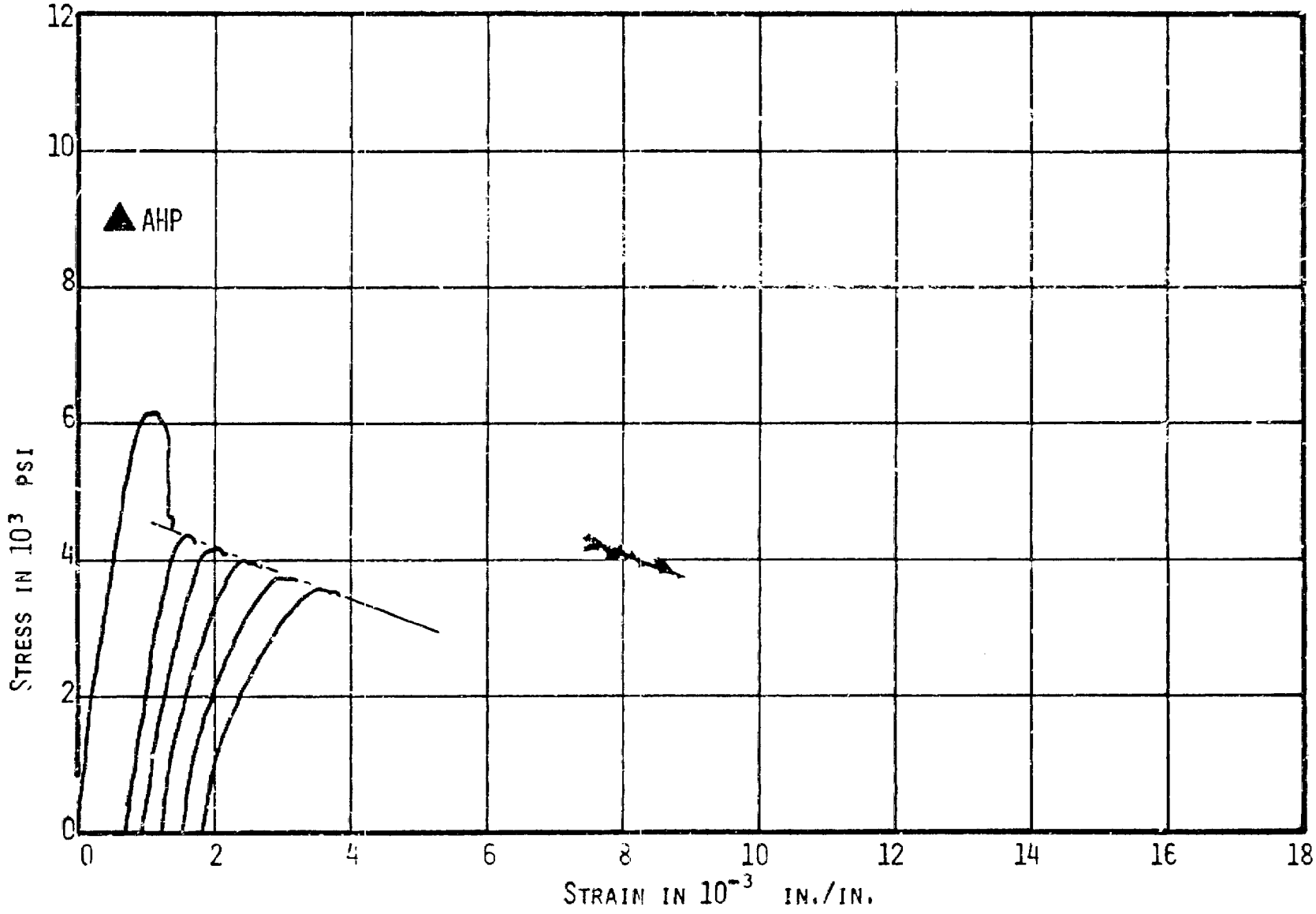

FIGURE 47. CIRCUMFERENTIAL COMPRESSION 3DCC CURVED SPECIMEN 4-0 - NO LATERAL SUPPORT SHOWING CUMULATIVE EFFECTS OF REPEATED LOADING

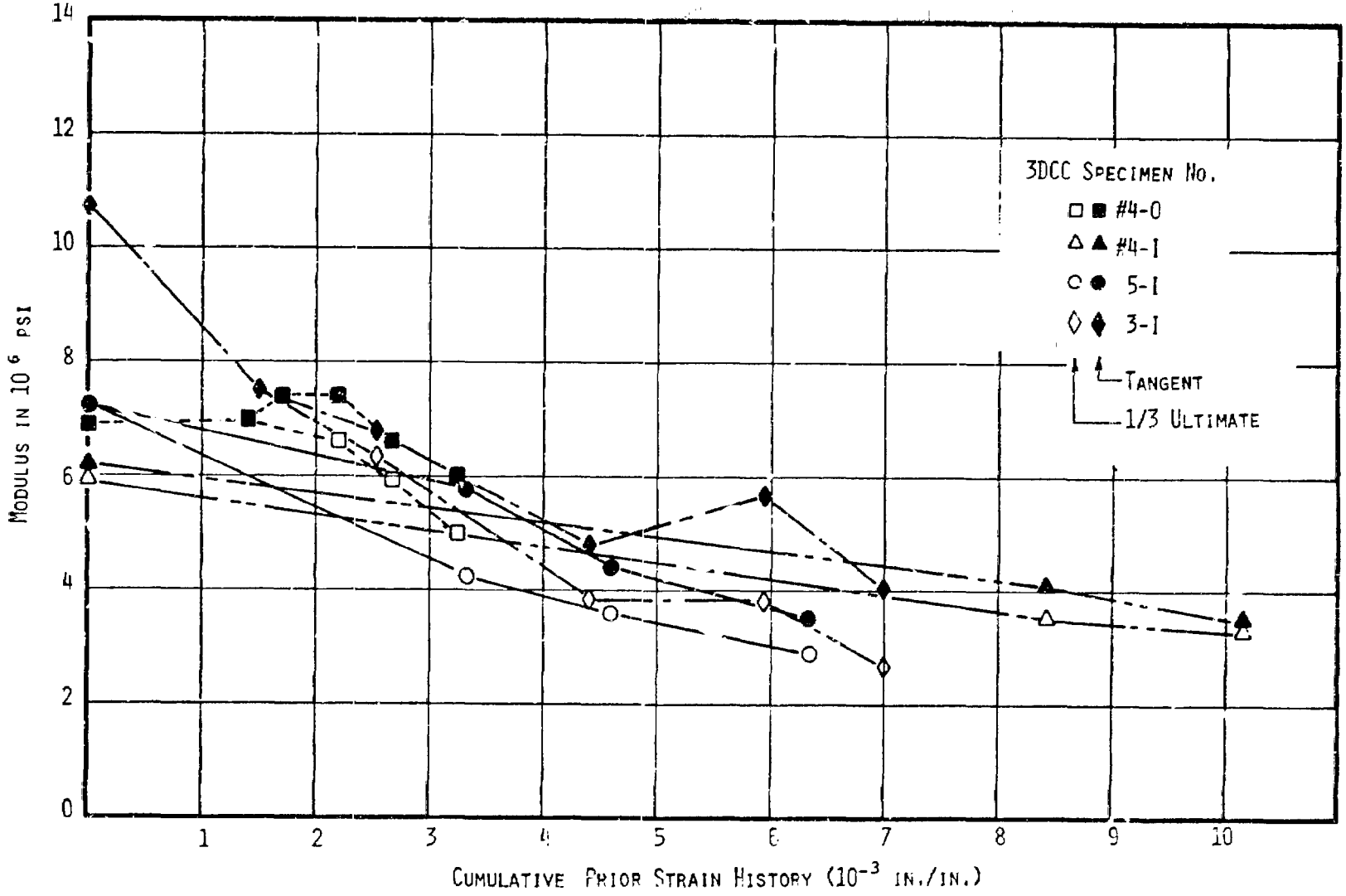

Figure 48. Compressive Modulus vs Strain History-Curved 3DCC - No Lateral Support

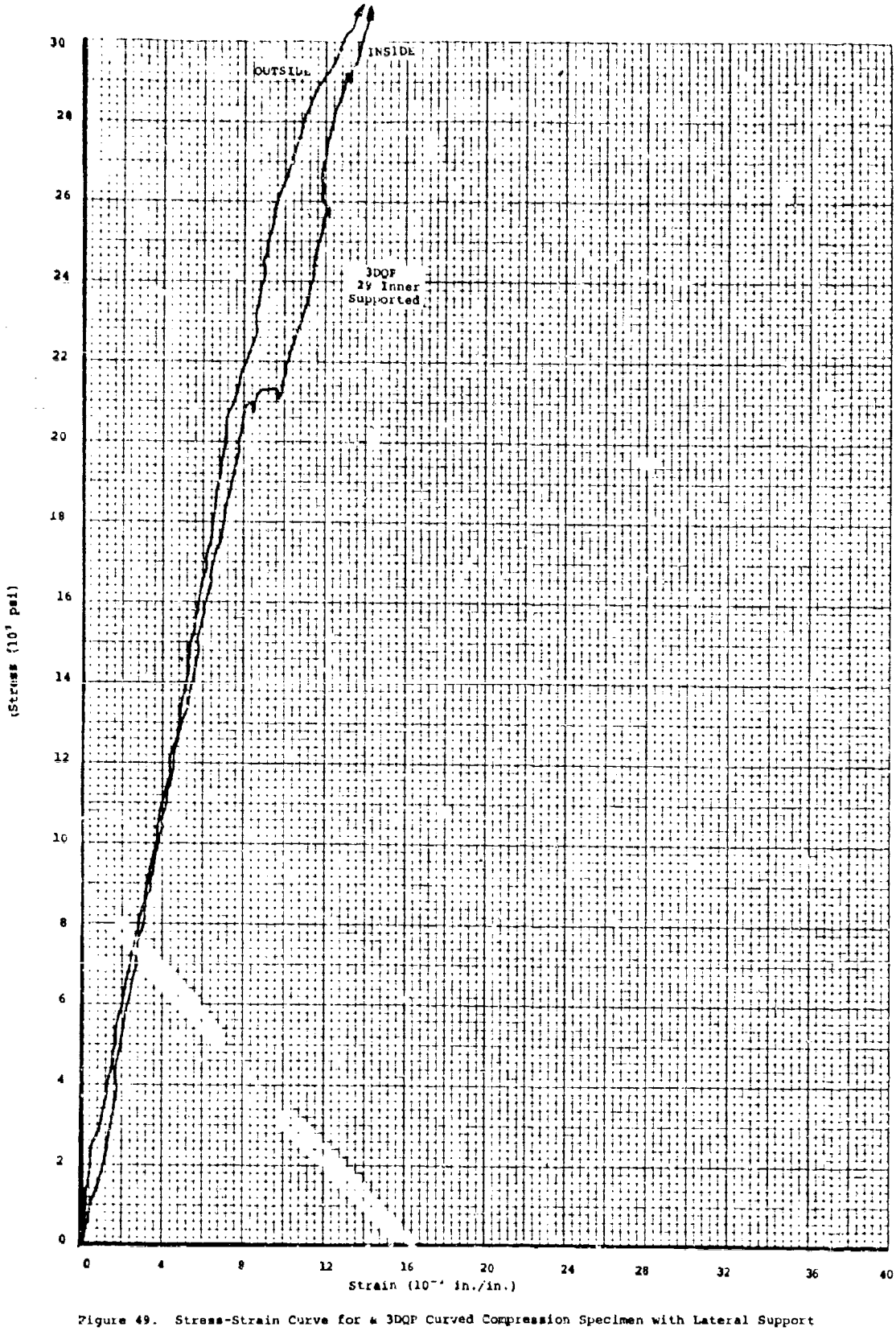

Figure 49. Stress-Strain Curve for a 3DQF Curved Compression Specimen with Lateral Support

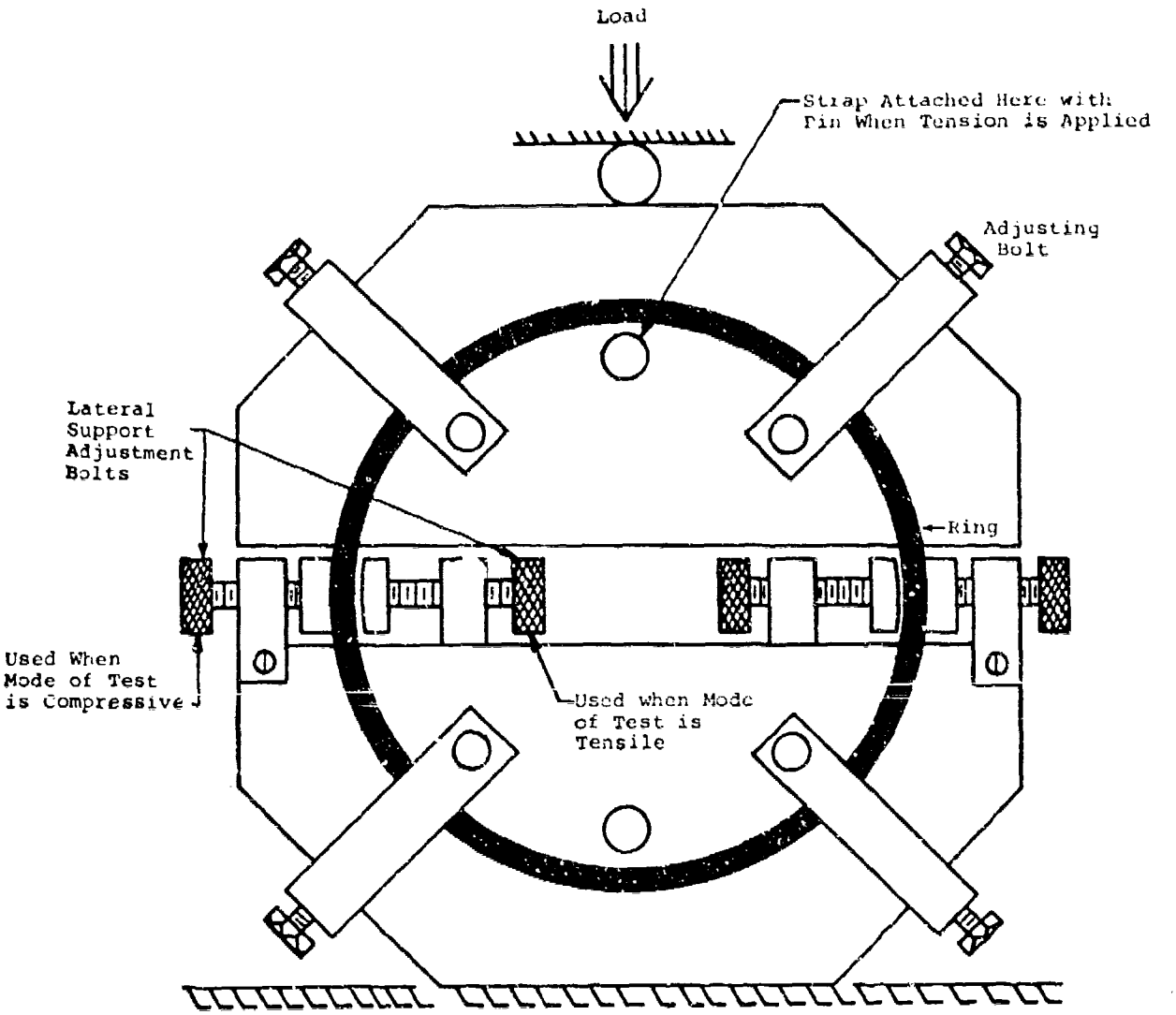

Figure 50. Schematic of Ring Segment Tension/Compression Fixture

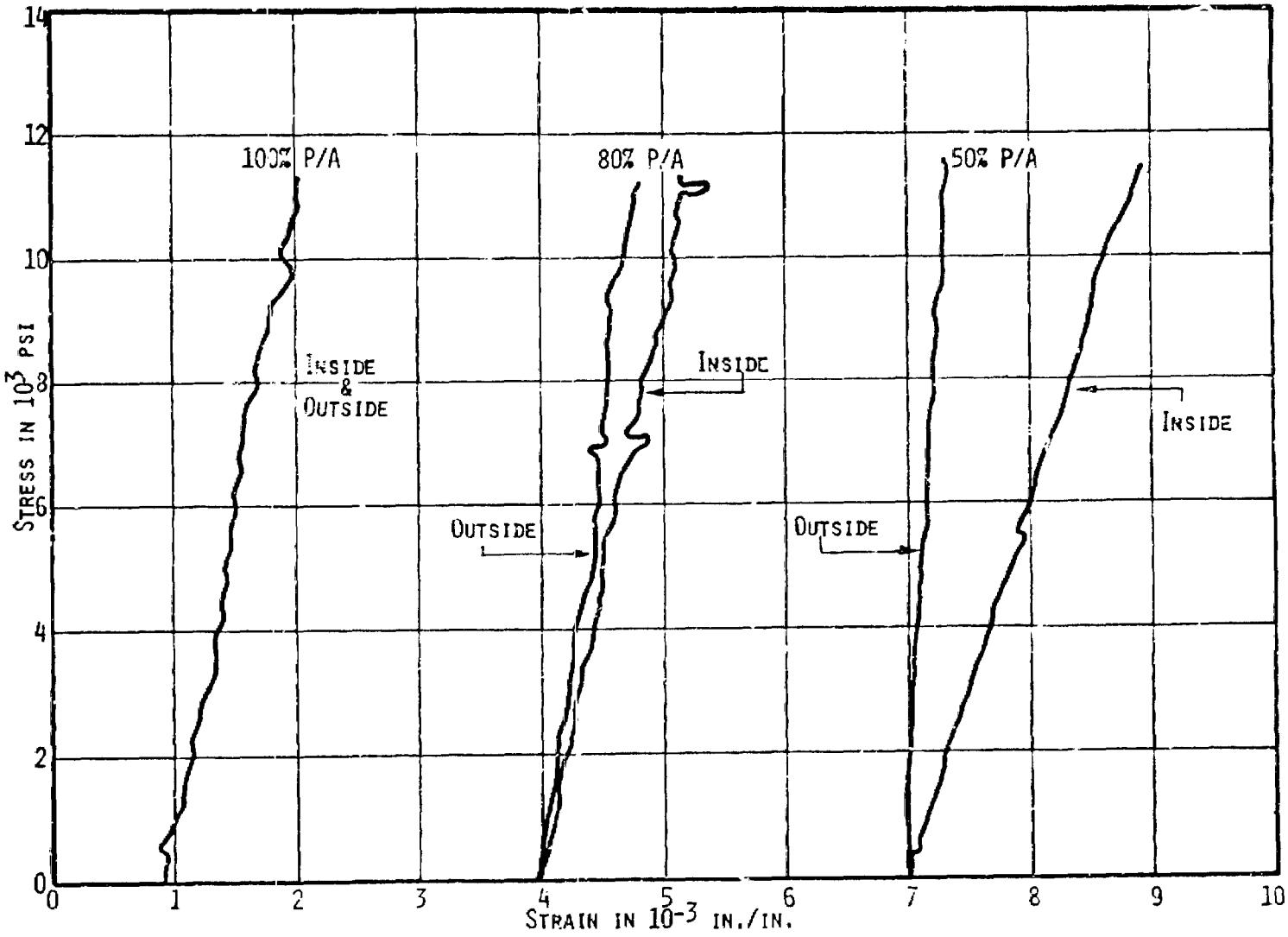

FIGURE 51. FELT CC RING SEGMENT COMPRESSION, RING #1

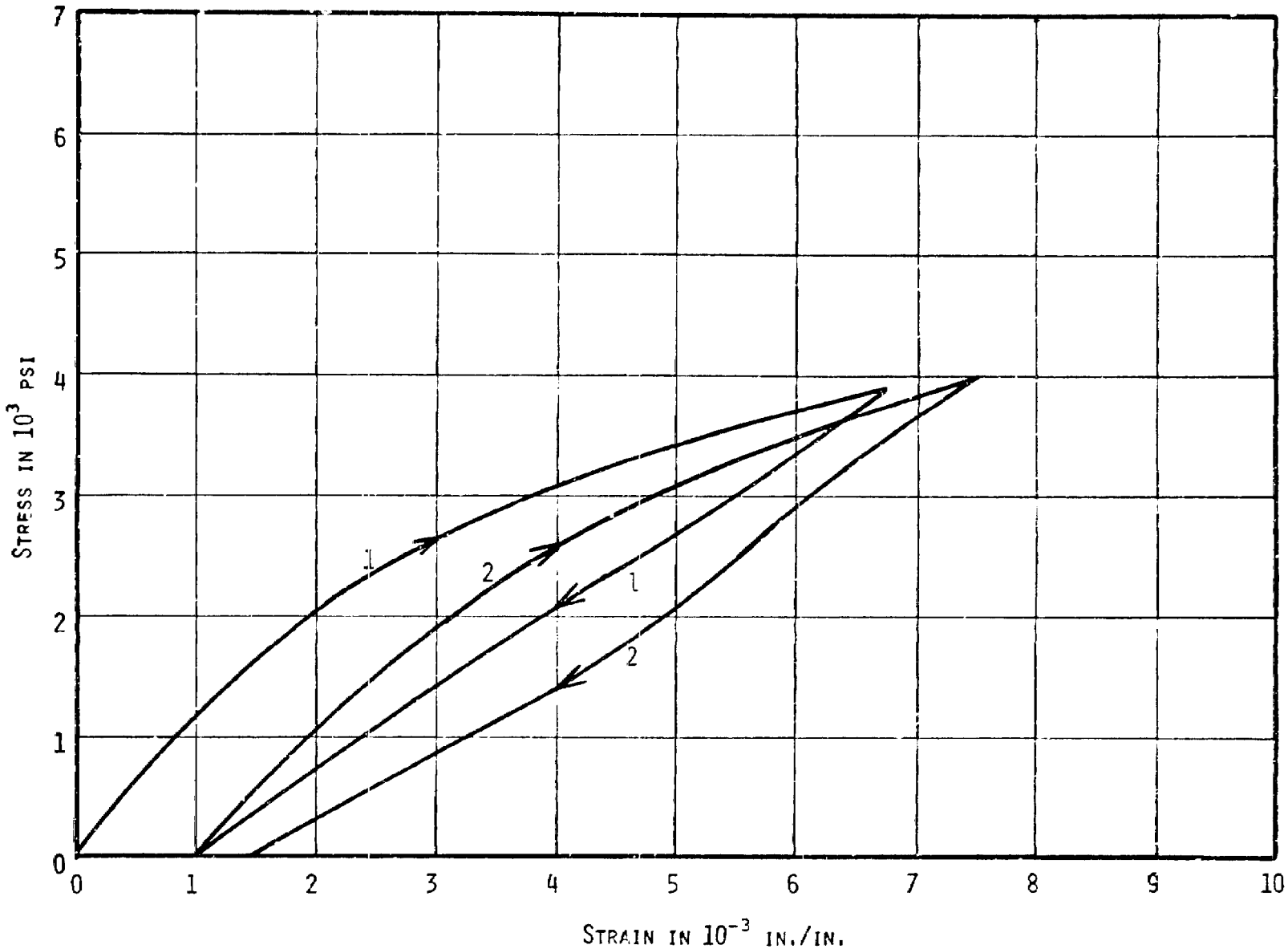

FIGURE 52. LOAD UNLOAD AT 100% P/A FELT CC RING #1 (DEBUG)

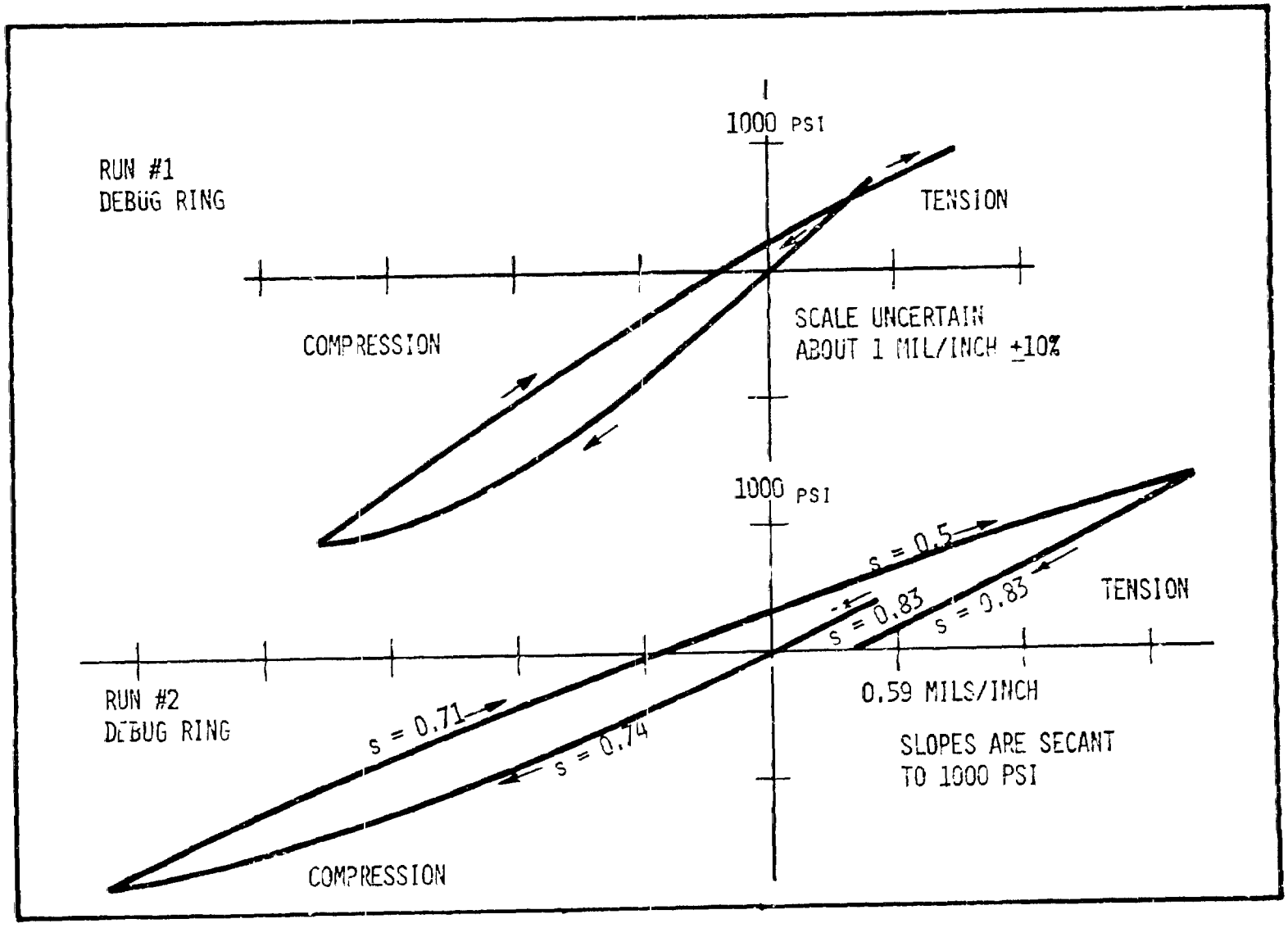

FIGURE 53. RING SEGMENT TENSILE/COMPRESSIVE CYCLE OF FELT CC

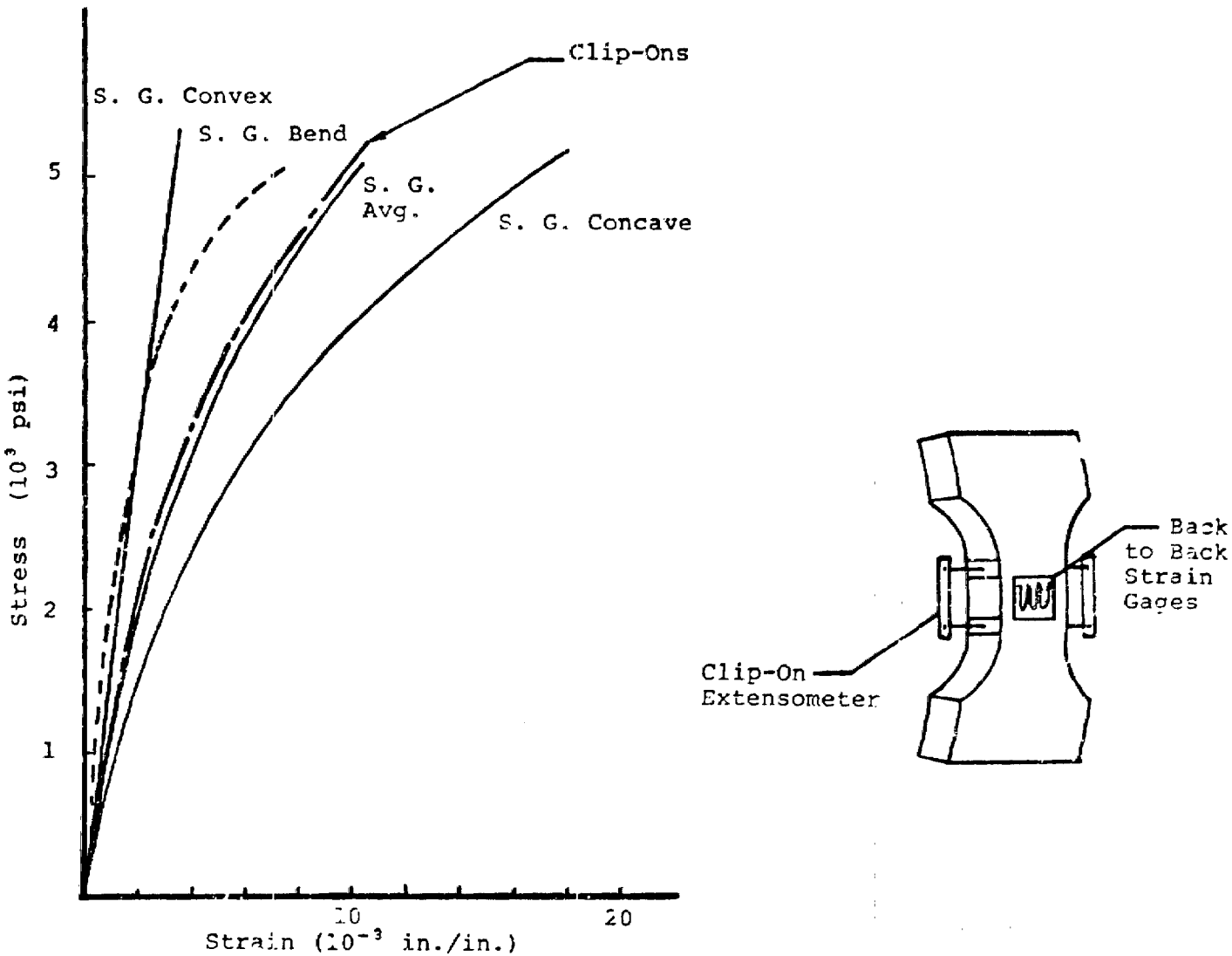

Figure 54. Comparison of Clip-On vs Strain Gage Data in Compression for Curved Felt CC Specimen 3-1-Unsupported

TABLE 1

EVALUATIONS COMPLETED ON RINGS FOR THE UNDERGROUND EXPOSURE PROGRAM

					Before Underground Exposure										After Underground Exposure									
Mat'l	Mfr.	Ring Identification	Selected By QC NDT	Designated By Mfr.	Visual	Density	Axial X-Ray	Velocity	Axial Velocity	Penetrants	Radial Transmission	40X[2]	Ring Flex	Hydro Compression	Visual	Density	Axial X-Ray	Radial Ultra Velocity	Axial Ultra Velocity	Thickness Profile	Penetrants	Radial Ultra Transmission	Ring Flex	Hydro Compression
R6300	AVCO	83301-400		✓	✓	✓	✓	✓		✓	✓		✓	✓	✓	✓	✓	✓	✓	✓	✓	✓	✓	...
		83301-305-1	✓		✓	✓	✓	✓		✓	✓		✓	✓	✓	✓	✓	✓	✓	✓	✓	✓	✓	...
		83301-305-4		✓	✓	✓	✓	✓		✓	✓		✓	✓	✓	✓	✓	✓	✓	✓	✓	✓	✓	...
3DCP	AVCO	#1	✓		✓	✓	✓	✓	✓	✓	✓[1]													
		#2	✓		✓	✓	✓	✓	✓	✓	✓[1]													
		#4	✓		✓	✓	✓[1]																	
		#8	✓		✓	✓	✓[1]																	
		#9	✓		✓	✓	✓	✓	✓	✓[1]														
		#11	✓		✓	✓	✓	✓	✓	✓[1]														
		83301-200		✓	✓	✓	✓	✓	✓	✓	✓		✓	✓										
		83301-202A		✓	✓	✓	✓	✓	✓	✓	✓		✓	✓										
		83301-305-2		✓	✓	✓	✓	✓	✓	✓	✓		✓	✓										
		83301-305-3		✓	✓	✓	✓	✓	✓	✓	✓		✓	✓										
3DC/QP	AVCO	#3	✓		✓	✓	✓	✓	✓	✓	✓[1]													
		83301-202B		✓	✓	✓	✓	✓	✓	✓	✓		✓	✓										
		83301-305-5		✓	✓	✓	✓	✓	✓	✓	✓		✓	✓										
3DCC	AVCO	1109-35 #2	✓		✓	✓	✓	✓	✓	✓	✓		✓	✓	✓	✓	✓	✓	✓	✓	✓	✓	✓	✓
		1109-35 #3	✓		✓	✓	✓	✓	✓	✓	✓		✓	✓	✓	✓	✓	✓	✓	✓	✓	✓	✓	✓
Belt CC	Sandia	9N-2		✓	✓	✓	✓	✓	✓	✓	✓		✓	✓	✓	✓	✓	✓	✓	✓	✓	✓	✓	✓
		9P-2		✓	✓	✓	✓	✓	✓	✓	✓		✓	✓	✓	✓	✓	✓	✓	✓	✓	✓	✓	✓

Note:

1. Worked stopped on these rings because of unexpected failure of 3DC/QP rings in flyer plate testing at Kaman Sciences.
2. Polishing techniques for entire ring using trimethylpentane was unsuccessful.
3. Hydrostatic compression was not run on the R6300 rings due to short time the rings were at Southern Research

TABLE 2

NDT AND MONITOR INSPECTION RESULTS ON AVCO R6300 RINGS BEFORE AND AFTER UNDERGROUND NUCLEAR EXPOSURE

Ring No.	Bulk Density (gm/cm³) Before	Bulk Density (gm/cm³) After	Orientation (Deg.)	Axial Velocity (in./μsec) Before	Axial Velocity (in./μsec) After	Radial Velocity (in./μsec) Before	Radial Velocity (in./μsec) After	Radial Ultra Transmission (added dB) Before	Radial Ultra Transmission (added dB) After	After Thickness Profile (inch)	Visual/X-ray/Liquid Penetrant Results
83301-305-1	1.338	1.343	0	0.1292	0.1254	0.1285	0.0887	Run 1-44 Run 2-41	Run 1-34 Run 2-35	See Fig. 10 for profile	Background: 1. Material similar to AHP R6300 reported in AFML-TR-72-160. 2. Residual Porosity to 20 mils, Figure 9a. 3. Occassional wrinkling in reinforcement, Figure 9b. Surface in 83301-305-1 only.
			45	0.1292	0.1255	0.1286	0.0996	44 43	40 40		
			90	0.1292	0.1297	0.1254	0.1235	44 43	43 44		
			135	0.1292	0.1320	0.1284	0.1226	44 43	45 45		
			180	0.1296	0.1319	0.1278	0.1233	44 43	45 45		
			225	0.1304	0.1325	0.1266	0.1250	44 43	45 45		
			270	0.1295	0.1315	0.1259	0.1253	44 43	45 45		
			315	0.1285	0.1292	0.1258	0.1011	44 44	43 42		
			Mean	0.1294	0.1297	0.1271	0.1136	44	43		
			sd	0.0005	0.0029	0.0013	0.0147	0.5	3.6		
83301-305-4	1.339	1.341	0	0.1286	0.1309	0.1242	0.1239	Run 1-49 Run 2-49	Run 1-47 Run 2-48	No Profile	Before Exposure Variations: 83301-305-1: 1. No surface flaws 2. 20 mil low-absorptive area near inner edge located at 180° by axial x-ray. 83301-305-4: Ring uniform throughout with no single flaws 83301-400: Ring uniform throughout with no flaws
			45	0.1279	0.1296	0.1243	0.1223	49 49	47 48		
			90	0.1282	0.1300	0.1240	0.1231	49 49	48 48		
			135	0.1279	0.1298	0.1231	0.1220	49 49	48 48		
			180	0.1279	0.1291	0.1216	0.1239	48 49	47 48		
			225	0.1289	0.1303	0.1244	0.1242	49 49	48 48		
			270	0.1283	0.1304	0.1238	0.1243	49 49	48 48		
			315	0.1283	0.1304	0.1239	0.1246	49 49	48 48		
			Mean	0.1283	0.1301	0.1237	0.1235	49	49		
			sd	0.0004	0.0006	0.0009	0.0010	0.4	0.4		
8330.-400	1.340	1.343	0	0.1282	0.1296	0.1230	0.1234	Run 1-49 Run 2-48	Run 1-47 Run 2-47	No Profile	Designated Exposure Centerlines 83301-305-1: SoRI 110° 83301-305-4: SoRI 180° 83301-400 : Any Exposure SoRI 0° After-Exposure Structural Change: 83301-305-1: 1. Matrix eroded and/or melted in outer surface at 275-0-75°. Figure 14 2. Higher porosity on inner surface at 295-0-60° size to 100 mils. 83301-305-4: No structural change 83301-400: Higher porosity on inner surface at 315-0-60° size to 80 mils.
			45	0.1262	0.1287	0.1231	0.1215	47 48	47 47		
			90	0.1278	0.1290	0.1233	0.1221	49 49	48 47		
			135	0.1276	0.1301	0.1239	0.1216	49 49	48 48		
			180	0.1281	0.1296	0.1240	0.1222	48 49	46 48		
			225	0.1284	0.1298	0.1240	0.1221	48 49	47 48		
			270	0.1280	0.1304	0.1242	0.1243	48 49	47 47		
			315	0.1282	0.1298	0.1241	0.1238	48 49	48 48		
			Mean	0.1278	0.1296	0.12.7	0.1226	48	47		
			sd	0.0007	0.0006	0.0005	0.0011	48 0.6	47 0.5		

Notes:

1. 83301-305-1 exposure ℄ was at SoRI 110°. Except for After-Exposure Radial Velocity, all data were measured on 45° increments starting at SoRI 90° or 340°. After-Hit Radial Velocity measurements were started at 0°.

2. Trimethylpentane was used as the penetrant.

TABLE 3

NDT AND MONITOR RESULTS ON AVCO 3DCP RINGS BEFORE UNDERGROUND NUCLEAR EXPOSURE

Ring No.	Bulk Density (gm/cm³) Before	Bulk Density (gm/cm³) After	SoRI Orientation (Deg.)	Axial Velocity (in./μsec) Before	Axial Velocity (in./μsec) After	Radial Velocity (in./μsec) Before	Radial Velocity (in./μsec) After	Radial Ultra Transmission (added db) Before	Radial Ultra Transmission (added db) After	After Thickness Profile (inch)	Visual/X-ray, Liquid Penetrant Results
1	1.406		0	0.3658		0.1646		26.5			Background:
			45	0.3710		0.1684		24.5			1. Material generally similar to AHP 3DCP reported in AFWL-TR-72-160.
			90	0.3687		0.1633		24			
			135	0.3691		0.1640		23			2. Reinforcement was workmanly placed.
			180	0.3822		0.1645		24.5			
			225	0.3711		0.1638		25.5			3. Material in Rings 1,2,4,8,9, and 11 had lower porosity and straighter circa than AHP material, Figure 15.
			270	0.3735		0.1641		27			
			315	0.3687		0.1643		26.5			
			Mean	0.3713		0.1646		25			
			sd	0.0050		0.0016		1.4			
2	1.415		0	0.3695		0.1595		28.5			4. Material in Rings 83301-200, 83301-202A, 83301-305-2, and 83301-305-3 had extremely high residual porosity along radials, Figure 16.
			45	0.3651		0.1615		27.5			
			90	0.3650		0.1659		27			
			135	0.3652		0.1646		27			
			180	0.3675		0.1673		28			
			225	0.3685		0.1642		28.5			
			270	0.3609		0.1625		28.5			
			315	0.3719		0.1638		28			
			Mean	0.3674		0.1637		28			
			sd	0.0024		0.0025		0.6			
4	1.409		0	*		*		*			Before-Exposure Variations:
			45								#1: No flaws
			90								#2:
			135								1. Resin starved areas around radials on outer surface by vision at following locations:
			180								
			225								
			270								
			315								
8	1.414		0	*		*		*			
			45								
			90								
			135								
			180								
			225								
			270								
			315								
			Mean								
			sd								
9	1.413		0	0.3562		0.1639		25			
			45	0.3549		0.1706		23.5			
			90	0.3538		0.1619		22			
			135	0.3571		0.1674		24.5			
			180	0.3563		0.1715		23			
			225	0.3516		0.1625		22			
			270	0.3698		0.1714		23			
			315	0.3665		0.1748		25.5			
			Mean	0.3583		0.1680		23.5			
			sd	0.0064		0.0048		1.3			

SoRI Orien. (Deg.)	Location from Bottom Edge (in.)
30 - 45	0.5 - 1.6
70 - 100	0.4 - 0.9
170 - 195	Bottom-Top Edge

Figure 17 shows typical

2. Volume oriented low-absorptive alignments by axial X-ray located at SoRI 15-65° and 70-105°.

3. Single 0.8 inch long low-absorptive alignment at SoRI 0° by axial X-ray

4. Top outer edge had been bumped resulting local matrix/reinforcement interface failure, Figure 18. Bumped area measured 0.4 inch.

TABLE 3 CONTINUED

Ring No.	Bulk Density (gm/cm³) Before	Bulk Density (gm/cm³) After	SoRI Orientation (Deg)	Axial Velocity (in./μsec) Before	Axial Velocity (in./μsec) After	Radial Velocity (in./μsec) Before	Radial Velocity (in./μsec) After	Radial Ultra Transmission (added db) Before	Radial Ultra Transmission (added db) After	After Thickness Profile (inch)	Visual/X-ray, Liquid Penetrant Results
11	1.404		0	0.3611		0.1646		32			#4: 1. Resin starved areas around radials on outer and inner surfaces by vision at following locations: Surface — SoRI Orien. (Deg.) — Location from Bottom Edge (in.) Outer 20 - 30 — 1.6 Outer 60 — 0.9 - 1.6 Inner 70 — 0.3 - 1.3 Outer 160 - 180 — 1.6 2. 0.32 inch low-absorptive area located at SoRI 20° by axial X-ray #8: 1. Resin starved areas around radials, Figure 19, on outer surface by vision located as follows: SoRI Orien. (Deg.) — Location from Bottom Edge (in.) 110-140 — 0.4-1.7 190-200 — 1.4-1.9 225 — 0.9-1.3 260 — 1.8 295-310 — 1.5-1.9 2. Part through-thickness low-absorptive alignments along radials by axial X-ray located SoRI 10-45°. 3. Single through-thickness low-absorptive alignment along radial located SoRI 340°. #9: 1. Resin starved areas around radials on outer outer surface by vision located SoRI 5-15° and 1 inch from bottom edge. 2. Through thickness low-absorptive alignments along radials at SoRI 135°, 140°, and 350° by axial X-ray. #11: 1. Missing matrix between reinforcement in outer surface located SoRI 165-200° and from bottom edge to 0.7 inch above bottom edge by vision. 2. Volume oriented low-absorptive alignments located SoRI 255-345° by axial X-ray. #3301-200: No flaws #3301-202A: No flaws #3301-305-2: Low absorptive alignments by axial X-ray located SoRI 310-330°. #3301-305-3: No flaws Designated Exposure Location: # 1: Any # 2: SoRI 270° # 4: See Note 2 # 8: " " " # 9: " " " #11: " " " #3301-200: SoRI 225° #3301-202A: SoRI 90° #3301-305-2: SoRI 135° #3301-305-3: SoRI 90° After-Exposure Structural Change See Note 1
			45	0.3619		0.1668		23			
			90	0.3688		0.1617		23.5			
			135	0.3688		0.1675		23			
			180	0.3673		0.1664		22			
			225	0.3781		0.1688		25			
			270	0.3780		0.1726		24			
			315	0.3735		0.1675		23.5			
			Mean	0.3697		0.1670		23			
			sd	0.0065		0.0032		1.0			
#3301-200	1.316		0	0.2862		0.1871		31			
			45	0.2873		0.1882		29			
			90	0.2834		0.1994		30			
			135	0.2839		0.1892		29			
			180	0.2819		0.1960		30			
			225	0.2832		0.2004		31			
			270	0.2830		0.1931		31			
			315	0.2824		0.1914		32			
			Mean	0.2839		0.1931		30.5			
			sd	0.0019		0.0051		1.1			
#3301-202A	1.317		0	0.2804		0.1873		25			
			45	0.2803		0.1862		26			
			90	0.2845		0.1854		27			
			135	0.2819		0.1854		29			
			180	0.2855		0.1799		29			
			225	0.2886		0.1978		25			
			270	0.2916		0.1868		25			
			315	0.2800		0.1910		28			
			Mean	0.2841		0.1875		26.5			
			sd	0.0043		0.0052		1.7			
#3301-305-2	1.316		0	0.2822		0.1908		28			
			45	0.2837		0.1870		25			
			90	0.2855		0.1875		27			
			135	0.2833		0.1960		26			
			180	0.2837		0.1878		25			
			225	0.2824		0.1951		25			
			270	0.2855		0.1876		26			
			315	0.2855		0.1930		29			
			Mean	0.2846		0.1904		26.5			
			sd	0.0022		0.0033		1.5			
#3301-305-3	1.321		0	0.2775		0.1891		29			
			45	0.2819		0.1813		29			
			90	0.2855		0.1925		27			
			135	0.2813		0.1940		25			
			180	0.2783		0.1923		26			
			225	0.2783		0.1833		27			
			270	0.2783		0.1896		31			
			315	0.2849		0.1893		29			
			Mean	0.2808		0.1891		28			
			sd	0.0032		0.0045		2.0			

Notes:

1. No after-hit NDT - application redirected.
2. Work stopped and application redirected on this ring after unexpected failure of 3DC/QP rings in flyer plate testing at Kaman.
3. Trimethylpentane was used as the liquid penetrant.

TABLE 4

NDT AND MONITOR INSPECTION RESULTS ON AVCO EDC/OF WRMOG BEFORE UNDERWATER NUCLEAR EXPOSURE

Ring No.	Bulk Density (gm/cm³) Before	Bulk Density (gm/cm³) After	SoRI Orientation (Deg.)	Axial Uniformity (in./inch) Before	Axial Uniformity (in./inch) After	Radial Uniformity (in./inch) Before	Radial Uniformity (in./inch) After	Radial Ultra Transmission Index dB Before	Radial Ultra Transmission Index dB After	Mean Thickness Profile (Inch)	Visual/X-ray/Liquid Penetrant Results
3[1]	1.476		0	0.3394		0.3564		36.5			Background:
			45	0.3378		0.3514		30.5			#1: Material workman like and similar to AHP EDC/OF reported in AFML-TR-72-160 except residual porosity and waviness in circs were less for this material, Figure 26.
			90	0.3418		0.3757		29.5			
			135	0.3412		0.3760		30.5			
			180	0.3405		0.3843		29.5			
			225	0.3445		0.3800		30			
			270	0.3420		0.3700		30.5			
			315	0.3452		0.3817		30			
			Mean	0.3420		0.3696		30.5			
			sd	0.0030		0.0084		1.5			
83301-202B	1.943		0	0.3352		0.3586		23			83301-202B
			45	0.3373		0.2980		21			83301-305-5:
			90	0.3461		0.3046		23			1. Reinforcement lay up workman like.
			135	0.3374		0.2979		22			2. Residual porosity between axials and along radials extremely high in outer materials, Figure 27a and b.
			180	0.3376		0.2980		24			
			225	0.3394		0.2983		23			
			270	0.3371		0.3071		22			
			315	0.3382		0.3089		27			
			Mean	0.3368		0.3026		21			
			sd	0.0021		0.0036		2.1			
83301-305-5	1.853		0	0.3042		0.1875		28			3. Missing pcs of axials and circs on inner and outer surfaces, Figure 27c.
			45	0.3052		0.1916		23			
			90	0.3016		0.1869		18			
			135	0.3060		0.1965		21			
			180	0.3062		0.1921		21			4. Residual porosity between one side of radial and axial on inner surface - porosity occasionally in succeeding radials in axial direction, Figure 27d.
			225	0.3048		0.1946		22			
			270	0.3075		0.1929		23			
			315	0.3011		0.1879		21			
			Mean	0.3042		0.1925		21.5			
			sd	0.0027		0.0037		1.7			

Notes:

1. No after-exposure NDT - application redirected.
2. Work stopped and application redirected on this ring after unannounced failure of EDC/OF rings in flyer plate testing at Kaman.
3. Trimethylpentane was used as the liquid penetrant.

Before-Exposure Variations:

#3: No flaws.

83301-202B: No flaws.

83301-305-5: No flaws.

SoRI Designated Exposure ℄ Locations:

#3: No designation - see Note 2.
83301-202B: SoRI 45°
83301-305-5: SoRI 225°

After-Exposure Structural Change:

See Note 1.

TABLE 5

NDT AND MONITOR INSPECTION RESULTS ON AVCO 3DCC RINGS BEFORE AND AFTER UNDERGROUND NUCLEAR EXPOSURE

Ring No.	Bulk Density (gm/cm^3) Before	Bulk Density (gm/cm^3) After	Orientation (Deg.)	Axial Velocity (in./μsec) Before	Axial Velocity (in./μsec) After	Radial Velocity (in./μsec) Before	Radial Velocity (in./μsec) After	Radial Ultra Transmission (added db) Before	Radial Ultra Transmission (added db) After	After Thickness Profile (inch)	Visual/X-ray/ Liquid Penetrant Results
1109-35-2	1.636	1.636	0	0.3789	0.3651	0.2408	0.2186	21	24.5	See Note 3	Background:
			45	0.3804	0.3718	0.2432	0.2195	18	22		1. Reinforcement lay up workman like, and, in general, material was similar to AHP 3DCC reported in AFML-TR-72-160. The frequency of delams along Circs was higher than for AHP, Figure 30. The delams were uniformly distributed throughout.
			90	0.3804	0.3682	0.2475	0.2155	21	22		
			135	0.3747	0.3703	0.2460	0.2187	16.5	23.5		
			180	0.3747	0.3538	0.2440	0.2101	16.5	22		
			225	0.3719	0.3553	0.2393	0.2182	20.5	21		
			270	0.3705	0.3596	0.2415	0.2157	16.5	21		
			315	0.3718	0.3574	0.2526	0.2265	17	19		
			Mean	0.3[illegible]6	0.3627	0.2444	0.2179	18	22		
			sd	0.0040	0.0071	0.0043	0.0046	2.1	1.7		

2. Occasional missing radials in machined surface.

Before-Exposure Variations:

1109-35-2: No flaws. Background circ delams most frequent from 30-315°.

1109-35-3: No flaws. Severest background circ delams were located at 55-175°, 190-235°, and 265-330°.

SORI Designated Exposure Locations:

1109-35-2: SORI 315°

1109-35-3: SORI 320°

After-Exposure Structural Change, 1109-35-2

A: Bottom Edge:

1. Missing and raised radials located 105-0 15°, Figure 35a
2. Spalled sections of matrix and discs over radials located [illegible], Figure 35b 90-150°.
3. Single 0.24" long circ crack located 0.25" from inner edge at 60-65°, Figure 35c.
4. Generally, evidence of circ cracking along pre-existing circ delams completely around ring.

B: Top Edge:

No apparent structural change from underground test.

C: Outer Surface:

1. Occasional front yarn lift located at 300-0-45°, Figure 35d.
2. Single 1-3/4" discolored (dark) areas located at 75-90° and 240-255°, Figure 35e.

D: Inner Surface:

No apparent structural change

Note: Penetrant absorption in the edges was higher in the exposed zone of this ring.

Reproduced from best available copy.

TABLE 5 CONTINUED

Ring No.	Bulk Density (gm/cm³) Before	After	Orientation (Deg.)	Axial Velocity (in./μsec) Before	After	Radial Velocity (in./μsec) Before	After	Radial Ultra Transmission (added db) Before	After	Wiper Thickness Profile (inch)	Visual/X-ray/Liquid Penetrant Results
1109-35-3	1.645	1.640	0°	0.3719	0.3529	0.2660	0.2454	19.5	23	See Note 3	1109-35-3 A: Bottom Edge: 1. Missing and raised radials located at 0-30°, Figure 36a 2. Generally, indications of cracking within pre-existing circ delams completely around ring with severest occurring at 285-0-45°, Figures 36b, c, d, and e. 3. Missing matrix between axials and missing ends of axials between radials located near outer edge at 350-0-15°. B: Top Edge: Generally, indications of cracking within pre-existing circ delams completely around ring with severest occurring at 300-0-75°, Figures 36f, g, and h. C: Outer Surface: Front yarn lift located 300-0-20°, Figure 36i. D: Inner Surface: No apparent structural change Notes: 1. Axial X-ray revealed a 1-1/2" long circ low-absorptive alignment at 315°. 2. Penetrant absorption indicated maximum cracking at 350-0-10° in bottom edge and at 15-45° in top edge.
			45	0.3735	0.3542	0.2383	0.2380	19.5	22.5		
			90	0.3789	0.3804	0.2456	0.2189	24.5	21.5		
			135	0.3816	0.3892	0.2438	0.2450	22.5	20		
			180	0.3769	0.3537	0.2417	0.2321	22	20		
			225	0.3789	0.3588	0.2414	0.2303	24	22.5		
			270	0.3760	0.3516	0.2441	0.2401	23	23.5		
			315	0.3774	0.3586	0.2514	0.2376	21.5	18		
			Mean	0.3769	0.3561	0.2467	0.2371	22	21.5		
			sd	0.0032	0.0032	0.0086	0.0060	1.7	2.4		

Notes:

1. 1109-35-3 Exposure C was at SGRI 330°. All after exposure data were measured at 45° increments starting at SGRI 315°.
2. Trimethylpentane was used as the liquid penetrant.
3. Thickness profiles based on average values from measurements at 15-degree increments located 1/4 inch from top and bottom edges and at center of rings:

Thickness (inch)

Ring	270°	285°	300°	315°	330°	345°	Exposure	15°	30°	45°	60°	75°	90°
1109-35-2	0.4984	0.4977	0.4990	0.4990	0.4995	0.4986	0.5003	0.5002	0.5006	0.4996	0.4997	0.4997	0.4993
1109-35-3	0.4971	0.4990	0.4974	0.4964	0.4974	0.4971	0.4986	0.4986	0.4992	0.4995	0.4990	0.5000	0.5000

TABLE 6

NDT AND MONITOR INSPECTION RESULTS ON SANDIA FELT CC RINGS BEFORE AND AFTER UNDERGROUND EXPOSURE

Ring No.	Bulk Density (gm/cm^3) Before	Bulk Density (gm/cm^3) After	Orientation[1] (Deg)	Axial Velocity (in./μsec) Before	Axial Velocity (in./μsec) After	Radial Velocity (in./μsec) Before	Radial Velocity (in./μsec) After	Radial Ultra Transmission (Added db) Before	Radial Ultra Transmission (Added db) After	After Thickness Profile (inch)	Visual/X-ray/Liquid Penetrant[2] Results
9N-2	1.813	1.814	0	0.1153	0.1131	0.1197	0.1117	52	49	See note 3	Background:
				-	(0.1139)	-	(0.1162)	--	--		
			45	0.1157	0.1136	0.1221	0.1166	51.5	49.5		Uniform and typical Felt CC. Residual porosity to approx. 12 mils, Figure 37a and b.
			90	0.1157	0.1161	0.1171	0.1169	51.5	49		
			135	0.1174	0.1145	0.1145	0.1183	51	49		
			180	0.1184	0.1131	0.1181	0.1199	51	49.5		
			225	0.1171	0.1147	0.1212	0.1194	52	49.5		
			270	0.1176	0.1166	0.1204	0.1197	52	49		
			315	0.1166	0.1155	0.1177	0.1100	52	49		
			Mean	0.1165	0.1146	0.1188	0.1166	51.5	45		
			sd	0.0009	0.0013	0.0025	0.0038	0.4	0.2		
											Before-Exposure Variations: 9N-2: 1. Skew low-absorptive alignments by axial X-ray located at 110 - 125° (SoRI 30 -45°) and 170 - 190° (SoRI 90 - 110°), Figure 38. 2. Single 0.15 inch long radial low-absorptive alignment by axial X-ray - extends from outer surface and located at 255° (SoRI 175°). 9P-2: Single 1/4 x 1/2 inch low-absorptive area by axial X-ray located near inner surface and at 225°.

TABLE 6 CONTINUED

Ring No.	Bulk Density (gm/cm³) Before	Bulk Density (gm/cm³) After	Orientation[1] (Deg)	Axial Velocity (in./μsec) Before	Axial Velocity (in./μsec) After	Radial Velocity (in./μsec) Before	Radial Velocity (in./μsec) After	Radial Ultra Transmission (Added db) Before	Radial Ultra Transmission (Added db) After	After Thickness Profile (inch)	Visual/X-ray/Liquid Penetrant Results[2]
9P-2	1.830	1.830	0	0.1109	0.1097	0.1180	0.1173	52.5	50	See note 3	SoRI Designated Exposure ℄ Location:
			45	0.1157	0.1089	0.1166	0.1154	51.5	51		9N-2: SoRI 260°
			90	0.1146	0.1123	0.1136	0.1208	52	50.3		9N-2: SoRI 0°
			135	0.1150	0.1134	0.1158	0.1186	52	50.5		After-Exposure Structural Change:
			180	0.1163	0.1150	0.1143	0.1171	52	51		9N-2:
			225	0.1166	0.1136	0.1154	0.1182	52	51		No significant structural change revealed. Material located on the bottom edge at 275 - 0 - 45° was slightly more porous appearing, Figure 42a shows bottom edge at 0°. Also, material located in outer surface at 270 - 0 - 90° was slightly discolored (dark), and texture was rougher, Figure 42b and c.
			270	0.1173	0.1126	0.1161	0.1249	52	51		
			315	0.1136	0.1127	0.1235	0.1095	52	50.5		
			Mean	0.1150	0.1123	0.1167	0.1177	52	50.5		
			sd	0.0020	0.0020	0.0031	0.0044	0.3	0.4		9P-2:
											A: Bottom Edge:
											1. No significant change such as cracking, Figure 43a.
											2. Porosity slightly higher due to 20 mil and smaller voids located 270-0-90°.
											3. 20 mil voids in surface (located 240-255°) and 270°, Figure 43b.
											B. Top Edge:
											1. No significant change such as cracking.
											2. Entire edge showed streaking discoloration (dark) with most apparent occuring at 345-0-60°
											3. Single 80 mil chip in outer edge at 315°, Figure 43c.
											C. Outer Surface: Material removal and discoloration located at exposure zone approx. 270-0-90°. Effects were continuous from top edge down to approx. 0.10 inch from bottom edge resulting in a ridge of virgin appearing material running along the bottom edge, Figure 43d and e. There was no significant change in porosity or surface texture in the exposed zone.
											D. Inner Surface: No structural change revealed.

Notes:

1. 9N-2 exposure ℄ was at SoRI 260°. All other monitor data were measured at 45° increments starting at SoRI 270° except as noted.

2. Trimethylpentane was used as the liquid penetrant.

3. Thickness profiles based on average values from measurements at 15-degree increments located 1/4 inch from top and bottom edges and at center of rings:

Ring	Thickness (inch) 270°	285°	300°	315°	330°	345°	Exposure ℄	15°	30°	45°	60°	75°	90°
9N-2	0.4991	0.4984	0.4977	0.4977	0.4975	0.4975	0.4974	0.4972	0.4977	0.4983	0.4991	0.4991	0.4990
9P-2	0.4992	0.4990	0.4970	0.4961	0.4962	0.4968	0.4975	0.4970	0.4967	0.4966	0.4974	0.4974	0.4992

TABLE 7

DIMENSIONS OF UNDERGROUND EXPOSURE AND KAMAN SCIENCES EQUIVALENT RINGS

Material	Exposure Location	Ring No.	Position	Outer Diameter-Heatshield: Before Assy (SoRI)	After Assy (Kaman)	Before Disassy (Kaman)	Before Disassy (SoRI)	After[1] Disassy (SoRI)	Out of Round Before/After	Inner Diameter-Be Ring: After Assy (Kaman)	Before Disassy (Kaman)	Before Disassy (SoRI)	After Disassy (SoRI)	Out of Round Before/After
3DCC	Underground Exposure Station 4	83301-404A	0°	9.001			8.998	8.998	4/3			7.730	7.730	1/-1
			45°				8.998	8.996				7.726	7.728	
		1109-35-#3	90°	8.999			9.002	9.001				7.731	7.729	
			135°				9.001	9.001				7.729	7.730	
				9.000			9.000	8.999				7.729	7.729	
	Underground Exposure Station 3	83301-304-1	0°	9.000			8.999	8.999	2/2			7.730	7.730	-2/0
			45°				9.000	9.000				7.728	7.730	
		1109-35-#2	90°	9.000			9.001	9.001				7.728	7.730	
			135°				8.999	8.999				7.726	7.730	
				9.000			9.000	9.000				7.728	7.730	
	Kaman		0°	9.001	9.003	8.998	8.998	8.999	13/13	7.731	7.725	7.727	7.731	9/5
			45°		9.002	9.002	9.003	9.003				7.731	7.728	
		1109-35-#4	90°	9.001	9.003	9.010	9.011	9.012		7.729	7.734	7.736	7.736	
			135°		9.002	9.002	9.002	9.002				7.731	7.732	
				9.001	9.002+	9.002	9.003+	9.004		7.730	7.730	7.731	7.732	
Felt CC	Underground Exposure Station 4	83301-404B	0°	8.998			8.996	8.993	10/14			7.453	7.460	11/0
			45°				9.002	9.001				7.459	7.459	
		9P-2	90°	8.998			9.006	9.007				7.464	7.460	
			135°				9.005	9.003				7.457	7.459	
				8.998			9.002	9.001				7.458	7.459+	
	Underground Exposure Station 3	83301-304-2	0°	9.001			8.995	8.992	14/16			7.455	7.459	11/2
			45°				8.997	8.997				7.454	7.458	
		9N-2	90°	8.999			9.009	9.008				7.466	7.461	
			135°				9.005	9.002				7.460	7.460	
				9.000			9.002	9.000				7.459	7.460+	
	Kaman		0°	9.002	9.006	9.008	8.985	8.982	32/37	7.46[illegible]	7.457	7.447	7.460	34/9
			45°		9.003	9.004	8.991	8.995				7.467	7.464	
		8P-1	90°	9.000	8.999	9.008	9.017	9.019		7.470	7.470	7.481	7.469	
			135°		8.999	8.997	8.999	9.004				7.469	7.462	
				9.000	9.002	9.004	8.998	9.000		7.465	7.463+	7.466	7.464	

[1] 3 Independent Measurements within 2 mils

TABLE 8

BULK MODULUS OF ELASTICITY FOR UNDERGROUND EXPOSURE AND KAMAN SCIENCES EQUIVALENT RINGS

Material	Exposure Location	Ring Identification	Before Exposur			After Exposure			Retained Modulus (Ratio)			AHP Cylinder Modulus			
			Ring Flexure		Hydro-static Compres-sions	Ring Flexure		Hydro-static Compres-sions	Ring Flexure		Hydro-static Compres-sions	Tension		Compression	
			From Deflec-tions	From Strain		From Deflec-tions	From Strain		From Deflec-tions	From Strain		Axial	Circ	Axial	Circ
3DCC	U. G. Station 4	83301-404A 1109-35-03	9.1[1]	11.3	15.1	7.60	9.51	14.1	0.84	0.84	0.93	11.8 to 14.9	11.8 to 15.3	6.9 to 15.0	7.7 to 10.4
	U. G. Station 3	83301-304-1 1109-35-02	9.7	11.1	14.1	9.03	10.6	16.2	0.93	0.96	1.15				
	Kaman (Equivalent to U. G. Station 4)	1109-35-04	---	---	---	7.22	10.3	14.8	(0.74 to 0.79)[2]	(0.91 to 0.93)	(0.98 to 1.0)	13.8	12.9	11.6	9.29
Felt CC	U. G. Station 4	83301-404B 9P-2	1.36	1.29	1.31	1.36	1.15	1.18	1.00	0.89	0.90	0.95 to 1.05	--	0.97 to 1.14	1.30 to 1.91
	U. G. Station 3	83301-304-2 9N-2	1.33	1.24	1.28	1.30	1.17	1.33	0.98	0.94	1.04				
	Kaman (Equivalent to U. G. Station 4)	8P-1	---	---	---	1.32	1.15	1.28	(0.97 to 0.99)	(0.89 to 0.93)	(0.98 to 1.0)	0.98		1.06	1.62
3DC/QP	U. G. Station 2	83301-202B	5.85	5.03	9.19	---	---	---	---	---	---	4.53 to 6.47	5.75 to 7.09	6.07 to 6.20	---
	U. G. Station 3	83301-305-5	6.09	5.15	9.51	---	---	---	---	---	---	5.50	6.42	6.14	
3DCP	U. G. Station 2	83301-200	8.93	9.56	11.2	---	---	---	---	---	---	5.12 to 5.91	12.2	5.32 to 10.2	5.21 to 8.41
	U. G. Station 2	83301-202A	8.93	9.66	12.3	---	---	---	--	---	---				
	U. G. Station 3	83301-305-2	8.76	9.56	11.9	---	---	---	---	---	---	5.51		7.29	6.81
	U. G. Station 3	83301-305-3	8.93	9.72	11.4	---	---	---	---	---	---				
R6300	U. G. Station 4	83301-400	1.48	1.26	1.49	1.45	---	---	0.98	---	---	1.05 to 1.24	1.45 to 1.56	1.07 to 1.17	1.36 to 1.52
	U. G. Station 3	83301-305-1	1.56	1.39	1.38	1.43	---	---	0.92	---	---				
	U. G. Station 3	83301-305-4	1.48	1.26	1.52	1.46	---	---	0.99	---	---	1.16	1.49	1.23	1.43

Notes:

1. All table values are in 10^6 psi.
2. Numbers in parentheses are the range of retained modulus based on the range of moduli for the other two rings of that particular carbon-carbon material.

TABLE 9

FELT CC CURVED COMPRESSION TEST RESULTS

[Fixed End Test]

Specimen	σ psi	E_I 10^6 psi	E_s 10^6 psi	ϵ in./in.
1-I	6530	1.22	1.08	0.0290
3-I	7520	1.34	1.10	0.0304
2-I (Supported)	9170	1.29	1.11	0.0378
1-C	6570	1.27	0.97	0.0282
3-C	6300	1.10	0.97	0.0275
2-C (Supported)	8350	1.23	0.97	0.0284
2-0	7000	1.27	1.27	0.0306
3-0	6820	0.91	0.85	0.0330
1-0 (Supported)	9220	1.27	0.96	0.0430
Averages				
Inner	7740	1.28	1.10	0.0324
Center	7073	1.20	0.97	0.0280
Outer	7680	1.15	1.03	0.0355
Supported	8910	1.26	1.01	0.0364
Unsupported	6790	1.18	1.04	0.0298

Note:

E_I = Initial Modulus

E_s = Secant Modulus at 1/3 $\sigma_{0.01}$

$\sigma_{0.01}$ = Stress at = 0.01 in./in. Strain

Specimens run with lateral support had approximately 60 percent P/A Stress.

TABLE 10

3DCC CURVED COMPRESSION TEST RESULTS

[Fixed End Test]

Specimen	σ psi	E_I 10^6 psi	E_s 10^6 psi	ϵ in./in.
1-I	6780	2.28	-	0.0020
3-I	6360	10.7	-	0.0008
3-0 (Supported)	9820	8.58	-	0.0018
4-I	6450	6.20	5.9	0.0016
4-0	6200	6.9	-	0.0012
5-I	7420	7.2	-	0.0012
5-0 (Supported)	12,450	15.4	-	0.0016

Note:

E_I = Initial Modulus

E_s = Secant Modulus at 1/3 $\sigma_{0.01}$

$\sigma_{0.01}$ = Stress at = 0.01 in./in. Strain

Specimens run with lateral support had approximately 60 percent P/A stress.

TABLE 11

COMPARISON OF CLIP-ON vs STRAIN GAGE DATA IN COMPRESSION FOR CURVED FELT CC SPECIMEN 3-1-UNSUPPORTED

Stress (psi)	Strain (μ in./in.)				
	Clip-Ons	S.G. Convex	S.G. Concave	S.G. Avg.	S.G. Bend
0	0	0	0	0	0
2000	1920	1225	3285	2255	1030
3000	3800	2045	6486	4265	2020
4000	6760	2912	11,275	7093	3181
5000	10,780	3629	18,865	11,247	7618

TABLE 12

COMPARISON OF MODULUS OF ELASTICITY AT DIFFERENT LOCATIONS FOR 300P RINGS

		MOE in 10^6 psi							
		0°		90°		180°		270°	
Ring	Test	Inside	Outside	Inside	Outside	Inside	Outside	Inside	Outside
AFWL-1	RST	3.39	3.24	3.42	3.54	3.48	3.37	3.45	3.52
	HST	3.73	3.69	3.66	3.51	3.67	3.69	3.65	3.51
	RSC	3.32	3.48	3.29	3.41	3.34	3.29	3.69	3.74
	HSC	3.33	3.06	3.33	3.56	3.33	3.06	3.45	3.56
AFWL-2	RST	Gage Damaged		3.34	3.22	3.24	3.21	3.22	3.19
	HST	3.73	3.40	3.84	3.49	3.55	3.40	3.22	3.49
	RSC	Gage Damaged		3.45	3.39	3.10	3.12	3.69	3.67
	HSC	3.37	2.78	2.84	3.09	3.31	2.78	3.32	3.09

HST = Hydrostatic Tension
HSC = Hydrostatic Compression
RST = Ring Segment Tension
RSC = Ring Segment Compression